UNIVERSIDAD POLITECNICA DE VALENCIA

motores térmicos

TRABAJO DE FIN DE MASTER

Simulación LES de flujos equivalentes a los chorros Diesel

Realizado por: Juan Manuel Mompó Laborda
Dirigido por: Sergio Hoyas Calvo

Valencia, Julio de 2011

Master en
Motores de Combustión Interna Alternativos
DEPARTAMENTO DE MÁQUINAS Y MOTORES TÉRMICOS

Contenidos:

1. INTRODUCCION

1.1. Antecedentes

Durante los últimos años se ha producido un gran avance en la comprensión de muchos fenómenos físicos en los chorros líquidos (sprays), tanto por medios experimentales de diagnóstico como técnicas CFD basadas principalmente en RANS (Reynolds Averaged Navier-Stokes). Estos métodos computacionales, aunque muy útiles para estudiar el flujo medio, no pueden proporcionar información sobre las fluctuaciones turbulentas ni sobre el comportamiento preciso de la frontera del chorro. En el extremo opuesto se encuentra la DNS (Direct Numerical Simuation) que resuelve todas las escalas significativas del flujo. Este método proporciona el máximo nivel de detalle de la fluido-dinámica sin necesidad de ningún modelo, pero el coste computacional crece con $Re^{9/4}$ con lo que los recursos necesarios para las condiciones de los chorros en un motor Diesel están por encima de la capacidad actual del hardware disponible.

Los métodos LES (Large Eddy Simulations, Simulación de Grandes Remolinos) por su parte, representan un compromiso entre modelado y coste computacional. Son computacionalmente más caros que los RANS pero al reducirse el modelado que requiere este método, son considerablemente más precisos. Además, los métodos LES permiten el estudio detallado de las estructuras complejas relacionadas con las zonas en las que las fluctuaciones turbulentas son importantes y que los métodos RANS, por definición, no pueden simular. Cabe destacar que dichas estructuras son determinantes durante los procesos de inyección y combustión y su correcta simulación y estudio detallado representan el paradigma necesario para seguir profundizando en la comprensión de los fenómenos físicos (y químicos) asociados a los chorros diésel . Así mismo, conocer mejor estos fenómenos resultará de gran ayuda en las tareas de reducir el consumo y minimizar las emisiones de los motores Diesel.

Además del modelado de la turbulencia, el spray diesel comprende un amplio rango de procesos fisicoquímicos complejos que han de ser incorporados a las simulaciones. Por lo que respecta a la naturaleza bifásica de los chorros, diferentes estudios experimentales demuestran que, a partir de una determinada distancia del inyector, los chorros diesel -tanto en condiciones evaporativas como no evaporativas- son procesos controlados por mezcla y por lo tanto pueden ser estudiados, en una primera aproximación, como los chorros gaseosos.

No obstante, los procesos de mezcla entre el combustible y el aire se ven afectados de forma significativa por la atomización del combustible y la colisión entre las gotas, por lo que la idea de aproximar la evolución de un chorro liquido por medio de la inyección de un gas, resulta una hipótesis demasiado restrictiva, teniendo en cuenta el nivel de descripción física de las simulaciones LES.

Originalmente los modelos LES se desarrollaron para flujos de una sola fase y, de la misma manera que con los modelos RANS, dispone en la actualidad de diferentes planteamientos para resolver flujos bifásicos. El enfoque euleriano-euleriano ha inspirado modelos como el mesoscópico o el VOF (Volume Of Fluid), mientras que el lagrangiano-euleriano se puede usar de forma directa, siempre y cuando se tengan en cuenta los modelos necesarios para describir la interacción entre ambas fases para los tamaños característicos de celda. No obstante, ambos presentan limitaciones dependiendo de la zona del chorro en que nos encontremos (densa o dispersa), de ahí que, ciertas líneas de investigación actual busquen un modelo valido para la totalidad del chorro. El modelo ELSA (Eulerian-Lagrangian Spray Atomization) es un modelo integral desde ese punto de vista,

puesto que captura la totalidad de la evolución del chorro. Este modelo está actualmente en proceso de desarrollo y validación en cálculos RANS donde ya ha demostrado un gran potencial y se presenta pues, como una alternativa lógica a implementar en los cálculos LES de chorros diesel.

1.2. Memoria

Durante el periodo de formación del programa de doctorado enmarcado dentro del Máster Universitario en Motores de Combustión Interna Alternativos, las actividades del investigador han estado orientadas al estudio del chorro diesel. De forma general, el trabajo desarrollado ha perseguido adaptar e implementar los métodos LES para la simulación de chorros diesel.

Forman parte del periodo de formación inicial, la instalación y manejo, paralelización, y ciertas técnicas de postratamiento de datos, específicos del programa con el que se realizaran las simulaciones: el código abierto OpenFOAM. Resulta oportuno mencionar este punto por las implicaciones prácticas que se derivan de las diferencias existentes entre OpenFOAM y los programas de código cerrado, más comunes por su uso extensivo (industrial) en simulación fluidodinámica.

Así pues, y a diferencia de estos programas comerciales, el hecho de tener acceso al código hasta el último nivel y carecer de entorno gráfico, repercute en la curva de aprendizaje pero posibilita la comprensión detallada de las variables en juego y los métodos de cálculo del código, y propicia la optimización del mismo para el caso particular de estudio, convirtiéndose en una herramienta idónea para la investigación en el campo de la simulación.

Siguiendo las ideas expuestas en la introducción el trabajo realizado se puede clasificar de la siguiente manera:

- Simulación LES de chorros gaseosos equivalentes un chorro diesel de referencia
- Simulación de chorros bifásicos con el método Lagrangiano-euleriano en condiciones
- Validación y análisis de los resultados del modelos ELSA aplicado a la simulación de chorros Diesel

Puesto que la paralelización de este tipo de cálculos es condición indispensable para su viabilidad en términos temporales, se realizó un estudio previo sobre la influencia de los parámetros que afectan la reducción temporal al paralelizar el cálculo RANS de un chorro diesel. El estudio, adjunto en los anexos, tiene en cuenta hasta 11 factores, entre los que inicialmente se encuentran los niveles de tolerancia para los residuales de los campos calculados, la condición CFL (Courant–Friedrichs–Lewy), y las variables que controlan la cantidad de veces que se pasa por los distintos bucles del algoritmo PISO (Pressure Implicit with Splitting of Operators) encargado de resolver las ecuaciones de Navier Stokes en problemas transitorios. Después de un primer análisis se sustituyó el número de Courant por el número de procesadores (2 y 4). El planteamiento se corresponde con un diseño de experimentos factorial fraccional, puesto que el número de combinaciones de un diseño factorial completo resulta demasiado alto para su procesamiento (2^{11}=2048 cálculos) y el interés se centra sobre todo en el efecto aislado de cada uno de los factores en el aumento de la velocidad al paralelizar el cálculo. De los resultados se pueden extraer dos conclusiones principales: los factores más significativos son los residuales de los campos relacionados con el modelo de turbulencia, la velocidad, la presión y la ecuación de la energía (entalpia); y el aumento del número de bucles internos para el algoritmo de resolución PISO no es comparable al de los residuales.

En cuanto a la simulación LES de chorros gaseosos, el caso de referencia se escogió de entre los que se disponía de más datos experimentales (analizados en el instituto CMT-Motores Térmicos).

La primera referencia que se puede encontrar de los mismos aparece en la tesis doctoral de Jaime Gimeno García "Desarrollo y Aplicación de la Medida del Flujo de Cantidad de Movimiento de un Chorro Diesel". Con los datos físicos necesarios para las condiciones de contorno, el estudio se centró fundamentalmente en la validación de la condición de entrada.

Una peculiaridad de las simulaciones LES, que resulta de su propia metodología de cálculo, es la necesidad de incluir un campo turbulento coherente y desarrollado en la condición de contorno de entrada o al menos, si no se incluyen de forma apropiada las variables turbulentas de los campos de entrada necesarios -por no disponer de la información-, es necesario extender el dominio aguas arriba de la región de interés para que la turbulencia se pueda desarrollar. En el caso concreto de la simulación de chorros esto supone un problema añadido, pues las alternativas no están exentas de inconvenientes:

- de un lado es necesario disponer de una condición de contorno de entrada (la salida del inyector) que imponga para cada paso temporal dichos campos turbulentos de forma coherente. Esto se puede conseguir a su vez de dos formas, la primera requiere disponer de ellos por cálculos LES (o DNS) previos, con las complicaciones derivadas del manejo y la interpolación de una gran cantidad de datos (debidos a la elevada resolución de malla y de paso temporal) y de la diferencia de tipología de malla asociada a cada problema (i.e. flujo interno en toberas, y flujo externo en la parte del chorro). Con la segunda forma los campos se generan de forma sintética (artificial) para cada paso temporal, pero los perfiles radiales de velocidad turbulenta para el flujo interno no son en absoluto estándar y requeriría de una programación ad hoc.
- Como ya se ha comentado, de otro lado cabe la posibilidad de extender la condición de contorno aguas arriba de la salida del inyector, lo que supondría simular el flujo dentro de la tobera, con el consiguiente aumento del número de celdas y el mismo problema asociado de la diferentes necesidades de malla del flujo confinado entre paredes y del asociado al chorro que no se ve afectado por las paredes.

En los cálculos de chorros gaseosos se optó por reducir el dominio computacional evitando intencionadamente la zona no perturbada del chorro. Dos razones fundamentales llevaron a tomar esta decisión. En primer lugar como preparación a los cálculos de chorros en los que se añade el término Lagrangiano, donde esta zona se omite porque la fracción de liquido es demasiado elevada para la resolución de malla. Además, a partir de la zona no perturbada se puede aplicar la hipótesis de chorro gaseoso y el perfil medio de velocidades teórico es conocido para dicha sección. El trabajo desarrollado ha sido expuesto en diversos congresos y aparece sintetizado en una publicación actualmente en revisión en una revista JCR. Tanto las contribuciones a los congresos como el artículo en revisión aparecen en los documentos anexos. Cabe destacar que la contribución al International Conference on Mechanical, Automotive and Aerospace Engineering 2011 ha sido seleccionada para su publicación en la revista IJVSMT (International Journal of Vehicle Simulation, Modeling and Testing).

Tomando como referencia estos cálculos y los conocimientos adquiridos acerca de la condición de contorno, se añade el método Lagrangiano-euleriano con lo que el flujo simulado se puede considerar ya bifásico. Los resultados de este estudio se presentaran en el próximo congreso internacional Mathematical Modelling for Engineering & Human Behaviour bajo el título "Large-Eddy Simulation of Diesel like particle-laden flows". Está previsto publicar este artículo en la revista Mathematical and Computer Modeling.

Por último, se ha colaborado en el análisis de los resultados del proceso de validación del modelo ELSA en un código comercial (cerrado). Supone una primera toma de contacto con un modelo capaz de simular la totalidad del chorro bifásico con el objetivo de plantear futuros estudios comparativos con el mismo modelo implementado en OpenFOAM para cálculos LES. Los resultados han aparecido en sendas contribuciones a congresos internacionales adjuntos en los anexos.

2. ANEXOS

2.1. DISEÑO DE EXPERIMENTOS

2.1.1. Design and analysis of various factors which affect the Diesel spray simulation using Fractional Factorial design 2^k and 2^{k-p}

Diseño De Experimentos

FINAL PROJECT

Project title:

Design and analysis of various factors which affect the Diesel spray simulation using Fractional Factorial design 2^k and 2^{k-p}

Students: Khuong Anh Dung &

Juan Manuel Mompó Laborda

Lecturer: Prof. Jose Miguel Carot Sierra

Date: 22th Jun 2010

1. DEFINE THE PROBLEM AND OBJECTIVES OF THE STUDY

1.1 Model used for the study

To realize a further optimization of the engine design, this requires a good understanding of the combustion process and how these processes are influenced by engine design and settings.

The spray behavior itself comprises a range of complex physical and chemical processes which are difficult to incorporate in the engine design or computer models. Therefore empirical relations have been developed for the spray behavior which are essential for the engine designer and the developers of multi-dimensional computational models.

For engine designers insight in the behavior of an evaporating fuel spray is of great importance. Improvements in injection equipment reduce emissions and increase power by a more effective combustion process. The major objective of this work is to numerically investigate the interacting physical and chemical phenomena that characterize the flow in a diesel fuel spray evaporation system.

Within this limited topic, the Numerical Simulation of Diesel Spray with the isothermal, non-vaporizing conditions is examed.

- **Isothermal**: indicating equal or constant temperatures.
- A **non-evaporating** fuel spray is defined as the spray produced under variable chamber pressure condition by maintaining the chamber temperature equal to the ambient temperature.

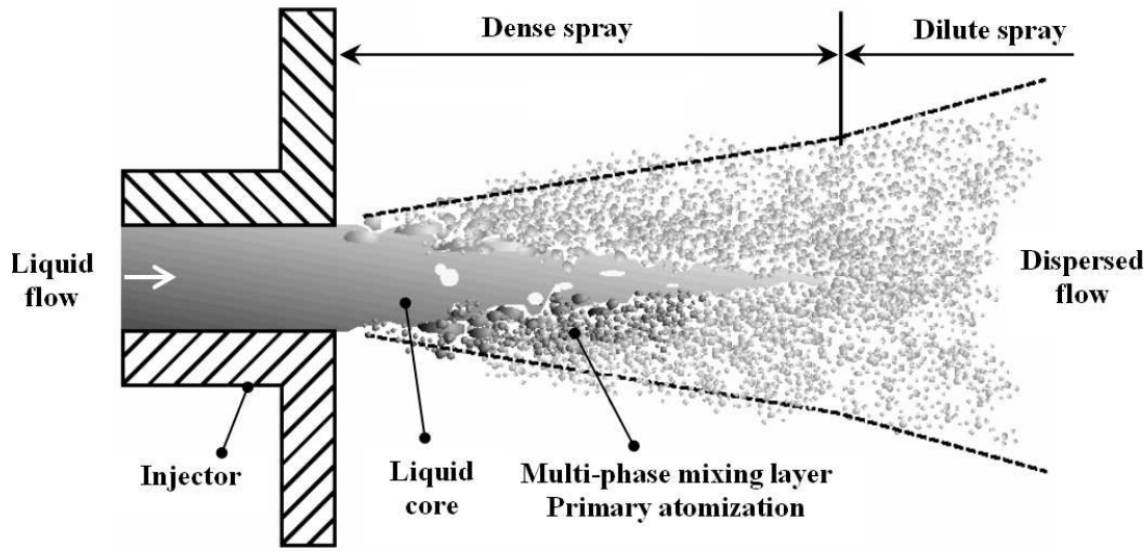

Figure 1: Spray structure

We used OpenFOAM with Computational fluid dynamics tool for the calculation, some detail techniques and methods are described shortly hereafter.

1.2 Computational fluid dynamics

Computational fluid dynamics (CFD) [1] is one of the branches of fluid mechanics that uses numerical methods and algorithms to solve and analyze problems that involve fluid flows. Computers are used to perform the millions of calculations required to simulate the interaction of liquids and gases with surfaces defined by boundary conditions. Even with high-speed supercomputers only approximate solutions can be achieved in many cases.

1.3 Overview of OpenFOAM

The OpenFOAM® [2] (Open Field Operation and Manipulation) CFD Toolbox is a free, open source CFD software package produced by a commercial company, OpenCFD Ltd. It has a large user base across most areas of engineering and science, from both commercial and academic organisations. OpenFOAM has an extensive range of features to solve anything from complex fluid flows involving chemical reactions, turbulence and heat transfer, to solid dynamics and electromagnetics.

The core technology of OpenFOAM is a flexible set of efficient C++ modules. These are used to build a wealth of: solvers, to simulate specific problems in engineering mechanics; utilities, to perform pre- and post-processing tasks ranging from simple data manipulations to visualisation and mesh processing; libraries, to create toolboxes that are accessible to the solvers/utilities, such as libraries of physical models.

OpenFOAM is supplied with numerous pre-configured solvers, utilities and libraries and so can be used like any typical simulation package. However, it is open, not only in terms of source code, but also in its structure and hierarchical design, so that its solvers, utilities and libraries are fully extensible.

OpenFOAM uses finite volume numerics to solve systems of partial differential equations ascribed on any 3D unstructured mesh of polyhedral cells. The fluid flow solvers are developed within a robust, implicit, pressure-velocity, iterative solution framework, although alternative techniques are applied to other continuum mechanics solvers. Domain decomposition parallelism is fundamental to the design of OpenFOAM and integrated at a low level so that solvers can generally be developed without the need for any 'parallel-specific' coding.

1.4 Parallel computing

The availability of parallel computing provides an opportunity for solving increasingly complex problems.

OpenFOAM employs domain decomposition to run cases on more than one processor. The domain is automatically decomposed into a number of sub-domains, each of which is solved on a separate processor. The communication between processors uses the MPI communications protocol (or shmem on Cray platforms).

OpenFOAM has been used for calculations with 10 million cells and has run on a 256 processor Cray T3E.

OpenFOAM displays excellent scaling performance, i.e. reduction in computing time with increase in number of processors. The table below presents timing data for a 3-D linear stress analysis problem on a Diesel injector valve seat with 360,000 cells. The calculation was performed on a 24 CPU Silicon Graphics Origin 2000 in non-dedicated mode, i.e. other jobs were running on the machine during the test.

No of CPUs	CPU time to convergence	Speedup
1	35620.4 s	1.00
2	22398.8 s	1.60
4	11406.6 s	3.10
8	4247.32 s	8.88
16	2872.58 s	12.4

Table 1: CPU time consuming

1.5 Fractional Factorial Designs:

A factorial design is one in which every possible combination of treatment levels for different factors appears.

Why do we need the factorial designs? For example, if there are , say, a levels of factor A, b levels of factor B, c levels of factors C, then a factorial design requires at least abc observations, and more if one wants to estimate the three way interaction among the factors. This can get expensive when experiments have many different factors.

To keep experimental costs in line, one approach is to use fractional factorial designs. In these, one does not take measurements upon every possible combination of factor levels, but only upon a very carefully chosen few.

These few are selected to ensure that the main effects and low-order interactions can be estimated and tested, at the expense of high-order interactions.

The scientific intuition is that it is unlikely for there to be complex interactions among many different factors; instead, there are probably only main effects and a few low-order interactions.

Thus one might design the collection in a fractional factorial so that all main effects and two-way interactions can be tested, but not three-way or higher interactions.

In this report, the experimental data will be analyzed using Statgraphics software.

A step-by-step analysis of a fractional factorial experiment for the case will be shown in this report.

1.6 Purposes of the study

- Reduced the calculation time by optimizing the calculation from 1 node into parallel computation.
- To determine the significant factors that affect the behaviour of the modelling.
- From the obtained results, an optimal reference will be used for future study.

2. Define the response variable

- The Speed of the spray.
- The magnitude directly calculates by the computer programming. The speed range is located from 0 – 300 m/s.

3. Selection of the factors and definition of the levels

Some numbers, controlling the numerical behaviour of the calculation, have been selected as the factors that affect the difference founded between the 1 node calculation and the parallelization. The tolerance for the residuals of the variables directly calculated by the code, the Courant–Friedrichs–Lewy condition (CFL) and the correctors present inside the PISO loop, are the factors studied.

The residual is ostensibly a measure of the error in the solution so that the smaller it is, the more accurate the solution. Besides, it is normalised in to make

it independent of the scale of problem being analysed. The solver **tolerance** should represents the level at which the residual is small enough that the solution can be deemed sufficiently accurate.

In mathematics, the **CFL** condition is a necessary condition for convergence while solving certain partial differential equations numerically. For example, if a wave is crossing a discrete grid, then the time step must be less than the time for the wave to travel adjacent grid points. As a corollary, when the CFL is reduced, the upper limit for the time step also decreases. At the OpenFOAM's use guide there are some suggested values for a given solver.

The number *v* is called the Courant number, and is set as a constant number in the current case, thus the time step changes to fulfill this factor of study in the cell with the highest ratio speed-time vs cell distance.

$$\nu = \frac{u \cdot \Delta t}{\Delta x}$$

Fluid dynamics solver applications in OpenFOAM use the pressure-implicit split-operator (**PISO**) algorithm for transient problems. This algorithm is an iterative procedure for solving equations for velocity and pressure, based on evaluating some initial solutions and then correcting them. Other algorithms only make 1 correction whereas PISO requires more than 1, but typically not more than 4. Therefore **nCorrectors** must be specified by the user between 2 and 4 (OF's recommendation) but , after some bibliography review, for the solver used for diesel sprays under chemical reactions, authors have set this number up to 8. Although no reactive conditions have been used in the current problem the students wanted to know its influence for a wider range since it may be used in future works.

nNonOrthogonalCorrectors stands for an additional correction to account mesh non-orthogonality. **nOuterCorrectors** specifies the number of outer loops around the complete system of equations.

The values for each of the factors are presented in the Table 1.

Factor	CFL	nCorrectors	nNonOrth	nOuterCor	p,rho,U,Yi,h,k,epsilon
Value	0,5; 0,1	2; 8	1; 5	1; 5	1e-6; 1e-10

Table 1: Factors value

4. Setup the test

The case is calculated up to 0.0003s, when the spray reaches the halve of the domain. By this time 8400 time steps have been calculated under a CFL=0.5. The U file calculated at 0.0003s with the domain splitted is compared with the

one calculated in one node. Specifically, the maximum absolute value of the difference of the speed axial component in the domain was identified to get the outcome variable analyzed in this study.

5. Number of observations

We use a factorial experimental design of 2 levels and 32 tries as presented in the Table 2.

6. Organize the experiments

In order to minimize the human error and save time, the run of the cases was automatized following a binary code that identifies the level of each of the factors of study. In the following script, the case pointer is taken from the case folder (i.e. reactingFoam_01111011001_2par) to change the value of the factors

```
setReactingFoam ()

{

# get the case pointer

   caseID=`pwd | grep reactingFoam | cut -d'_' -f2`

# ascribe the value to the factor
   CFL=`expr substr $caseID 1 1`

   nCorrectors=`expr substr $caseID 2 1`
   nNonOrth=`expr substr $caseID 3 1`
   nOuterCor=`expr substr $caseID 4 1`
   p=`expr substr $caseID 5 1`
   rho=`expr substr $caseID 6 1`
   U=`expr substr $caseID 7 1`
   Yi=`expr substr $caseID 8 1`
   h=`expr substr $caseID 9 1`
   k=`expr substr $caseID 10 1`
   epsilon=`expr substr $caseID 11 1`
```

```
# change the level when required

if [ $CFL = 1 ]

then

   sed\
   -e s/"\(maxCo[ \t]*\) 0.5;"/"\1 0.1;"/g \
   $controlDict > temp.$$
   mv temp.$$ $controlDict
fi


if [ $nCorrectors = 1 ]

then

   sed\
   -e s/"\(nCorrectors *\) 2;"/"\1 8;"/g \
   $fvSolution > temp.$$
   mv temp.$$ $fvSolution
fi
```

7. Conduct the experiment

caso	CFL	nCorrectors	nNonOrth	nOuterCor	p	rho	U	Yi	h	k	epsilon	caso	
1	0	0	0	0	0	0	0	0	0	0	0	reactingFoamCase_	0 0 0 0 0 0 0 0 0 0 0 0
2	1	0	0	0	0	1	0	0	1	1	0	reactingFoamCase_	1 0 0 0 0 1 0 0 1 1 0
3	0	1	0	0	0	1	1	0	0	0	1	reactingFoamCase_	0 1 0 0 0 1 1 0 0 0 1
4	1	1	0	0	0	0	1	0	1	1	1	reactingFoamCase_	1 1 0 0 0 0 1 0 1 1 1
5	0	0	1	0	0	1	1	1	1	0	0	reactingFoamCase_	0 0 1 0 0 1 1 1 1 0 0
6	1	0	1	0	0	0	1	1	0	1	0	reactingFoamCase_	1 0 1 0 0 0 1 1 0 1 0
7	0	1	1	0	0	0	0	1	1	0	1	reactingFoamCase_	0 1 1 0 0 0 0 1 1 0 1
8	1	1	1	0	0	1	0	1	0	1	1	reactingFoamCase_	1 1 1 0 0 1 0 1 0 1 1
9	0	0	0	1	0	0	1	1	1	1	1	reactingFoamCase_	0 0 0 1 0 0 1 1 1 1 1
10	1	0	0	1	0	1	1	1	0	0	1	reactingFoamCase_	1 0 0 1 0 1 1 1 0 0 1
11	0	1	0	1	0	1	0	1	1	1	0	reactingFoamCase_	0 1 0 1 0 1 0 1 1 1 0
12	1	1	0	1	0	0	0	1	0	0	0	reactingFoamCase_	1 1 0 1 0 0 0 1 0 0 0
13	0	0	1	1	0	1	0	0	0	1	1	reactingFoamCase_	0 0 1 1 0 1 0 0 0 1 1
14	1	0	1	1	0	0	0	0	1	0	1	reactingFoamCase_	1 0 1 1 0 0 0 0 1 0 1
15	0	1	1	1	0	0	1	0	0	1	0	reactingFoamCase_	0 1 1 1 0 0 1 0 0 1 0
16	1	1	1	1	0	1	1	0	1	0	0	reactingFoamCase_	1 1 1 1 0 1 1 0 1 0 0
17	0	0	0	0	1	0	0	1	0	1	1	reactingFoamCase_	0 0 0 0 1 0 0 1 0 1 1
18	1	0	0	0	1	1	0	1	1	0	1	reactingFoamCase_	1 0 0 0 1 1 0 1 1 0 1
19	0	1	0	0	1	1	1	1	0	1	0	reactingFoamCase_	0 1 0 0 1 1 1 1 0 1 0
20	1	1	0	0	1	0	1	1	1	0	0	reactingFoamCase_	1 1 0 0 1 0 1 1 1 0 0
21	0	0	1	0	1	1	1	0	1	1	1	reactingFoamCase_	0 0 1 0 1 1 1 0 1 1 1
22	1	0	1	0	1	0	1	0	0	0	1	reactingFoamCase_	1 0 1 0 1 0 1 0 0 0 1
23	0	1	1	0	1	0	0	0	1	1	0	reactingFoamCase_	0 1 1 0 1 0 0 0 1 1 0
24	1	1	1	0	1	1	0	0	0	0	0	reactingFoamCase_	1 1 1 0 1 1 0 0 0 0 0
25	0	0	0	1	1	0	1	0	1	0	0	reactingFoamCase_	0 0 0 1 1 0 1 0 1 0 0
26	1	0	0	1	1	1	1	0	0	1	0	reactingFoamCase_	1 0 0 1 1 1 1 0 0 1 0
27	0	1	0	1	1	1	0	0	1	0	1	reactingFoamCase_	0 1 0 1 1 1 0 0 1 0 1
28	1	1	0	1	1	0	0	0	0	1	1	reactingFoamCase_	1 1 0 1 1 0 0 0 0 1 1
29	0	0	1	1	1	1	0	1	0	0	0	reactingFoamCase_	0 0 1 1 1 1 0 1 0 0 0
30	1	0	1	1	1	0	0	1	1	1	0	reactingFoamCase_	1 0 1 1 1 0 0 1 1 1 0
31	0	1	1	1	1	0	1	1	0	0	1	reactingFoamCase_	0 1 1 1 1 0 1 1 0 0 1
32	1	1	1	1	1	1	1	1	1	1	1	reactingFoamCase_	1 1 1 1 1 1 1 1 1 1 1

Table 2: The value 0 sets the first level of the factors, and 1 the second level

After running all the cases the students realized that most of the cases with the lower CFL didn't progress. As it had been said above “when the CFL is reduced, the upper limit for the time step also decreases”, therefore, the residuals at the beginning of their calculation loops are sometimes lower than the tolerance set. These generate some instabilities leading to the calculation diverged.

Consequently, the experiment was re-design, taking in account only the higher CFL (CFL=0,5) and swapping the first factor (CFL) by a new one in order to take advantage of the cases which were already calculated. The new factor substituting CFL is number of processors (**nproc**). Thus, the cases were run in 2 and 4 nodes. Level 0 = 4 processors; level 1 = 2 processors.

case	nproc	nCorrectors	nNonOrth	nOuterCor	p	rho	U	Yi	h	k	epsilon	max speed diff
1	0	0	0	0	0	0	0	0	0	0	0	1,651
2	1	0	0	0	0	1	0	0	1	1	0	1,4514
3	0	1	0	0	0	1	1	0	0	0	1	0,1779
4	1	1	0	0	0	0	1	0	1	1	1	0,0155
5	0	0	1	0	0	1	1	1	1	0	0	1,6699
6	1	0	1	0	0	0	1	1	0	1	0	1,533
7	0	1	1	0	0	0	0	1	1	0	1	2,322
8	1	1	1	0	0	1	0	1	0	1	1	0,0511
9	0	0	0	1	0	0	1	1	1	1	1	0,0934
10	1	0	0	1	0	1	1	1	0	0	1	0,0342
11	0	1	0	1	0	1	0	1	1	1	0	5,8886
12	1	1	0	1	0	0	0	1	0	0	0	1,175
13	0	0	1	1	0	1	0	0	0	1	1	0,4616
14	1	0	1	1	0	0	0	0	1	0	1	4,936
15	0	1	1	1	0	0	1	0	0	1	0	1,4933
16	1	1	1	1	0	1	1	0	1	0	0	1,0986
17	0	0	0	0	1	0	0	1	0	1	1	0,0409
18	1	0	0	0	1	1	0	1	1	0	1	0,0339
19	0	1	0	0	1	1	1	1	0	1	0	1,9963
20	1	1	0	0	1	0	1	1	1	0	0	0,9997
21	0	0	1	0	1	1	1	0	1	1	1	0,0282
22	1	0	1	0	1	0	1	0	0	0	1	0,0336
23	0	1	1	0	1	0	0	0	1	1	0	1,1333
24	1	1	1	0	1	1	0	0	0	0	0	0,4792
25	0	0	0	1	1	0	1	0	1	0	0	1,1397
26	1	0	0	1	1	1	1	0	0	1	0	0,8998
27	0	1	0	1	1	1	0	0	1	0	1	0,0621
28	1	1	0	1	1	0	0	0	0	1	1	0,0173
29	0	0	1	1	1	1	0	1	0	0	0	1,8359
30	1	0	1	1	1	0	0	1	1	1	0	1,884
31	0	1	1	1	1	0	1	1	0	0	1	0,0676
32	1	1	1	1	1	1	1	1	1	1	1	0,0165

Table 3: Observation factors and results.

8. Data analysis

Table 4: Initial data

Source	*Sum of Squares*	*Df*	*Mean Square*	*F-Ratio*	*P-Value*
A:nproc	0,912229	1	0,912229	0,73	0,4316
B:nCorrectors	0,0167674	1	0,0167674	0,01	0,9122
C:nNonOrth	0,354293	1	0,354293	0,28	0,6170
D:nOuterCor	1,75158	1	1,75158	1,40	0,2894
E:p	5,59828	1	5,59828	4,49	0,0877
F:rho	0,172593	1	0,172593	0,14	0,7252
G:U	4,59507	1	4,59507	3,68	0,1131
H:Yi	0,650798	1	0,650798	0,52	0,5026
I:h	3,66196	1	3,66196	2,93	0,1474
J:k	0,0158465	1	0,0158465	0,01	0,9147
K:epsilon	10,0541	1	10,0541	8,06	0,0363
AB+CF+GI+JK	5,42316	1	5,42316	4,35	0,0915
AC+BF+DI+HJ	1,73133	1	1,73133	1,39	0,2919
AD+CI+EJ+FG	0,37008	1	0,37008	0,30	0,6094
AE+DJ+HI	0,0724758	1	0,0724758	0,06	0,8191
AF+BC+DG+HK	3,58363	1	3,58363	2,87	0,1509
AG+BI+DF	0,0554528	1	0,0554528	0,04	0,8414
AH+CJ+EI+FK	3,76168	1	3,76168	3,01	0,1430
AI+BG+CD+EH	0,07997	1	0,07997	0,06	0,8102
AJ+BK+CH+DE	0,822756	1	0,822756	0,66	0,4537
AK+BJ+FH	2,62875	1	2,62875	2,11	0,2064
BD+CG+EK+FI	0,151071	1	0,151071	0,12	0,7421
BE+DK+GH	0,0717731	1	0,0717731	0,06	0,8200
BH+CK+EG+FJ	4,1441	1	4,1441	3,32	0,1280
CE+DH+GK+IJ	0,243236	1	0,243236	0,19	0,6773
EF+GJ+IK	0,18327	1	0,18327	0,15	0,7173
Total error	6,23968	5	1,24794		
Total (corr.)	57,346	31			

Table 5: Final data

Source	Sum of Squares	Df	Mean Square	F-Ratio	P-Value
A:nproc	0,912229	1	0,912229	1,26	0,2762
D:nOuterCor	1,75158	1	1,75158	2,42	0,1371
E:p	5,59828	1	5,59828	7,74	0,0123
F:rho	0,172593	1	0,172593	0,24	0,6311
G:U	4,59507	1	4,59507	6,35	0,0214
H:Yi	0,650798	1	0,650798	0,90	0,3554
I:h	3,66196	1	3,66196	5,06	0,0372
J:k	0,0158465	1	0,0158465	0,02	0,8840
K:epsilon	10,0541	1	10,0541	13,90	0,0015
AF+DG+HK	3,58363	1	3,58363	4,95	0,0390
AH+EI+FK	3,76168	1	3,76168	5,20	0,0350
EG+FJ	4,1441	1	4,1441	5,73	0,0278
GI+JK	5,42316	1	5,42316	7,50	0,0135
Total error	13,0209	18	0,723384		
Total (corr.)	57,346	31			

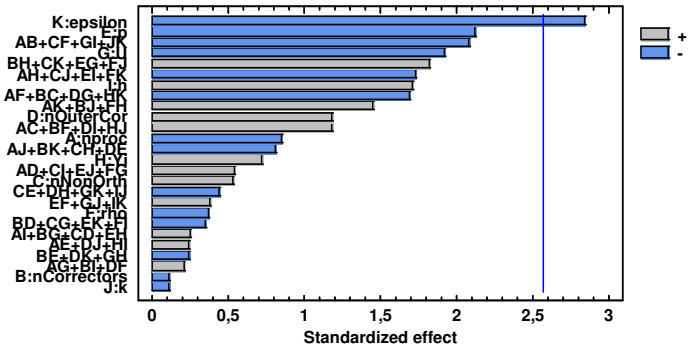

Figure 2: Standardized pareto chart of maximum speed difference

In the initial data, standard errors are based on total error with 5 d.f, whereas the final selection of the factors, standard errors are based on total error with 18 d.f .

The estimation in decreasing order of significance is plotted by Pareto Chart in Figure 2. Using this graph and the values of P-Value shown in Table 4, the non-significant cross factors were taken out in the downward order, one by one, because the elimination of each factor imply the modification of the values of Table 4, specifically the P-Value. The reduction processes started with the combined factors, then following by each individual factors respectively. The Factors were erased in the following order:

	Factors	Reasons
1	AG+BI+DF	P-Value higher than 0.05
2	BE+DK+GH	P-Value higher than 0.05
3	AE+DJ+HI	P-Value higher than 0.05
4	AI+BG+CD+EH	P-Value higher than 0.05
5	BD+CG+EK+FI	P-Value higher than 0.05
6	AF+BC+DG+HK	P-Value higher than 0.05
7	CE+DH+GK+IJ	P-Value higher than 0.05
8	AD+CI+EJ+FG	P-Value higher than 0.05
9	AJ+BK+CH+DE	P-Value higher than 0.05
10	AC+BF+DI+HJ	P-Value higher than 0.05
11	AK+BJ+FH	P-Value higher than 0.05

At this stage all the p-values of the cross interactions were lower than 0.05. A closed observation on the residual log file (the program file which used for setting up the calculation) show that the variables under **nNonOrthogonal** loop were no calculated because the initial residual value was already lower than the tolerance imposed because the calculation performed in the outer loops. Thus, the C factor call nNonOrth and its correlations were taken out of the analysis list

	Old factor	New factor	Reasons
12	AF+BC+DG+HK	AF +DG+HK	C factor no contribution
13	AH+CJ+EI+FK	AH +EI+FK	C factor no contribution
14	BH+CK+EG+FJ	BH +EG+FJ	C factor no contribution
15	AB+CF+GI+JK	AB +GI+JK	C factor no contribution

Then the lower contribution of cross factors due to higher P-Value was removed.

	Old factor	New factor	Reasons
16	AB +GI+JK	GI+JK	AB factor lower contribution compare with G, I, K
17	BH +EG+FJ	EG+FJ	BH factor lower contribution compare with E, G

As B (nCorrectors) does not appear anymore crossed with any other factors and the simply effect has a P-Value higher than 0.05, it was removed from the analysis.

Regarding the rest of factors, no further reason is found in which needs to eliminate their cross effect. Although some of the P-Values for the single effect are higher than 0.05, this factors can not be deleted because their presence in the cross effect. The

Table 5 show the final parameters remain for our investigation.

The final configuration gave us the following results:

- **R-squared = 77,2941 percent**
- **R-squared (adjusted for d.f.) = 60,8954 percent**
- **Standard Error of Est. = 0,85052**

The R-square is slightly low but acceptable in our case. This parameter indicates how linear is the behaviour of the factors studied, suggesting future studies of 3 levels for some of the factors must be performed in order to take in account non-linearity.

The optimization approach is to minimize the speed difference, given that the ideal minimum for a difference between results is zero [Table 6]. In this case the optimum value has a negative sign, which has no mathematical sense. However, the values of the factors to minimize the difference are reasonable. The tolerances should be set to level 1, which means a lower tolerance. Also, lower number of processors will reduce the difference with the solution calculated in one processor. Although this is unlikely expectation, the factor “number of processors” is insignificant, and it is not the main target in this exercise.

9. Conclusion

From our analysis we can use the results as a reference for future calculations to reduce the time and the effect of insignificant factors.

Appendix A

INITIAL DATA

Estimated effects for SpeedDiff

Effect	*Estimate*	*Stnd. Error*	*V.I.F.*
average	1,08502	0,197479	
A:nproc	-0,337681	0,394958	1,0
B:nCorrectors	-0,0457812	0,394958	1,0
C:nNonOrth	0,210444	0,394958	1,0
D:nOuterCor	0,467919	0,394958	1,0
E:p	-0,836531	0,394958	1,0
F:rho	-0,146881	0,394958	1,0
G:U	-0,757881	0,394958	1,0
H:Yi	0,285219	0,394958	1,0
I:h	0,676569	0,394958	1,0
J:k	-0,0445063	0,394958	1,0
K:epsilon	-1,12106	0,394958	1,0
AB+CF+GI+JK	-0,823344	0,394958	1,0
AC+BF+DI+HJ	0,465206	0,394958	1,0
AD+CI+EJ+FG	0,215081	0,394958	1,0
AE+DJ+HI	0,0951813	0,394958	1,0
AF+BC+DG+HK	-0,669294	0,394958	1,0
AG+BI+DF	0,0832563	0,394958	1,0
AH+CJ+EI+FK	-0,685719	0,394958	1,0
AI+BG+CD+EH	0,0999812	0,394958	1,0
AJ+BK+CH+DE	-0,320694	0,394958	1,0
AK+BJ+FH	0,573231	0,394958	1,0
BD+CG+EK+FI	-0,137419	0,394958	1,0
BE+DK+GH	-0,0947188	0,394958	1,0
BH+CK+EG+FJ	0,719731	0,394958	1,0
CE+DH+GK+IJ	-0,174369	0,394958	1,0
EF+GJ+IK	0,151356	0,394958	1,0

Standard errors are based on total error with 5 d.f

The StatAdvisor

This table shows each of the estimated effects and interactions. Also shown is the standard error of each of the effects, which measures their sampling error. Note also that the largest variance inflation factor (V.I.F.) equals 1,0. For a perfectly orthogonal design, all of the factors would equal 1. Factors of 10 or larger are usually interpreted as indicating serious confounding amongst the effects.

To plot the estimates in decreasing order of importance, select Pareto Charts from the list of Graphical Options. To test the statistical significance of the effects, select ANOVA Table from the list of Tabular Options. You can then remove insignificant effects by pressing the alternate mouse button, selecting Analysis Options, and pressing the Exclude button.

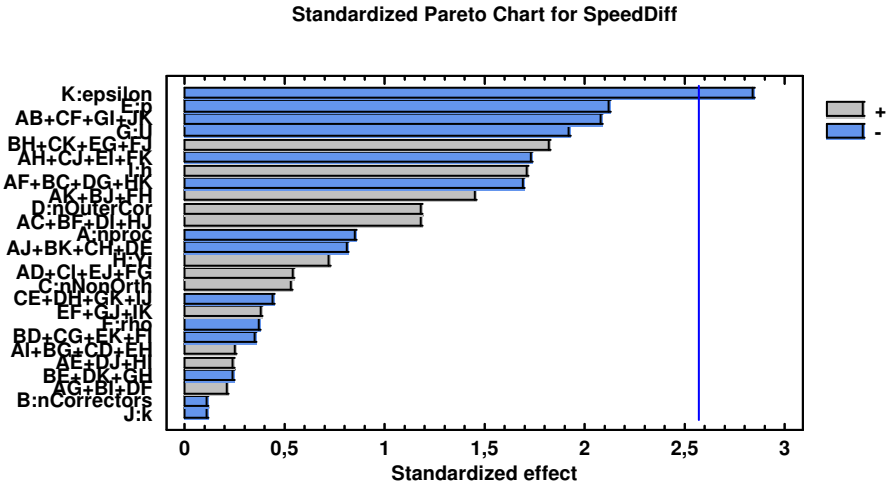

Analysis of Variance for SpeedDiff

Source	*Sum of Squares*	*Df*	*Mean Square*	*F-Ratio*	*P-Value*
A:nproc	0,912229	1	0,912229	0,73	0,4316
B:nCorrectors	0,0167674	1	0,0167674	0,01	0,9122
C:nNonOrth	0,354293	1	0,354293	0,28	0,6170
D:nOuterCor	1,75158	1	1,75158	1,40	0,2894
E:p	5,59828	1	5,59828	4,49	0,0877
F:rho	0,172593	1	0,172593	0,14	0,7252
G:U	4,59507	1	4,59507	3,68	0,1131
H:Yi	0,650798	1	0,650798	0,52	0,5026
I:h	3,66196	1	3,66196	2,93	0,1474
J:k	0,0158465	1	0,0158465	0,01	0,9147
K:epsilon	10,0541	1	10,0541	8,06	0,0363
AB+CF+GI+JK	5,42316	1	5,42316	4,35	0,0915
AC+BF+DI+HJ	1,73133	1	1,73133	1,39	0,2919
AD+CI+EJ+FG	0,37008	1	0,37008	0,30	0,6094
AE+DJ+HI	0,0724758	1	0,0724758	0,06	0,8191
AF+BC+DG+HK	3,58363	1	3,58363	2,87	0,1509
AG+BI+DF	0,0554528	1	0,0554528	0,04	0,8414
AH+CJ+EI+FK	3,76168	1	3,76168	3,01	0,1430
AI+BG+CD+EH	0,07997	1	0,07997	0,06	0,8102
AJ+BK+CH+DE	0,822756	1	0,822756	0,66	0,4537
AK+BJ+FH	2,62875	1	2,62875	2,11	0,2064
BD+CG+EK+FI	0,151071	1	0,151071	0,12	0,7421
BE+DK+GH	0,0717731	1	0,0717731	0,06	0,8200
BH+CK+EG+FJ	4,1441	1	4,1441	3,32	0,1280
CE+DH+GK+IJ	0,243236	1	0,243236	0,19	0,6773
EF+GJ+IK	0,18327	1	0,18327	0,15	0,7173
Total error	6,23968	5	1,24794		
Total (corr.)	57,346	31			

R-squared = 89,1192 percent

R-squared (adjusted for d.f.) = 32,5393 percent

Standard Error of Est. = 1,11711

Mean absolute error = 0,364605

Durbin-Watson statistic = 2,51078 (P=0,6752)

Lag 1 residual autocorrelation = -0,255401

The StatAdvisor

The ANOVA table partitions the variability in SpeedDiff into separate pieces for each of the effects. It then tests the statistical significance of each effect by comparing the mean square against an estimate of the experimental error. In this case, 1 effects have P-values less than 0,05, indicating that they are significantly different from zero at the 95,0% confidence level.

The R-Squared statistic indicates that the model as fitted explains 89,1192% of the variability in SpeedDiff. The adjusted R-squared statistic, which is more suitable for comparing models with different numbers of independent variables, is 32,5393%. The standard error of the estimate shows the standard deviation of the residuals to be 1,11711. The mean absolute error (MAE) of 0,364605 is the average value of the residuals. The Durbin-Watson (DW) statistic tests the residuals to determine if there is any significant correlation based on the order in which they occur in your data file. Since the P-value is greater than 5,0%, there is no indication of serial autocorrelation in the residuals at the 5,0% significance level.

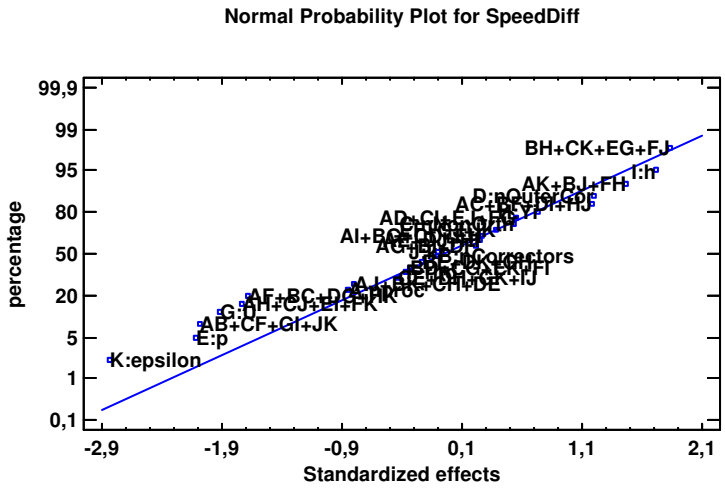

Appendix B

SELECTION OF FINAL PARAMETERS

Analyze Experiment - SpeedDiff

Estimated effects for SpeedDiff

Effect	*Estimate*	*Stnd. Error*	*V.I.F.*
average	1,08502	0,150352	
A:nproc	-0,337681	0,300704	1,0
D:nOuterCor	0,467919	0,300704	1,0
E:p	-0,836531	0,300704	1,0
F:rho	-0,146881	0,300704	1,0
G:U	-0,757881	0,300704	1,0
H:Yi	0,285219	0,300704	1,0
I:h	0,676569	0,300704	1,0
J:k	-0,0445063	0,300704	1,0
K:epsilon	-1,12106	0,300704	1,0
AF+DG+HK	-0,669294	0,300704	1,0
AH+EI+FK	-0,685719	0,300704	1,0
EG+FJ	0,719731	0,300704	1,0
GI+JK	-0,823344	0,300704	1,0

Standard errors are based on total error with 18 d.f.

The StatAdvisor

This table shows each of the estimated effects and interactions. Also shown is the standard error of each of the effects, which measures their sampling error. Note also that the largest variance inflation factor (V.I.F.) equals 1,0. For a perfectly orthogonal design, all of the factors would equal 1. Factors of 10 or larger are usually interpreted as indicating serious confounding amongst the effects.

To plot the estimates in decreasing order of importance, select Pareto Charts from the list of Graphical Options. To test the statistical significance of the effects, select ANOVA Table from the list of Tabular Options. You can then remove insignificant effects by pressing the alternate mouse button, selecting Analysis Options, and pressing the Exclude button.

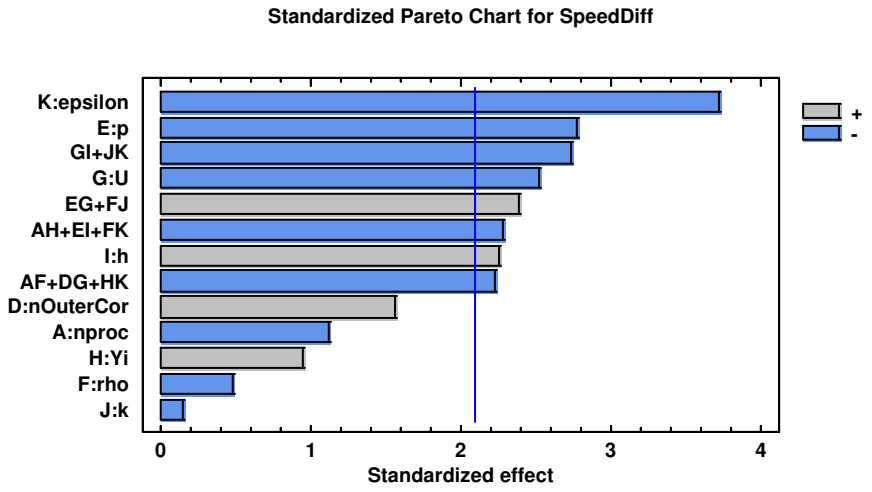

Analysis of Variance for SpeedDiff

Source	*Sum of Squares*	*Df*	*Mean Square*	*F-Ratio*	*P-Value*
A:nproc	0,912229	1	0,912229	1,26	0,2762
D:nOuterCor	1,75158	1	1,75158	2,42	0,1371
E:p	5,59828	1	5,59828	7,74	0,0123
F:rho	0,172593	1	0,172593	0,24	0,6311
G:U	4,59507	1	4,59507	6,35	0,0214
H:Yi	0,650798	1	0,650798	0,90	0,3554
I:h	3,66196	1	3,66196	5,06	0,0372
J:k	0,0158465	1	0,0158465	0,02	0,8840
K:epsilon	10,0541	1	10,0541	13,90	0,0015
AF+DG+HK	3,58363	1	3,58363	4,95	0,0390
AH+EI+FK	3,76168	1	3,76168	5,20	0,0350
EG+FJ	4,1441	1	4,1441	5,73	0,0278
GI+JK	5,42316	1	5,42316	7,50	0,0135
Total error	13,0209	18	0,723384		
Total (corr.)	57,346	31			

R-squared = 77,2941 percent

R-squared (adjusted for d.f.) = 60,8954 percent

Standard Error of Est. = 0,85052

Mean absolute error = 0,471606

Durbin-Watson statistic = 2,25152 (P=0,7096)

Lag 1 residual autocorrelation = -0,143933

The StatAdvisor

The ANOVA table partitions the variability in SpeedDiff into separate pieces for each of the effects. It then tests the statistical significance of each effect by comparing the mean square against an estimate of the experimental error. In this case, 8 effects have P-values less than 0,05, indicating that they are

significantly different from zero at the 95,0% confidence level.

The R-Squared statistic indicates that the model as fitted explains 77,2941% of the variability in SpeedDiff. The adjusted R-squared statistic, which is more suitable for comparing models with different numbers of independent variables, is 60,8954%. The standard error of the estimate shows the standard deviation of the residuals to be 0,85052. The mean absolute error (MAE) of 0,471606 is the average value of the residuals. The Durbin-Watson (DW) statistic tests the residuals to determine if there is any significant correlation based on the order in which they occur in your data file. Since the P-value is greater than 5,0%, there is no indication of serial autocorrelation in the residuals at the 5,0% significance level.

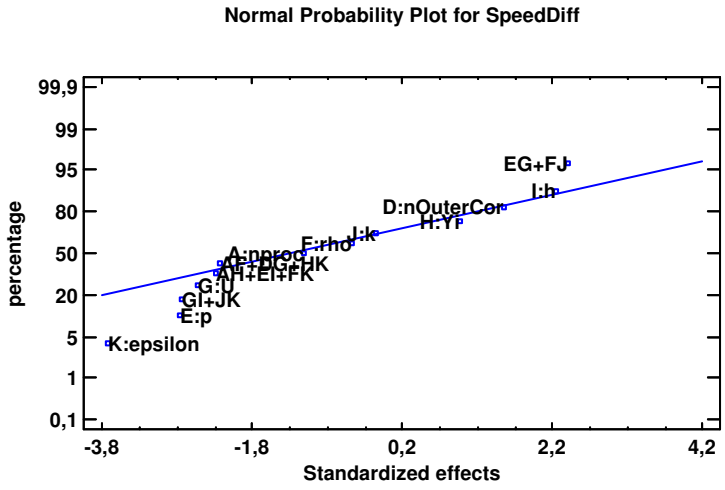

Optimize Response

Goal: minimize SpeedDiff

Optimum value = -0,976133

Factor	*Low*	*High*	*Optimum*
nproc	-1,0	1,0	0,999627
nCorrectors	-1,0	1,0	0,339439
nNonOrth	-1,0	1,0	0,999152
nOuterCor	-1,0	1,0	-1,0
p	-1,0	1,0	0,731128
rho	-1,0	1,0	0,984508
U	-1,0	1,0	0,999058
Yi	-1,0	1,0	0,990301
h	-1,0	1,0	0,977513
k	-1,0	1,0	0,232391
epsilon	-1,0	1,0	1,0

Table 6: Factor levels

The StatAdvisor

This table shows the combination of factor levels which minimizes SpeedDiff over the indicated region. Use the Analysis Options dialog box to indicate the region over which the optimization is to be performed. You may set the value of one or more factors to a constant by setting the low and high limits to that value.

10. REFERENCES

1. Computational Fluid Dynamics:
   http://en.wikipedia.org/wiki/Computational_fluid_dynamics
2. OpenFOAM
   http://www.openfoam.com

2.2. PUBLICACIONES

2.2.1. On the boundary condition setup of Large Eddy Simulation of Diesel sprays. Modelling for Addictive Behaviour, Medicine and Engineering 2010. pp. 87-99. I.S.B.N.: 978-84-693-9537-0

On the boundary condition setup of Large Eddy Simulation of Diesel sprays.*

S. Hoyas† A. Gil, J. M. Mompó-Laborda, D. Khuong-Anh

CMT - Motores Térmicos,

Universidad Politécnica de Valencia,

Edificio 6D,46022, Valencia, Spain.

October 10, 2010

1 Introduction

For engine designers insight in the behaviour of an evaporating fuel spray is of great importance. Improvements in injection equipment reduce emissions and increase power by a more effective combustion process. Therefore, a deep understanding of the physics of Diesel spray will provide some fundamental knowledge for the design of more efficient, less consuming and cleaner engines.

During the last years great advances on the comprehension of several physical phenomena in liquid jets and sprays have been achieved, both by means of diagnosis experimental tests and CFD techniques mainly based on RANS (Reynolds Averaged Navier-Stokes) to simulate turbulence. These computational methods are very useful to study the averaged flow, but they do not provide any information neither about the turbulent fluctuations nor about the flow on the jet boundary. In this paper we present an implementation of a LES (Large Eddy Simulations) method in an non-reactive sprays. LES methods are computationally more expensive than RANS, but modelling required by RANS is reduced, and therefore they are more accurate. Furthermore, a detailed study of the flow characteristics in zones where turbulent fluctuations are significant is allowed by means of LES, while RANS, by definition, cannot model these features. For a comprehensive description of both methods, the book of Pope [1] is an excellent starting point.

Regarding Diesel spray injection, the most commonly used codes in the automotive industry, until very recently, are based on the RANS approach because of their reasonably accurate results and relatively lower computational cost. However as the RANS approach

*This research was funded by the Spanish Government (ENE2010-18542), the Universidad Politécnica de Valencia (PAID-2759) and the Generalitat Valenciana (GV/2010/039)

†Correspondig author.

has the highest level of modelling it can be seen as a successful interpolation between experimental data sets. On the contrary, direct numerical simulation (DNS) methods solve all the significative scales of the flow, so no modelling is require and it provides the highest level of description of the flow. Since the smallest structures of the flow have to be solved, the computational cost increases as $Re^{9/4}$ and the resources required for most practical cases are above current computer hardware limitations (and will probably be in the next 20 years). While the use of LES increases the computational cost, these methods are able to consistently simulate the complex structures related with turbulent mixing, which is decisive in the injection and combustion processes and invisible for RANS solvers ([2], and [3]).

The main goal of this work is to numerically investigate the influence of the inlet boundary conditions on a LES of the flow in a Diesel fuel spray evaporation system. This is the first part of a research project where the idea is to obtain a LES solver able to reproduce the different turbulent patterns that appear in the free shear flow of Diesel sprays, as well as the velocities profiles. In this paper we limited ourselves to the numerical simulation of Diesel spray with the isothermal, isodense and non-vaporizing conditions. Following the characteristic features of this congress, the paper concentrates on the mathematical aspects of the simulation. Thus, the chemical and physical analysis have also not discussed in this article and will be published elsewhere. The results are compared with the classical numerical RANS method with both Eulerian-Eulerian and Lagrangian-Eulerian approaches and are simultaneously validated with experimental data. Our algorithm has been implemented in the free all-purposes CFD code OpenFOAM © 2004-2010 OpenSource Ltd.

2 Numerical Technique

As mentioned above, the RANS approach has been traditionally used in order to model Diesel spray injections[4]. The RNG (Renormalization Group Theory) k-epsilon turbulence model with the default coefficients for the turbulent dissipation rate equation and turbulent viscosity is used for both Euler – Euler and Lagrangian – Euler spray calculations. Previous works [5] showed that RANS accurately predicts average velocity profiles and average spray's shape (i.e. dispersion rate, penetration), since the mean velocity profile and the spreading rate are independent of Re. Nevertheless, RANS is not valid if higher level of turbulence structure description is required during the calculations [3]. Table 1 resume the main characteristics of RANS models compared to LES formulation. Differences are based on the statistical treatment of the turbulence (RANS) and the use of the self-similarity theory of Kolmogorov (LES). Also differences can be found on the time-averaging of the Navier-Stokes equations and the spatial filtering for the RANS and LES respectively, see Table 2.

Application of the filtering operation to the continuity and momentum equations [1] yields:

Table 1: Comparison between RANS and LES.

RANS Reynolds-averaged Navier-Stokes	LES Large Eddy Simulation
Statistical phenomena	Kolmogorov theory of self similarity [1]
Time-averaged NS [2]	Spatial filtered NS
k - ϵ model (Jones and Launder, 1972) RNG k - ϵ model (Yakhot, 1992)	Smagorinsky (Smagorinsky, 1963) One Equation model (Yoshizawa,1985)
Less computationally demanding	Predict transient flows better

[1]Large eddies of the flow are dependent on the flow geometry, while smaller eddies are self similar and have a universal character.

[2]NS: Navier-Stokes Equations

$$\nabla \cdot \overline{u} = 0 \tag{1}$$

$$\frac{\partial \overline{u}}{\partial t} + \nabla \cdot \overline{uu} = -\frac{1}{\rho}\nabla \overline{p} + \nu \nabla^2 \overline{u} - \nabla \tau \tag{2}$$

where $\overline{u}$ is the filtered velocity field, t is the time, $\overline{p}$ is the filtered pressure, ρ is the fuel density, ν is the uniform kinematic viscosity and τ is the stress-like tensor ($\tau = \overline{uu} - \overline{uu}$). Eqs. (1) and (2) govern the evolution of the large (energy-carrying) scales of motion and the modelled stress term is τ . Also, this SGS stress tensor provides the communication between the resolved scales and the dissipation scales [6].

Closure is obtained by modelling the residual-stress tensor. The Smagorinsky [7] model is used for the sub-grid scale tensor:

$$\tau_{ij}^d = -2\mu_{SGS} S_{ij} \tag{3}$$

where τ_{ij}^d is the deviatoric SGS stress with $\mu_{SGS} = \overline{\rho}\,(C_S \Delta^2) \left\| \widetilde{S_{ij}} \right\|$. C_S is the Smagorinsky constant, a theoretical value (0.065–0.2) and $\left\| \widetilde{S_{ij}} \right\|$ is the Frobenious norm $\left\| \widetilde{S_{ij}} \right\| = \sqrt{2\widetilde{S_{ij}}\widetilde{S_{ij}}}$ of the filtered strain tensor, $\widetilde{S_{ij}} = \frac{1}{2}\left(\frac{\partial \overline{u_i}}{\partial \overline{x_j}} + \frac{\partial \overline{u_j}}{\partial \overline{x_i}}\right)$. Δ is the filter width, here assigned to be the cube root of the local cell volume.

3 Boundary conditions

Experimental results have confirmed the hypothesis that spray evolution is controlled by fuel-air mixing rates and thus they can be analysed in the same way as a gas jets [5]. Besides

Table 2: Time Averaging vs. Spatial Filtering.

Instantaneous = Average + Fluctuations ($u = \overline{u} + u'$) Averaging or filtering of NS equations gives identical equations for the averaged/filtered variables plus averaged fluctuation terms.	
Time Averaging	Spatial Filtering
$u_i(x) = \frac{1}{T}\int_t^{t+T} \overline{u_j}(x,s)\,ds.$	$u(x_0) = \int_\Omega u(x,t)\,G(x_0,x,\Delta)\ {}^{\llcorner 3}dx.$
$\overline{u_i'} = 0$, and $\overline{\overline{u_i}} = \overline{u_i}$.	$\overline{u_i'} \neq 0$, and $\overline{\overline{u_i}} \neq \overline{u_i}$.
Reynolds Stress Tensor	SGS[4] Stress Tensor
$\tau_{ij}^R = \overline{u_j' u_i'}$	$\tau_{ij}^S = -\left(\overline{\overline{u_i}u_j'} + \overline{u_i'\overline{u_j}} + \overline{u_i'u_j'}\right) = \overline{u_i u_j} - \overline{u_i u_j}$

[3]Spatial filter $G(x_0, x, \Delta)$ with filter size Δ

[4]Subgrid Scale

the simplifications brought by the experimental researches, CFD still remains limitations in term of the modelling of the atomisation process of the nearby zone which is not the goal of the present study. In addition, the present work can be seen as a previous approach to the inclusion of droplets (Lagrangian term) as a source of mass and momentum. Hence, to keep the same computational domain will provide a better application of present conclusions to future Lagrangian-Eulerian LES calculation and a more suitable framework for further comparison between them. Consequently, the simplification of the computational domain presented by Vuorinen [8] is also assumed. In his work the inlet boundary condition is set far enough from the nozzle avoiding the problems of the void fraction limits which grid resolution required by LES makes it more restrictive. As presented below, turbulent gas jet theory will be applied to set the fields in the inlet boundary conditions of the domain.

Studies show how under certain conditions, for any section perpendicular to the spray axis in the steady region of the gas jet or diesel spray, momentum flux is conservative, and thus equal to that existing at the nozzle exit ([9], [10]). Therefore, a proper implementation of the inlet boundary condition would perform the same spray development independent of where it would be placed. Consequently, the inlet boundary condition must be perpendicular to the spray axis, contain the whole spray and the same momentum flux as at the nozzle exit and in order to ensure a more realistic development of the flow the boundary inlet has to reproduce the same profile of the fields as in a steady spray.

Since momentum flux can be obtained from experimental data, the unknown factors to set up the BC. can be identified by integrating momentum over the whole spray section:

$$\begin{aligned}\dot{M}_0 &= \frac{\pi}{2\alpha}\cdot\rho_a\cdot\tan^2\left(\frac{\theta_u}{2}\right)\\ &\cdot x^2\cdot U_{axis}^2\cdot\sum_{i=0}^{\infty}\frac{1}{\left(1+i\frac{S_C}{2}\right)}\\ &\cdot\left[\left(\frac{U_{axis}}{U_0}\right)\left(\frac{1+S_C}{2}\right)\left(\frac{\rho_f-\rho_a}{\rho_f}\right)\right]^i\end{aligned} \tag{4}$$

Desantes et al. obtain the previous expression for the spray momentum [11] assuming a Gaussian radial profile [12] for fuel concentration and axial velocity. Here the Schmidt number (S_C) represents the relative rate of momentum and mass transport and θ_u is the spray cone angle. The point of interest for the present work can be seen in Figure 1 where the axis velocity equals the injected velocity ($U_{axis} = U_0$) and a Gaussian radial profile can be assumed. The spray injected under the physical conditions shown in Table 3 has been simulated [13]. In these conditions the end of the non-perturbed zone for the isodense case is located at 4.073mm, approximately $8d_{eq}$ from the nozzle exit (with $d_{eq} = d_0\sqrt{\rho_f/\rho_a}$) and the spray diameter is 2.07mm which is set as the inlet boundary condition diameter. Since LES calculation requires perturbed inlet boundary conditions, the velocity and concentration reference profiles at the inlet boundary condition are Gaussian profiles randomly perturbed a 10% as a first simplify approximation. The discussion of the convenience of this hypothesis will be discussed in the followings sections.

Table 3: Definition of experimental and gas jet CFD simulation $\dot{M} = 1.11N$.

	reference[13]	simulation
Fuel	$C_{13}H_{28}$(l)	fuel (N_2)
Air	N_2	N_2
P_{inj} (MPa)	73.995	-
$P_{a,\infty}$ (MPa)	3.5	3.55
$T_{f,0}$ (K)	307.58	307.58
$T_{a,\infty}$	307.58	307.58
$\rho_{f,0}/\rho_{a,\infty}$	21.26	1
U_0 m/s	373.27	373.27
d_{inlet} μm	112	2070
d_{eq} μm	516	516

The computational domain is a cylindrical volume (d = 40mm, L = 70mm) that represents the shape of the injection test rig chamber. The meshing methodology is fairly the same for the RANS and LES calculations, with different grid densities depending on

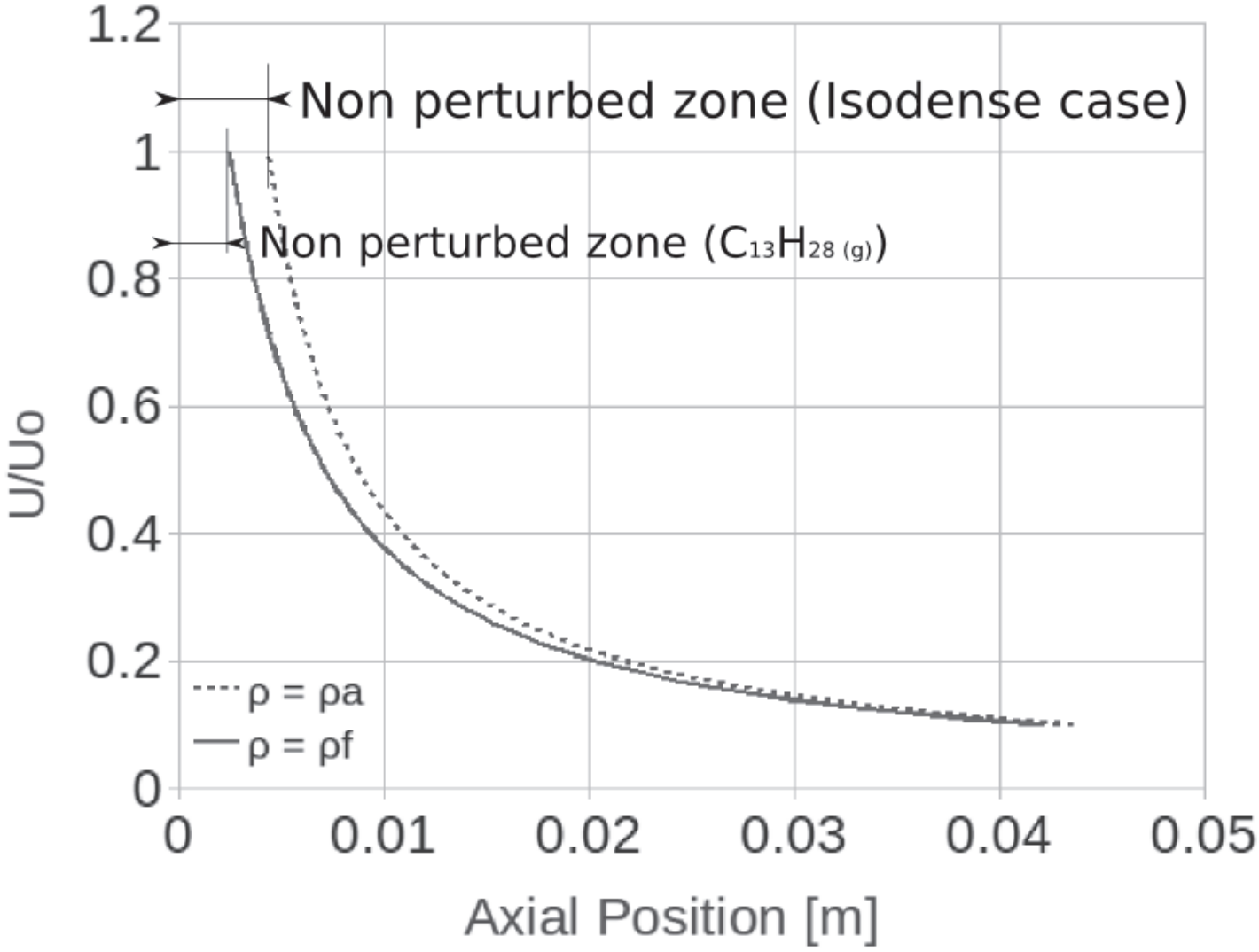

Figure 1: Axis velocity. Red line: Isodense case, Blue line: $C_{13}H_{28}$(g) case

Table 4: Definition of gas jet CFD boundary conditions.

Surface	Boundary type	Defining variables
Spray inlet diameter	Velocity turbulent inlet	$U_0(r)\&C(r)$, T_f
Wall	rigid wall, non-slip condition	–
outlet	constant pressure,	$P_{a,\infty}$;
	wave Transmissive boundary	$T_{a,\infty}$

the turbulence formulation. Hexahedral cells have been preferred for the grid generation, since they provide better accuracy and stability than tetrahedral cells. The computational domain has been decomposed into hexahedral subparts in order to get a semi-structured topology mesh, as shown in Figure 2(a). Cells are concentrated around the spray diameter (d = 2.07mm) to get a cell size of 60 μm and 20 μm for the RANS and LES meshes respectively. Downstream the nozzle the mesh is progressively adapted to the shape of the computational domain in order to obtain a homogeneous cell size at sections located downstream the inlet boundary condition, see circular sections on the right of Figure 2(a) &(b). The number of cells is around $4\text{x}10^5$ and $5.5\text{x}10^6$ for the RANS and LES formulation respectively. Also, an evolution on the LES mesh has been performed in order to optimize skewness, uniformity and number of cells (reduced to $4.9\text{x}10^6$ elements) of the mesh along the fluid zone occupied by the spray. Previous studies performed on RANS Euler – Euler [14] in similar spray conditions show that the structure of the mesh and cell size are enough to get a grid independent solution. Also, the meshes used for the LES formulation have comparable and also smaller cell sizes than recent LES studies [8] for sprays characterization where the grid independence is proved. Finally, three boundary conditions are assigned in the computational domain as depicted in Table 4.

4 Numerical results

The obtained numerical results are contrasted with those predicted by classical RANS models and compared with experimental data. Experimental results have been obtained from previously published data from the authors' research group [10], [15], [13].

Temporal evolution of the axial velocity at 25mm of the virtual nozzle has been used to justify the beginning for the statistical measurements. In Figure 3 (first of temp ev.) the criteria of a constant spray angle was used to set the radial position range of the probes. It is also shown the velocity value imposed in the center of the inlet boundary condition (4.073mm from the virtual nozzle under the isodense conditions). The difference in both the frequency content and the width of the velocity signals in the inlet boundary condition and the axis velocity at 25mm show a lack of precision of the spray fields simulated at the inlet boundary condition and justify the transient period needed for the turbulent

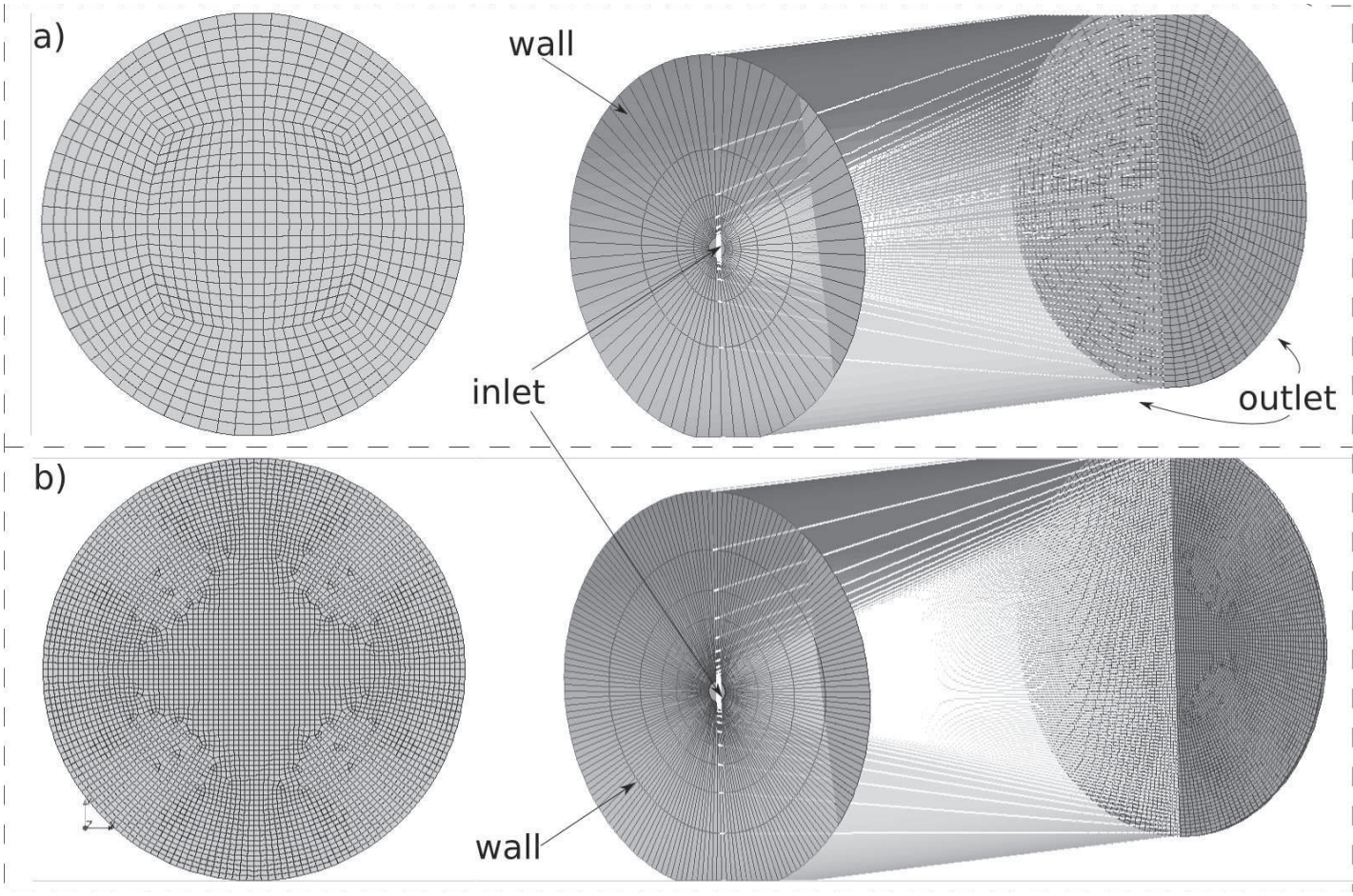

Figure 2: Calculation domain and boundary conditions. a) RANS case, b) LES case

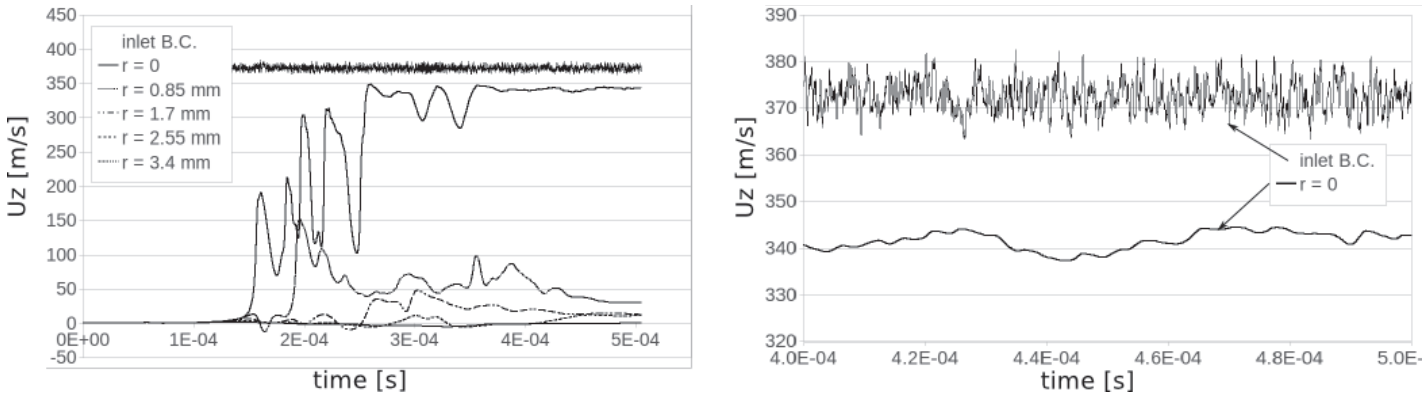

Figure 3: Measurements of radial probes (x=25mm)

evolution. Its effect in LES in terms of the classical parameters to characterize the spray is decisive as shown in Figures 4 and 5

The maximum axial distance for a 1% fuel concentration is the criteria used to define the penetration at Figures 4. Notice that this distance is located at the edge of the spray for theoretical and RANS calculations but not necessarily for LES simulations as shown in Figures 5. RANS and LES (E-E) calculations correspond to isodense cases detailed in previous sections and to obtain the RANS (L-E) penetration a Lagrangian formulation is coupled with an Eulerian one to track the particle dispersion and solve the gas phase variables.

The over prediction of both the RANS and LES Eulerian-Eulerian penetration at is affected by: the different injection mass flow rate shape, the fact that spray is more effective in transferring injection momentum to the ambient than the gas jet [16] and the non-fulfilment of the isodense hypothesis up to $30d_{eq}$. Furthermore, for the LES calculation, the first 5mm can be seen as a length required to develop turbulence Figure 5. Thus, the first assumption of a 1% of velocity fluctuation at the inlet boundary condition is not a good enough turbulent initialization of the flow. Although the inlet is placed at the end of an not well-known zone, authors think a more realistic turbulent conditions can be achieved by applying more realistic measured or calculated profiles of velocity variation [17], [18]. The Figure 5 show iso-surfaces of fuel concentration for the LES simulation at 0.3ms. The red line and the green line mark the stoichiometric iso-surface for LES and RANS (E-E) simulations respectively. These areas have a relevant importance in combustion processes. The upper part of the figure plots the radial distance of these surfaces where detached surfaces far from the jet can be found.

A comparison with the Gaussian radial profiles is shown in Figure 6. In both the axial velocity has been normalized with the axis velocity. In Figure 6(left) the radial distance is normalized with the jet's half-width as defined by Pope [1] where in Figure 6(right) is normalized with the axial distance. A spatial average at 25mm of the nozzle of the axial velocity (t= 0.5ms) shows a good agreement with the theoretical Gaussian profile from the edge to the 30% of the axis speed Figure 6(left). Differences in simulated profiles at 20

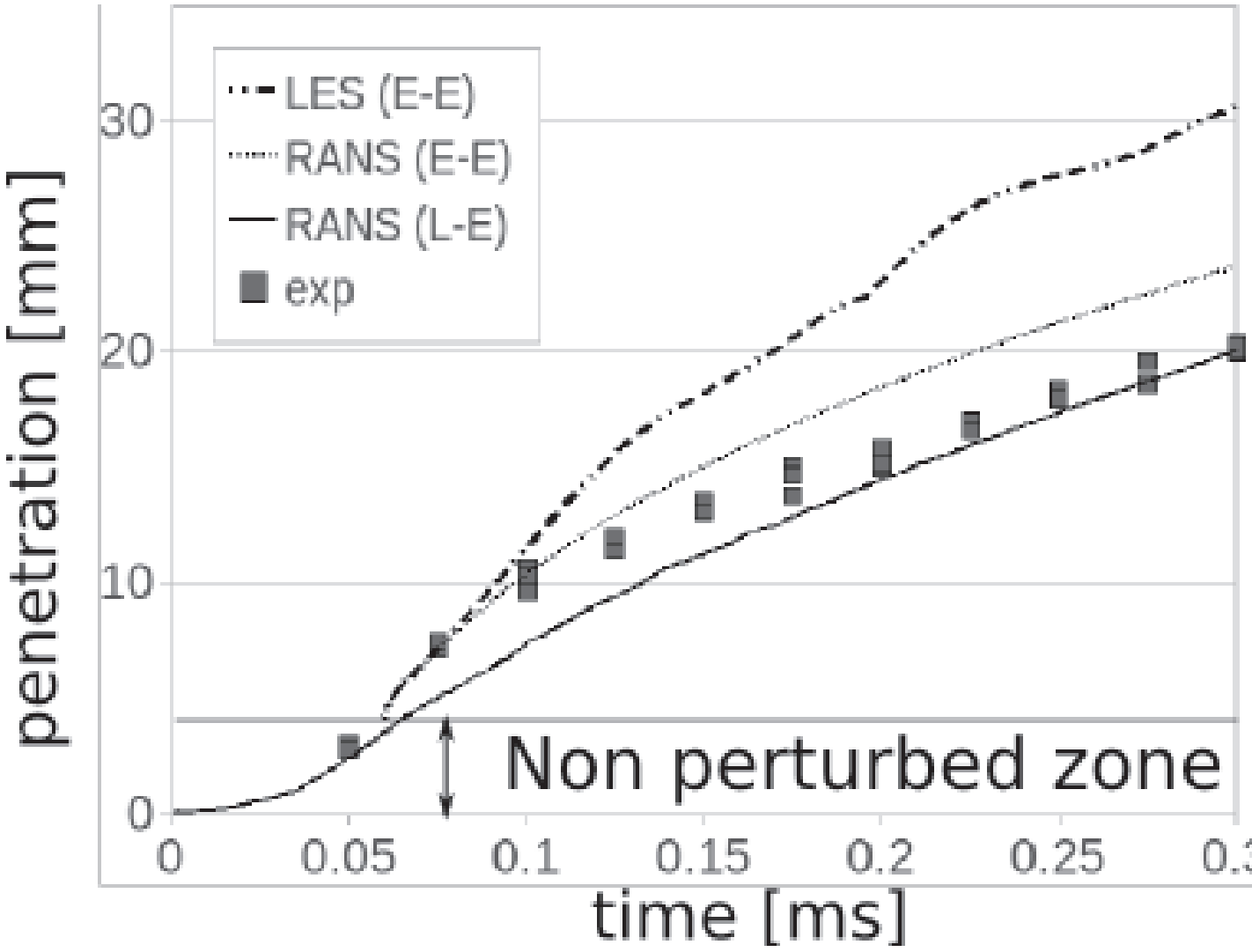

Figure 4: Comparison between experimental spray tip penetration (symbols) and CFD simulations (lines). The time axis is referred to the start of injection.

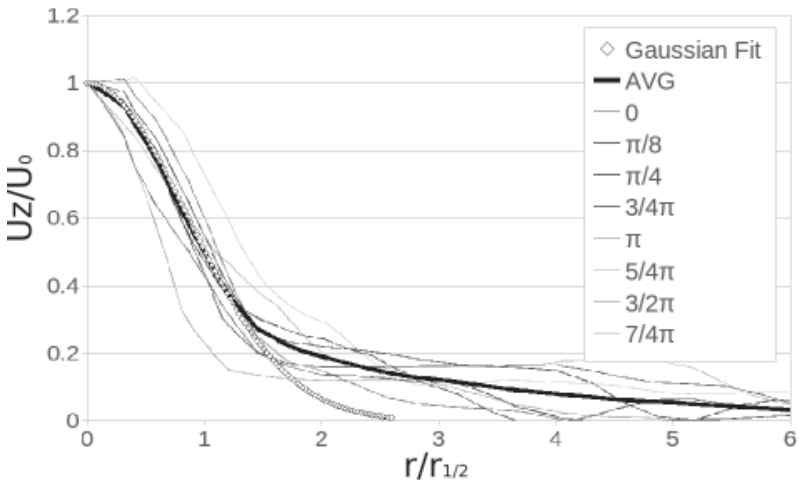

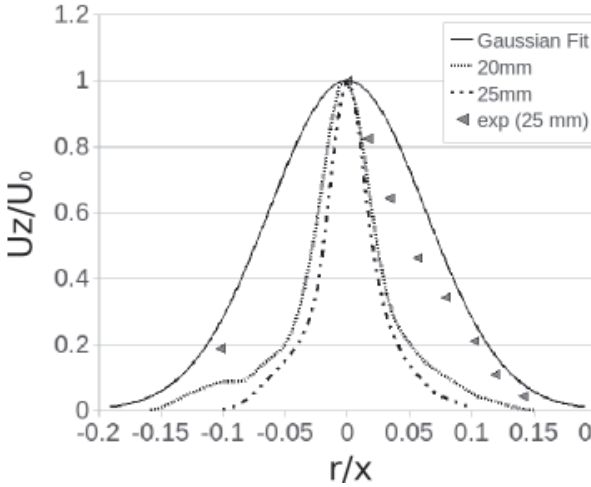

Figure 6: Radial velocity profiles (t=0.5ms). Left: Spatial average of eight different angles, Right: Time-averaged.

and 25 mm in Figure 6(right) can be affected by the amount of statistics for each location (around 0.05ms of data less at 25mm). Experimental data is close to LES simulated profile near the edge of the spray but moves to the Gaussian one as r increases.

5 Conclusions

Using the OpenFOAM code, the authors have performed a completed simulation of diesel spray in LES. Even the results do not match completely with the experimental results and RANS simulation, however; it performs a correct trend of spray simulation. These depict the complicate of modelling of spray processes with many direct or indirect parameters involved. Some specific needs are presented in our paper as challenges to overcome. The future research is now focusing on identifying the important parameters that affect the model and on improving the stability and accuracy of algorithms within OpenFOAM code. By so doing, the better spray simulation will be performed and a reliable tool will be used in modelling the spray simulation in the near future. Hence, LES modelling can become the practical tool in both industry and academic in the design process of combustion systems.

References

[1] Pope S. B., Turbulent Flows, Cambridge University Press, 2000. 771 pp.

[2] J.J. Riley, Review of large-eddy simulation of non-premixed turbulent combustion, J Fluids Eng 128 (2006), pp. 209-215.

[3] Pitsch, H., Large-Eddy Simulation of Turbulent Combustion, Annual Review of Fluid Mechanics, Vol. 38, No. 1, 2006, pp. 453-482.

[4] Fabian Peng-Krrholm, Numerical modelling of diesel spray injection, turbulence and combustion, Ph.D. Thesis, Chalmers Uni. of Technology, 2008.

[5] J.M. Desantes and J.V. Pastor and J.M. García-Oliver and J.M. Pastor, A 1D model for the description of mixing-controlled reacting diesel spray, Combustion and Flame, 2009, 156, pp 234 - 249.

[6] R. Payri and B. Tormos and J. Gimeno and G. Bracho, The potential of Large Eddy Simulation (LES) code for the modeling of flow in diesel injectors, Mathematical and Computer Modelling, Volume 52, Issues 7-8, 2010, Pages 1151-1160.

[7] J.S. Smagorinsky, General circulation experiments with the primitive equations. I. The basic experiment, Mon. Weather Rev. 91 (1963), pp. 99–164.

[8] Ville Vuorinen, LES of Certain Droplet Size Effects in Fuel Sprays, PhD Thesis, the Aalto University School of Science and Technology, 2010.

[9] Desantes JM, Payri R, Salvador FJ, Gimeno J. Measurements of spray momentum for the study of cavitation in diesel injection nozzles. SAE Paper 2003-01-0703; 2003.

[10] R. Payri, J.M. García, F.J. Salvador and J. Gimeno, Using spray momentum flux measurements to understand the influence of Diesel nozzle geometry on spray characteristics, Fuel 84 (2005), pp. 551–561.

[11] J.M. Desantes, R. Payri, J.M. Garcí

a and F.J. Salvador, A contribution to the understanding of isothermal diesel spray dynamics, Fuel 86 (2007), pp. 1093–1101.

[12] Correas D. Theoretical and experimental study of isothermal Diesel free sprays (In Spanish), PhD Thesis, Universidad Politcnica de Valencia; 1998.

[13] D. Jaime Gimeno Garca, Desarrollo y aplicacin de la medida del flujo de cantidad de movimiento de un chorro diesel, PhD thesis, Universidad Politécnica de Valencia, 2008.

[14] Abraham J, What is Adequate Resolution in the Numerical Computations of Transient Jets? SAE 970051 pp 81-95

[15] L. Araneo, V. Soare, R. Payri, J. Shakal, Setting up PDPA system for measurement in a diesel spray, Journal of Physics, 45, 2006, 85-93.

[16] Abraham J, Magi V, Macinnes J, Bracco FV. Gas versus Spray Injection: Which Mixes Faster? SAE paper 940895; 1994, pp163-177

[17] Hussein HJ, Capp and George WK. Velocity measurements in a high-Reynolds-number, momentum-conserving, axisymetric, turbulent jet, J Fluid Mech (1994). 258, 31-75.

[18] Levy Y, Lockwood FC, Combust. Flame 40, 333 (1981)

2.2.2. A Large-Eddy Simulation of Diesel-like gas jets. International Conference on Mechanical, Automotive and Aerospace Engineering 2011 (selected for submission to IJVSMT)

A Large-Eddy Simulation of Diesel-like gas jets.

Sergio Hoyas, Antonio Gil, Juan Manuel Mompó-Laborda, Dung Khuong-Anh
CMT – Motores Térmicos,
Universidad Politécnica de Valencia
Camino de Vera S/N, 46022 Valencia, Spain
E-mail: [serhocal, angime, juamomla, ankh2]@mot.upv.es

Abstract— **Some aspects of the transient evolution of Diesel-liked gas jets by means of Large-Eddy Simulation (LES) are discussed in this work. In order to understand the relationship between the inlet boundary condition and the development of the turbulent motions of the Diesel sprays, a 3D injection chamber is simulated. The main assumption of the set up is the turbulent gas jet theory hypothesis applied to the inlet boundary conditions. Validation of the results is achieved by comparing with both experimental diesel spray measurements and trusted Reynolds-Averaged Navier-Stokes (RANS) simulations. Results show that reasonable simulation of turbulent patterns from one diameter far away of the inlet boundary condition is achieved.**

LES Methods; Diesel sprays; biphasic flows (key words)

I. INTRODUCTION

For engine designers, insight in the behaviour of an evaporating fuel spray is of great importance. Improvements in injection equipment reduce emissions and increase power by a more effective combustion process. Therefore, a deep understanding of the physics of Diesel spray will provide some fundamental knowledge for the design of more efficient, less consuming and cleaner engines.

During the last years great advances on the comprehension of several physical phenomena in liquid jets and sprays have been achieved, both by means of diagnosis experimental tests and Computational Fluid Dynamics (CFD) techniques. Simulation of turbulence is still one of the most challenging problems in physics and there is a general agreement that this simulation can be done within three levels of accuracy. The most used approaches to simulate turbulence are based on RANS. These computational methods are very useful to study the averaged flow, but they do not provide any information neither about the turbulent fluctuations nor about the flow on the jet boundary. Regarding Diesel spray injection, the most commonly used codes in the automotive industry, until very recently, are based on this approach because of their reasonably accurate results and relatively lower computational cost. However as the RANS approach has the highest level of modelling it can be seen as a successful interpolation between experimental data sets, and without a careful check of the results against experiments, little can be said. On the contrary, direct numerical simulation (DNS) methods solve all the significative scales of the flow, so no modelling is required and it provides the highest level of description of the flow. Since the smallest structures of the flow have to be solved, the computational cost increases as $Re^{9/4}$ and the resources required for most practical cases are above current computer hardware limitations (and will probably be in the next 20 years) [1], [2]. In this paper we present an implementation of the third method: LES. It is computationally more expensive than RANS, but modelling required by RANS is reduced, and therefore it is more accurate. Furthermore, a detailed study of the flow characteristics in zones where turbulent fluctuations are significant is allowed by means of LES, while RANS, by definition, cannot model these features. For a comprehensive description of these methods, the book of Pope [3] is an excellent starting point.

As it has been said, LES increases the computational cost, but these methods are able to consistently simulate the complex structures related with turbulent mixing, which is decisive in the injection and combustion processes and invisible for RANS solvers [4], [5]. A good knowledge of this part of the spray is crucial in order to reduce the Diesel emissions. Apart from the turbulence modelling, the spray behaviour itself comprises a range of complex physical and chemical processes which are difficult to incorporate in the engine design or computer models. The nozzle internal flow greatly affects the fuel atomization characteristics and so the subsequent engine combustion and exhaust emissions [6], [7]. The transient nature of the flow is greatly affected by the needle movement which associated with cavitation has dominated recent studies as the key phenomenon connecting internal flow and spray behaviour [8], [9]. Thus simulating the transient behaviour inside the nozzle [10] and predicting the real spray characteristics is of great importance.

Experimental information (refereed by Pastor [11]) shows that Diesel sprays under both non-evaporising and vaporising conditions can be properly described with a mixing-controlled approach, and thus they can be analysed in the same way as a gas jets. However, since fuel-air mixing process is significantly influenced by fuel atomization, breakup and collision, the idea to approximate the spray evolution using gas injection cannot be completely acceptable for LES due to its degree of physical description. LES was originally developed to deal with turbulence in single phase flows. Therefore different approaches have been recently implemented in LES, in order to deal with this a priori complicated two-phase problem. The eulerian-eulerian approach (E-E) for two-phase flow has based models like the mesoscopic [12] or the VOF (volume of fluid) [13].

Regarding the lagrangian-eulerian approach (L-E), a direct use in LES can be performed by taking into account the models needed for the sub-grid two-phase interaction (viscous work, dissipation rate, turbulent viscosity, heat flux, species flux) [14]. Each of them has both advantages and disadvantages in the various regions of spray consisting of the dense zone and the downstream dilute zone. Hence, the Eulerian-Lagrangian Spray Atomization (ELSA) is an integrated model for capturing the whole spray evolution in RANS calculations [15]. Consequently, LES of atomization seems to be a necessarily step forward as depicted by Chesnel [16].

The main goal of this work is to numerically investigate the influence of the inlet boundary conditions on a LES of the flow in a Diesel fuel spray evaporation system. Therefore, in this paper we limited ourselves to the numerical simulation of Diesel-liked gas jet in a combustion chamber. By including in future works those phenomena and conditions omitted here, the effect of more complex/realistic hypothesis on the physical behavior of the spray will be noticed and its contribution on the fuel-air mixing process could be quantified. The results are compared with the classical numerical RANS method with both eulerian-eulerian and lagrangian-eulerian approaches and are simultaneously validated with experimental data. Our algorithm has been implemented in the free all-purposes CFD code OpenFOAM.

The paper is structured as follows: after the introduction, the basis of the LES methodology and the main differences with RANS provide the needed mathematical background. In a subsequent section, the detailed description of the assumptions to set the boundary conditions together with the computational domain are presented. Finally, the numerical results with the main conclusions are exposed.

II. Numerical Technique

As we said in the introduction, there are basically three types of methods to solve a CFD problem depending on the modelling and the description of turbulence: RANS, LES and DNS. DNS was the first developed method, but it is inapplicable in most practical cases. Both RANS and LES methods where developed more or less at the same time in the sixties. LES methods where first described by Smagorinsky in 1963 [17], [18] but, due to the computational resources required, it has not been wide applied in engineering until very recently.

Pope, in his book [3] gives an excellent introduction to LES that we are going to follow here. There are three conceptual steps in LES. First, define a filtering operation to decompose the velocity field as:

$$u(x,t) = \overline{u}(x,t) + u'(x,t). \tag{1}$$

Here the filtered component ū represents the motion of the large scales while the small scale motions that occur on length scales smaller than the mesh spacing are included in the residual component u′. The motion of these sub-grid scales (SGS) can not be captured and therefore their effect on the large scales is modelled in a subsequent step.

In a second stage, the Navier-Stokes equations are spatially filtered assuming that the filtering operator is commutative with the differential operator. The filtering operation is defined as:

$$\overline{f}(x,t) = \int_{\Omega} G(x - x'; \Delta(x))\, f(x',t)\, dx', \tag{2}$$

where G is the filter function and Δ is the filter width, here assigned to be the cube root of the local cell volume. As the isodense condition was set, the introduction of density filter quantities $\widetilde{f} = \overline{\rho f}/\overline{\rho}$ is negligible. A deep explanation can be found in [10]. In this study the conservation equations governing the filtered velocity field ū(x',t) are obtained by applying the filtering operation to the Navier–Stokes equation, for an incompressible flow of a Newtonian fluid. Thus, the filtered continuity equation and the filtered momentum equation become:

$$\nabla \cdot \overline{u} = 0, \tag{3}$$

$$\frac{\partial \overline{u}}{\partial t} + \nabla \cdot \overline{uu} = -\frac{1}{\rho}\nabla \overline{p} + \nu \nabla^2 \overline{u} - \nabla \tau, \tag{4}$$

where ū is the filtered velocity field, t is the time, $\overline{p}$ is the filtered pressure, ρ is the fuel density, ν is the uniform kinematic viscosity and τ is the stress-like tensor $(\tau = \overline{uu} - \overline{u}\,\overline{u})$. Notice that the filtered product $\overline{uu}$ differs from the product of the filtered velocities $\overline{u}\,\overline{u}$. Eqs. (3) and (4) govern the evolution of the large (energy-carrying) scales of motion and the modelled stress term is τ . Also, this sub-grid scale SGS stress tensor provides the communication between the resolved scales and the dissipation scales [10].

In the last step, closure is obtained by modelling the residual-stress tensor. The Smagorinsky [16] model is used for the sub-grid scale tensor:

$$\tau_{ij}^{d} = -2\mu_{SGS} S_{ij}, \tag{5}$$

where τ_{ij}^{d} is the deviatoric SGS stress with: $\mu_{SGS} = \overline{\rho}(C_S \Delta^2)\left\|\widetilde{S_{ij}}\right\|$

C_S is the Smagorinsky constant, with a theoretical value in the interval (0.065–0.2) and $\left\|\widetilde{S_{ij}}\right\|$ is the Frobenious norm $\left\|\widetilde{S_{ij}}\right\| = \sqrt{2\widetilde{S_{ij}}\widetilde{S_{ij}}}$ of the filtered strain tensor, $\widetilde{S_{ij}} = \frac{1}{2}\left(\frac{\partial \overline{u_i}}{\partial \overline{x_j}} + \frac{\partial \overline{u_j}}{\partial \overline{x_i}}\right)$

The Smagorinsky constant varies with both grid mesh aspect ratio as pointed out by Scotti in [19] and the mean shear ([20], [21]). Although some dynamic implementations of the Smagorinsky model allow to determine C_S as a function of time and position ([22], [23]), there is little to be gained by the use of more complex SGS models in the case of high Reynolds number free flows of the type considered. As it was shown clearly in the previous results [24], the standard Smagorinsky model and even more simple models [25] give good results for free flows.

The time derivative terms in Eqs. (3) and (4) are discretized using a first order Euler scheme. The discretization scheme for the diffusive term in Eq. (4) is a second order gaussian integration interpolated linearly by a centred scheme. The convection term in Eq. (3) and (4) is discretized implicitly using a second order Gaussian limited linear differencing scheme. The PISO [26] method is used to solve the pressure correction equation.

As mentioned above, the RANS approach has been traditionally used in order to model Diesel spray injections [27]. The RNG (Renormalization Group Theory) k-epsilon turbulence model with the default coefficients for the turbulent dissipation rate equation and turbulent viscosity is used for both Euler-Euler and Lagrangian-Euler spray calculations. Previous works [11] showed that RANS accurately predicts average velocity profiles and average spray's shape (dispersion rate, penetration), since the mean velocity profile and the spreading rate are independent of Reynolds number. Nevertheless, RANS is not valid if higher level of turbulence structure description is required during the calculations [5].

Table 1 resumes the main characteristics of RANS models compared to LES formulation. Differences are based on the statistical treatment of the turbulence (RANS) and the use of the self-similarity theory of Kolmogorov (LES). Consequently, differences can be found on the time-averaging of the Navier-Stokes equations and the spatial filtering for the RANS and LES respectively, see Table 2.

Solutions schemes for the Eulerian-Eulerian spray simulations with the RANS formulation are exactly the same to those used and described in the previous section for the LES Eulerian-Eulerian spray calculations.

TABLE I. COMPARISON BETWEEN RANS AND LES

RANS	***LES***
Statistical phenomena	Kolmogorov theory of self similarity [a]
Time-averaged NS [b]	Spatial filtered NS
k - ε model (Jones&Launder, 1972) RNG k - ε model (Yakhot, 1992)	Smagorinsky (Smagorinsky, 1963) One Eq. model (Yoshizawa,1985)
Less computationally demanding	Predict transient flows better

a. Large eddies of the flow are dependent on the flow geometry, while smaller eddies are self similar and have a universal character.

b. NS: Navier-Stokes Equations

TABLE II. TIME AVERAGING VS. SPATIAL FILTERING.

Instantaneous = Average + Fluctuations ($u = \bar{u} + u'$)

Averaging or filtering of NS equations gives identical equations for the averaged/filtered variables plus averaged fluctuation terms.

Time Averaging	Spatial Filtering
$u_i(x) = \frac{1}{T}\int_t^{t+T} \overline{u_j}(x,s)\,ds.$	$u(x_0) = \int_\Omega u(x,t)\,G(x_0,x,\Delta)$ [3] $dx.$
$\overline{u_i'} = 0$, and $\overline{\overline{u_i}} = \overline{u_i}.$	$\overline{u_i'} \neq 0$, and $\overline{\overline{u_i}} \neq \overline{u_i}.$
Reynolds Stress Tensor	SGS[4] Stress Tensor
$\tau_{ij}^R = \overline{u_j' u_i'}$	$\tau_{ij}^S = -\left(\overline{\overline{u_i}u_j'} + \overline{u_i'\overline{u_j}} + \overline{u_i'u_j'}\right) = \overline{u_i u_j} - \overline{u_i}\,\overline{u_j}$

3. Spatial filter G (x_0 , x, Δ) with filter size Δ

4. Sub-grid Scale

III. BOUNDARY CONDITIONS

In Diesel engines the fuel is injected into a cylinder by a high pressure atomizer with a nozzle hole diameter d_0 which creates the fuel spray. In terms of computational difficulty the flow is not statistically stationary and has 3 directions of statistical inhomogeneity. Those conditions together with the two phase appearing in the fuel at high velocity sets the spray evolution as one of the most complicated turbulent flow to simulate [3][16]. As depicted at the introduction, besides the simplifications brought by the experimental researches, CFD still presents limitations in term of the modelling of the atomisation process of the nearby zone which is not the goal of the present study. Consequently, the simplification of the computational domain presented by Vuorinen [25] is also assumed. In this work the inlet boundary condition is set far enough from the nozzle avoiding the problems of the void fraction limits which grid resolution required by LES makes it more restrictive. In addition, the present work can be seen as a previous approach to the inclusion of droplets (Lagrangian term) as a source of mass and momentum. These particle-laden gas jets are considered by the authors as the logical following step as it has been widely used to analyze dilute sprays [28][29]. As it can be inferred from the description of the computational domain this is the region of the spray where the research is focused. Furthermore, by keeping the same computational domain will provide a better application of present conclusions to future Lagrangian-Eulerian LES calculation and a more suitable framework for further comparison between them. As presented below, turbulent gas jet theory will be applied to set the fields in the inlet boundary conditions of the domain.

Studies show how under certain conditions, for any section perpendicular to the spray axis in the steady region of the gas jet or diesel spray, momentum flux is conservative, and thus equal to that existing at the nozzle exit [30][31]. Therefore, a proper implementation of the inlet boundary condition would perform the same spray development independent of where it would be placed. Hence, the inlet boundary condition must be perpendicular to the spray axis, contain the whole spray and the same momentum flux as at the nozzle exit and -in order to ensure a more realistic development of the flow- the boundary inlet has to reproduce the same profile of the fields as in a steady spray.

Since momentum flux can be obtained from experimental data, the unknown factors to set up the boundary condition

can be identified by integrating momentum over the whole spray section:

$$\dot{M}_0 = \dot{M}(x) = \int_0^R 2\pi\rho(x,r)\,U(x,r)\,rU(x,r)\,dr, \tag{6}$$

where the x-coordinates coincides with the spray axis and the r-coordinate is the radial position (perpendicular to the spray axis), ρ is the local density in the Diesel spray and U is the axial velocity. Writing the density at an internal point of the spray in terms of local concentration and assuming a Gaussian radial profile [32] for fuel concentration and axial velocity, Desantes et al, obtained the following expression for the spray momentum [33]:

$$\dot{M}_0 = \frac{\pi}{2\alpha}\cdot\rho_a\cdot\tan^2\left(\frac{\theta_u}{2}\right)\cdot x^2\cdot U_{axis}^2 \cdot\sum_{i=0}^{\infty}\frac{1}{\left(1+i\frac{S_C}{2}\right)}\cdot\left[\left(\frac{U_{axis}}{U_0}\right)\left(\frac{1+S_C}{2}\right)\left(\frac{\rho_f-\rho_a}{\rho_f}\right)\right]^i. \tag{7}$$

Here the Schmidt number (S_C) represents the relative rate of momentum and mass transport and θ_u is the spray cone angle. The point of interest for the present work can be seen in Fig. 1 where the $U_{axis} = U_0$. The spray injected under the physical conditions shown in Table 3 has been simulated [32]. In these conditions the end of the non-perturbed zone for the isodense case is located at 4.073mm, approximately $8d_{eq}$ from the nozzle exit (with $d_{eq} = d_0\sqrt{\rho_f/\rho_a}$) and the gas jet diameter is 2.07mm which is set as the inlet boundary condition diameter. The velocity and concentration reference profiles are defined as:

$$U(x,r) = U_{axis}(x)\cdot\exp\left(-\alpha\left(\frac{r}{R}\right)^2\right), \tag{8}$$

$$C(x,r) = C_{axis}(x)\cdot\exp\left(-\alpha\cdot S_C\cdot\left(\frac{r}{R}\right)^2\right), \tag{9}$$

with α (= 4.6) the shape factor of the Gaussian distribution. Since LES calculation requires perturbed inlet boundary conditions, the reference signal is randomly perturbed a 10% as a first approximation. The discussion of the convenience of this hypothesis will be overcome in the followings sections.

The computational domain is a cylindrical volume (d = 40mm, L = 70mm) that represents the shape of the injection test rig chamber. The meshing methodology is fairly the same for the RANS and LES calculations, with different grid densities depending on the turbulence formulation. Hexahedral cells have been preferred for the grid generation, since they provide better accuracy and stability than tetrahedral cells. The computational domain has been decomposed into hexahedral subparts in order to get a semi-structured topology mesh, as shown in Fig. 2(a). Cells are concentrated around the spray diameter (d = 2.07mm) to get a cell size of 57.5µm and 22.5µm for the RANS and LES meshes respectively. Downstream the nozzle the mesh is progressively adapted to the shape of the computational domain in order to obtain a homogeneous cell size at sections located downstream the inlet boundary condition, see circular sections on the right of Fig. 2. The numbers of cells are 4.05×10^5 and 4.9×10^6 for the RANS and LES formulation respectively.

TABLE III. DEFINITION OF EXPERIMENTAL AND GAS JET CFD SIMULATION.

	exp.[32] (M = 1.11N)	***simulation***
Fuel	$C_{13}H_{28}$ (l)	fuel (N_2)
Air	N_2	N_2
P_{inj} (MPa)	73.995	-
$P_{a,\infty}$ (MPa)	3.5	3.55
$T_{f,0}$ (K)	307.58	307.58
$T_{a,\infty}$ (K)	307.58	307.58
$\rho_{f,0}/\rho_{a,\infty}$	21.26	1
U_0 (m/s)	373.27	373.27
d_{inlet} (µm)	112[a]	2070[b]
d_{eq} (µm)	516	516

a. Nozzle diameter

b. Jet diameter at the end of the non perturbed zone

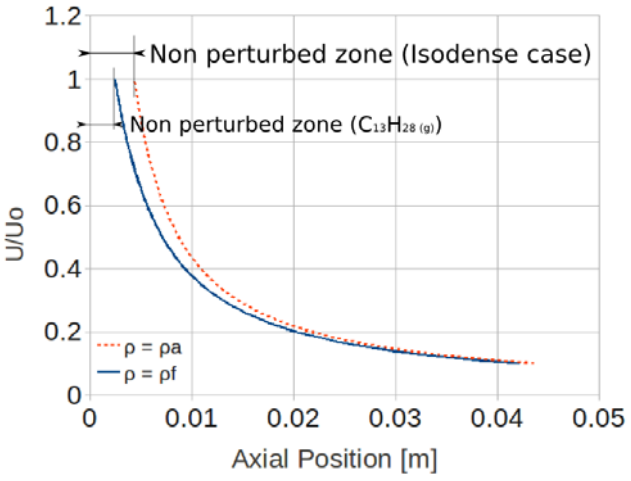

Figure 1. Axis velocity. Red dot line: Isodense case, Blue solid line: $C_{13}H_{28}$ (g) case

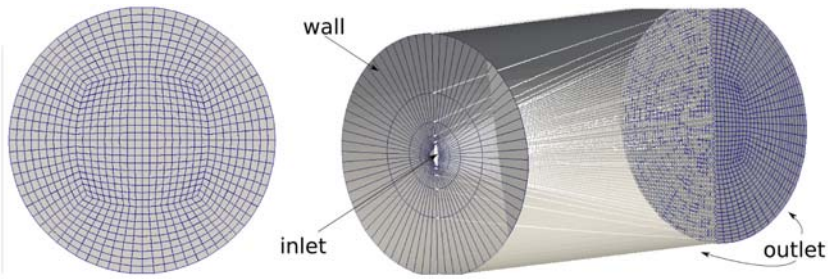

Figure 2. Calculation domain and boundary conditions for the RANS case. LES grid is a finer version of this one

In this mesh, the circular faces of the cylinder are splitted in to four parts and then meshed with a non-structured hexahedral mesh using the same cell size than that described above. Previous studies performed on RANS euler-euler [35] in similar spray conditions show that the structure of the mesh and cell size are enough to get a grid independent solution. Also, the meshes used for the LES formulation have comparable and also smaller cell sizes than recent LES studies [25] for sprays characterization where the grid independence is proved. Finally, three boundary conditions are assigned in the computational domain as depicted in Table 4.

TABLE IV. DEFINITION OF GAS JET CFD BOUNDARY CONDITIONS.

Surface	***Boundary type***	***Defining variables***
inlet	turbulent velocity inlet	U_0 (r)&C(r), T_f
wall	rigid wall, non-slip cond.	-
outlet	constant pressure, wave Transmissive	$P_{a,\infty}$ $T_{a,\infty}$

IV. NUMERICAL RESULTS

The obtained numerical results are contrasted with those predicted by classical RANS models and compared with experimental data. Experimental results have been obtained from previously published data from the authors' research group. Momentum flux data was achieved by measuring the impact force of the spray in a surface with a piezo-electric sensor [31]. The droplet velocity measurements have been performed under non-vaporising conditions inside a SF6 (a dense gas) atmosphere at room temperature (298K). The environmental density at low pressure (0.5MPa) was 40Kg/m^3, close to the reference case [36].

Temporal evolution of the axial velocity at 25mm of the virtual nozzle has been used to justify the beginning for the statistical measurements. In Fig. 3 the criteria of a constant spray angle was used to set the radial position of the probes. Thus the first probe in the isodense calculation is located at the edge of the spray and the last at 4.25mm from the edge. Since no significant velocity variation was detected by the most far-off probe, its measurements do not appear. It is also shown the velocity value imposed in the center of the inlet boundary condition (4.073mm from the virtual nozzle under the isodense conditions).

Differences in both the frequency content and the width of the velocity signals in the inlet boundary condition and the axis velocity at 25mm show a lack of precision of the spray fields simulated at the inlet boundary condition Its effect in LES in terms of the classical parameters to characterize the spray is decisive as shown in Fig. 4.

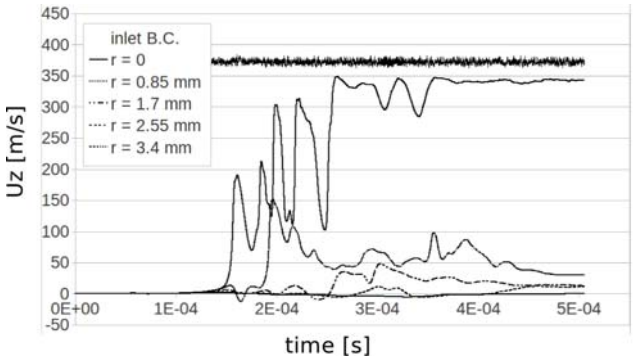

Figure 3. Measurements of radial probes (x=25mm)

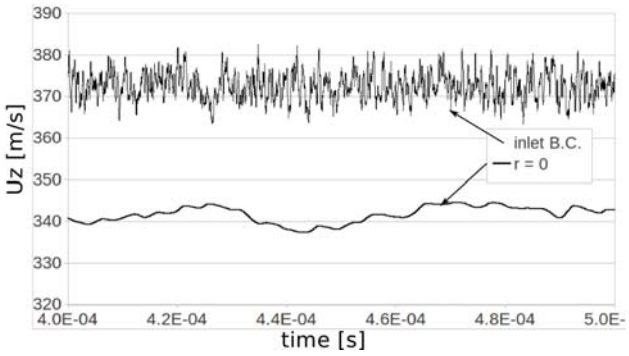

Figure 4. Measurements of axys velocity

The maximum axial distance for a 1% fuel concentration is the criteria used to define the penetration. Notice that this distance is located at the edge of the spray for theoretical and RANS calculations but not necessarily for LES simulations as shown in Fig. 5 (solid red line). RANS and LES (E-E) calculations correspond to isodense gas jets cases detailed in previous sections. A description of the Lagrangian-Eulerian approach will be done in future works when comparing RANS with LES Lagrangian-Eulerian calculations. This approach is outside of the scope of the present paper and has been shown as a reference of a good experimental estimation to compare with.

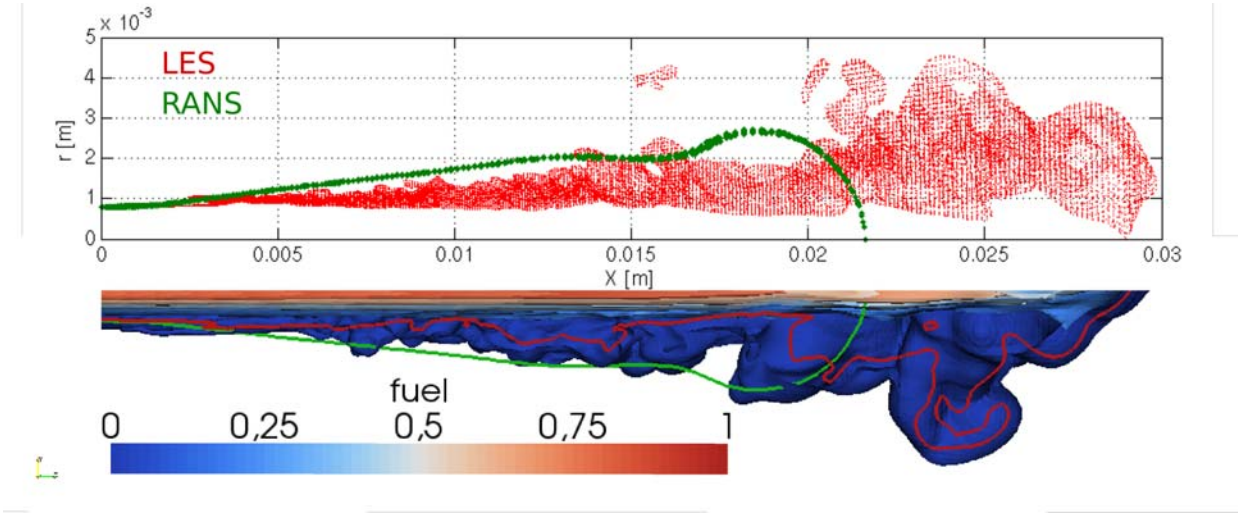

Figure 5. Comparison between RANS and LES concentration iso-surfaces t=(0.3ms). Lower part: longitudinal clip of fuel concentration contours, Upper part: Radial coordinates of stoichiometric iso-surfaces

The over prediction of both the RANS and LES Eulerian-Eulerian penetration is highly affected by the different injection mass flow rate shape. The L-E injection follows the experimental progressive evolution while the E-E injection is a constant value, simplified in this way to avoid disguising the first stages of the jet with this variable.

The over prediction of both the RANS and LES Eulerian-Eulerian penetration at is also affected by the fact that spray is more effective in transferring injection momentum to the ambient than the gas jet [37]. In the L-E approach the Lagrangian term carries the 45% of the momentum at 8deq of the nozzle.

Furthermore, in this initial part of the spray the local density is far from the assumption of constant density of the gas jets. Therefore the isodense hypothesis that allows to compare the gas jet with the Diesel spray is so restrictive from the actual boundary condition placed at 8deq. The assumption is acceptable beyond the developing region (x/deq > 30) where differences in axis velocity under turbulent gas jet theory are less than 3%.

Moreover, for the LES calculation, the first 5mm can be seen as a length required developing turbulence Fig. 5. Thus, the first assumption of a 10% of velocity fluctuation at the inlet boundary condition is not a good enough turbulent initialization of the flow. Given that the inlet is placed at the end of a not well-known zone, authors think a more realistic turbulent conditions can be achieved by applying measured or more accurate calculated profiles of velocity variation [38], [39]. The Fig. 5 shows iso-surfaces of fuel concentration for the LES simulation at 0.3ms. The red line and the green line mark the stoichiometric iso-surface for LES and RANS (E-E) simulations respectively. These areas have a relevant importance in combustion processes. The upper part of the figure plots the radial distance of these surfaces where detached surfaces far from the jet can be found.

A comparison with the Gaussian radial profiles is shown in Fig. 6 and Fig. 7. In both the axial velocity has been normalized with the axis velocity. In Fig. 6 the radial distance is normalized with the jet's half-width as defined by Pope [1] where in Fig. 7 is normalized with the axial distance. A spatial average at 25mm of the nozzle of the axial velocity (t = 0.5ms) shows a good agreement with the theoretical Gaussian profile from the edge to more than the half of the jet radius (up to 30% of the axis speed) Fig. 6. Differences in simulated profiles at 20 and 25 mm in Fig. 7 can be affected by the amount of statistics for each location (around 0.05ms less data at 25mm). Experimental data is close to LES simulated profile near the edge of the spray but moves to the Gaussian one as r increases.

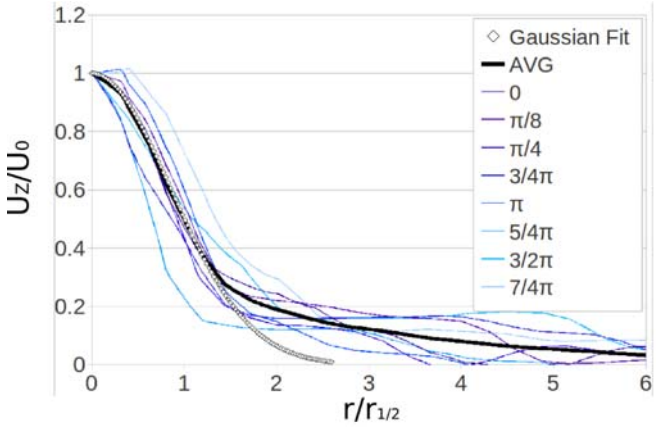

Figure 6. Radial velocity profiles (t=0.5ms). Spatial average of eight different angles

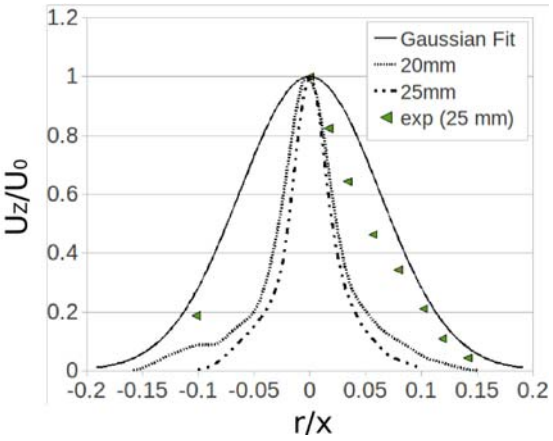

Figure 7. Radial velocity profiles (t=0.5ms). Time-averaged.

V. CONCLUSIONS

Using the OpenFOAM code, the authors have performed a completed simulation of diesel spray in LES. A comparison between the propose method and trusted (E-E) RANS sprays simulations has been performed, obtaining a very good agreement. Configuration and turbulent boundary conditions election have been justified and validated. Internal structure of the spray has been deeply studied, showing some characteristics of the spray. LES results have been also validated against experimental measurements of the velocity field. Some specific needs are presented in our paper as challenges to overcome. LES modelling can become the practical tool in both industry and academic in the design process of combustion system. The future research is now focusing on identifying the important parameters that affect the model and on improving the stability and accuracy of algorithms within OpenFOAM code. By so doing, the better spray simulation will be performed and a reliable tool will be used in modelling the spray simulation in the near future.

ACKNOWLEDGMENT

This research has been funded by the Spanish Government in the frame of the Project "Métodos LES para la simulación de chorros multifásicos", Ref.ENE2010-18542. The authors also acknowledge the financial support of the Universidad Politécnica de Valencia under the contract Reference PAID-2759 and the Generalitat Valenciana, under the contract GV/2010/039. We are also grateful to Dr. Franciso Javier Salvador, and Dr. José Manuel Pastor for providing experimental data and fruitful advices. In addition, we gratefully acknowledge helpful discussions with many researchers in CMT-Motóres Térmicos, specially Ms Palma González and Ms Mariany Chávez.

REFERENCES

[1] J Jiménez, Journal of Turbulence, J. turbul Vol. 4 (2003) Article Number: 022.

[2] Hoyas S., Jiménez J. Scalling of the velocity fluctuations in turbulent channels up to Re_tau=2000. Phys. Fluids, Vol. 18 (2006), Article Number: 011702

[3] S.B. Pope, Turbulent Flows, Cambridge University Press, 2000. 771 pp.

[4] J.J. Riley, Review of large-eddy simulation of non-premixed turbulent combustion, J Fluids Eng 128 (2006), pp. 209-215.

[5] H. Pitsch, Large-Eddy Simulation of Turbulent Combustion, Annual Review of Fluid Mechanics, Vol. 38, No. 1, 2006, pp. 453-482.

[6] J.M. Desantes, R. Payri, F.J. Salvador, J. de la Morena, Influence of cavitation phenomena on primary break-up and spray behaviour at stationary conditions. Fuel 89(10), pp.3033-3041.

[7] R. Payri, F.J. Salvador, J. Gimeno, J. de la Morena, Effects of nozzle geometry on the direct injection diesel engine combustion process Appl. Therm. Eng. 29 (2009) pp.2051-2060.

[8] F. Payri, X. Margot, S. Patouna, F. Ravet, M. Funk, A CFD Study of the Effect of the Needle Movement on the Cavitation Pattern of Diesel Injectors, Proceedings ICE2009 SAE Naples Section 2009-24-0025.

[9] X. Margot, S. Hoyas, P. Fajardo, S. Patouna, A moving mesh generation strategy for solving an injector internal flow problem, Mathematical and Computer Modelling (2010) 52 pp.1143-1150.

[10] R. Payri, B. Tormos, J. Gimeno, G. Bracho, The potential of Large Eddy Simulation (LES) code for the modeling of flow in diesel injectors, Mathematical and Computer Modelling, Volume 52, Issues 7-8, (2010), Pages 1151-1160.

[11] J.V. Pastor, J.J. López, J.M. García, J.M. Pastor, A 1Dmodel for the description of mixing-controlled inert diesel sprays. Fuel 87(08), pp.2871-2885.

[12] Fevrier P, Simonin O, Squires KD, Partitioning of particle velocities in gas-solid turbulent flows into a continuous field and a spatially uncorrelated random distribution: theoretical formalism and numerical study. J. Fluid Mech.Vol 533,(2005) pp. 1-46

[13] B. Befrui, G. Corbinelli, D. Robart, W. Reckers, LES simulation of the internal flow and near-field spray structure of an outward-opening gdi injector and comparison with imaging data. SAE paper 2008-01-0137; (2008), pp. 163-177.

[14] N. Bharadwaj, C.J. Rutland, A Large-Eddy Simulation study of sub-grid two-phase interaction in particle-laden flows and diesel engine sprays. Atomization and Spray (2010) 20(8), pp. 673-695.

[15] A. Deportes, M. Zellat, G. Desoutter, Y. Liang, F. Ravet, Application of the Eulerian-Lagrangian Spray Atomization (ELSA) Model for the Diesel Injection Simulation. THIESEL (2010)

[16] J. Chesnel, J. Réveillon, T. Ménard, A. Berlemont, F.X. Demoulin, Large Eddy Simulation of liquid atomization: From the resolved scales to subgrid spray. International Conference on Multiphase Flow (ICMF) (2010)

[17] J.S. Smagorinsky, General circulation experiments with the primitive equations. I. The basic experiment, Mon. Weather Rev. 91 (1963), pp. 99–164.

[18] B.E. Launder, D.B. Spalding, The numerical computation of turbulent flows, Computer Methods in Applied Mechanics and Engineering, Volume 3, Issue 2, March 1974, Pages 269-289.

[19] A. Scotti, C. Meneveau, D.K. Lilly (1993), Generalized Smagorinsky model for anisotropic grids. Phys. Fluids A 5, pp. 2306-2308.

[20] K. Horiuti, A proper velocity scale for modelling subgrid-scale eddy viscosities in large eddy simulation, Physics of Fluids (1993), 5, 146-157.

[21] A. Yakhot, S. Orszag, V. Yakhot, M. Israeli, Renormalization group formulation of large-eddy simulations, J. Sci. Comput. (USA), 4, 2, pp.139-58, (1989).

[22] U. Piomelli, J. Liu, Large-eddy simulation of rotating channel flows using a localized dynamic model Phys. Fluids 7 (4) (1995) 839-848.

[23] M. Germano, Turbulence: the filtering approach, J. Fluid Mech. 238 (1992) 325-336.

[24] W.P. Jones, S. Lyra, A.J. Marquis, Large Eddy Simulation of evaporating kerosene and acetone sprays, International Journal of Heat and Mass Transfer, Volume 53, Issues 11-12, May (2010), Pages 2491-2505.

[25] V. Vuorinen, LES of Certain Droplet Size Effects in Fuel Sprays, PhD Thesis, the Aalto University School of Science and Technology, (2010).

[26] I. E. Barton, Comparison of simple- and piso-type algorithms for transient flows. International Journal for Numerical Methods in Fluids, (1998).

[27] F. Peng-Krrholm, Numerical modelling of diesel spray injection, turbulence and combustion, Ph.D. Thesis, Chalmers Uni. of Technology, (2008).

[28] G.M. Faeth, Mixing, transport and combustion in sprays. Prog. Energy Combust. Sci (1987), 13, pp.293-345.

[29] G.M. Faeth, Spray combustion phenomena. 26th International Symposium on Combustion (1996), pp.1596-1612.

[30] J.M. Desantes, R. Payri, F.J. Salvador, J. Gimeno, Measurements of spray momentum for the study of cavitation in diesel injection nozzles. SAE Paper 2003-01-0703; (2003).

[31] R. Payri, J.M. García-Oliver, F.J. Salvador and J. Gimeno, Using spray momentum flux measurements to understand the influence of Diesel nozzle geometry on spray characteristics, Fuel 84 (2005), pp. 551–561.

[32] D. Correas, Theoretical and experimental study of isothermal Diesel free sprays (In Spanish), PhD Thesis, Universidad Politcénica de Valencia;(1998).

[33] J.M. Desantes, R. Payri, J.M. García-Oliver, F.J. Salvador, A contribution to the understanding of isothermal diesel spray dynamics, Fuel 86 (2007), pp. 1093–1101.

[34] D. Jaime Gimeno. García, Desarrollo y aplicación de la medida del flujo de cantidad de movimiento de un chorro diesel, PhD thesis, Universidad Politécnica de Valencia, (2008).

[35] J. Abraham, What is Adequate Resolution in the Numerical Computations of Transient Jets? SAE 970051 (1997) pp. 81-95.

[36] L. Araneo, V. Soare, R. Payri, J. Shakal, Setting up PDPA system for measurement in a diesel spray, Journal of Physics, 45, (2006), pp. 85-93.

[37] J. Abraham, V. Magi, J. Macinnes, F.V. Bracco, Gas versus Spray Injection: Which Mixes Faster? SAE paper 940895; (1994), pp. 163-177.

[38] H.J. Hussein, Capp, W.K. George, Velocity measurements in a high-Reynolds-number, momentum-conserving, axisymetric, turbulent jet, J Fluid Mech (1994). 258, 31-75.

[39] Levy Y, Lockwood FC, Combust. Flame 40, 333 (1981).

2.2.3. Evaluation of the Eulerian-Lagrangian Spray Atomization (ELSA) in spray simulations. International Conference on Mechanical, Automotive and Aerospace Engineering 2011

Evaluation of the Eulerian-Lagrangian Spray Atomization (ELSA) in spray simulations

Sergio Hoyas, J.M. Pastor, Dung Khuong-Anh, Juan Manuel Mompó-Laborda
CMT – Motores Térmicos,
Universidad Politécnica de Valencia
Camino de Vera S/N, 46022 Valencia, Spain
E-mail: [serhocal, jopasen, ankh2, juamomla] @mot.upv.es

Frederic Ravet
Renault
1 avenue du golf 78288, Guyancourt, France
E-mail: frederic.ravet@renault.com

***Abstract*: There are many approaches have been developing to simulate the spray structure especially in modeling fuel sprays, i.e. Eulerian, Lagrangian, Lagrangian-Eulerian, Eulerian-Eulerian and Eulerian-Lagrangian approaches. The present study uses an Eulerian-Lagrangian Spray Atomization (ELSA) method which is an integrated model for capturing the whole spray evolution starting directly from injector nozzle still the end.**

Our goal in this study is to evaluate the ELSA model which is implementing into the commercial software Star-CD, for numerically modeling of Diesel sprays. There are two key studies in these validations, at first we examine the turbulent parameters through the three different scenarios and then we study mesh dependency. The results show in form of liquid penetrations, droplet velocity, and axial velocity profiles. All numerical results are compared with experimental data from our research institute, CMT-Motores Térmicos.

Keywords: spray penetration, droplet, injection, ELSA, atomization, turbulence.

I. INTRODUCTION

Everybody knows the auto world has shifted. New efficiency standards are requiring a fleet-wide fuel economy. Within this purpose, car manufacturers have paid more attention to enhance the improvement of R&D resources in automotive industry. There is a variety of research fields included Noise, Vibration and Harshness (NVH), simulation of vehicle performance, dynamics, safety, durability, etc. Even though there have been big advances over the last decade in the efficiency of the diesel engine, automakers insist there is still much to improve about the humble combustion engines, especially in the Diesel injection simulation.

In the 1980s, Lefebvre (1989) described the complexity of spray structure and its related theories. Fuel injection process and subsequent fuel-air mixing formation play a major role on combustion and pollutant emissions on internal combustion engines. As the development of a spray is dependent on many parameters and coefficients, simulation studies try to assess the impact of complex phenomena. It is characterized by orifice diameter, nozzle shape, pressure, density, temperature, physical chemistry components, contraction coefficient, discharge coefficient, vaporization, etc.

Thus an accurate prediction of these processes is required in order to perform reliable engine combustion and pollutants formation simulations.. Fuel spray injection is one of the most important phenomena in internal combustion engine which is still under development and it has been attracted a high concerns from both academic and scientific researchers. Diesel fuel injection and spray formation modeling is still a challenging task due to the complex interrelated phenomena taking place. Still now some of them such as primary atomization or nozzle cavitation are not fully understood.

Even though many models are mentioned in the abstract but each of them has both advantages and disadvantages in the various regions of spray consisting of the dense zone and the downstream dilute zone or atomization.

In order to enhance CFD spray simulations, the ELSA model has been developing in recent years and integrated into the Star-CD CFD code by Renault. This model is based in an Eulerian approach for the description of the dense spray region, where standard Discrete Droplet Model (DDM) method is not suited for. Hence, the ELSA is an integrated model for capturing the whole spray evolution. Within the diluted spray region the ELSA model could switch to the traditional Lagrangian description of the liquid phase, taking advantage from well established previously developed submodels.

The theoretical aspects of the model have been developing in the last decade, however we need to make it real and stable for engineering applications. The ELSA model has been implementing into Star-CD code. Through the toughest structuring period, we continued to validate and evaluate heavily to ensure the prompt correction in preliminary stage.

Targeting this general objective, it is included to evaluate and validate the different parameters, improve the simply model for computation and identify the well-described phenomena involved in Diesel spray formation and development from nozzle outflow to complete fuel vaporization. As a result, we form the set of correct models for producing a diesel engine simulation in real-life operation. This work is part of a more ambitious project, with the general objective of developing and validating a new spray model tool for practical applications on CFD engine calculations.

Renault and VECOM (Vehicle Concept Modeling) Marie Curie Initial Training Network (ITN)

II. THE EULERIAN – LANGRANGIAN SPRAY ATOMIZATION (ELSA) MODEL

In this section the Eulerian-Lagrangian spray atomization approach is described. The goal of the ELSA model is to realistically describe the dense zone of the spray. The ELSA model has been developed from 2001 ignited by Vallet et al. and during the time has been under development [Beau (2006); Lebas (2007); De Lucas M. (2007); Ning W. (2007); Blokkeel et al. (2003)].

The ELSA model is used for situations when it assumes the following hypotheses:

- In the situation of high-speed turbulent sprays where Reynolds and Weber numbers are high.
- And it exams a turbulent mixing process between the liquid and surrounding gaseous phases as a single-phase turbulent fluid flow with mean properties.

Basically, we can divide ELSA approach into three broad zones:

- **Eulerian mixture zone**: in the first part, single phase CFD code to describe the liquid/gas mixture in the dense part of the spray. In this region, liquid and gas phase are considered as a unique mixture flow. The classical Eulerian model is used to solve this single phase flow.

- **Transition zone**: switch from Eulerian to Lagrangian calculation, and

- **Lagrangian zone**: classical Lagrangian tracking for droplets in the diluted spray zone

Once the difference of velocity of a liquid jet with respect to the surrounding gas is very strong, atomization of the jet occurs, and droplets are formed (atomization regime).

In two papers of A. Desportes et al. (2010), the author had summarized the key formulae as following, and we include here for completeness. Mean liquid mass fraction $\tilde{Y}_l$

$$\tilde{Y} = \frac{\overline{\rho Y}}{\overline{\rho}} \tag{1}$$

where $\overline{Y}$ is the mean liquid volume fraction,

The mean properties of this effective fluid or mixture (like mean density $\overline{\rho}$ or Favre averaged mean velocity $\tilde{U}_i$) are defined with the following relationships:

The state equation is obtained as

$$\overline{\rho} = \rho_l \overline{Y} + \rho_g \left(1 - \overline{Y}\right) \tag{2}$$

ρ_l is the liquid density and ρ_g is the gas density, which is expressed in terms of $\tilde{Y}_l$ as

$$\frac{1}{\overline{\rho}} = \frac{\tilde{Y}_l}{\rho_l} + \frac{1-\tilde{Y}_l}{\rho_g} \tag{3}$$

$$\tilde{U}_i = \tilde{Y}_l U_{l,i} + \left(1-\tilde{Y}_l\right) U_{g,i} \tag{4}$$

and the equation of state

$$\overline{P} = \frac{\left(1-\tilde{Y}_l\right)\overline{\rho} R_g T_g}{1-\tilde{Y}_l \cdot \overline{\rho}/\rho_l} \tag{5}$$

In the equation of state (5), we take into account the volume occupied by liquid.

Then, the classical transport equations are solved for these mean variables:

$$\frac{\partial \overline{\rho}}{\partial t} + \frac{\partial \overline{\rho} \tilde{U}_j}{\partial x_j} = S_{EL}^{\tilde{Y}_l} \tag{6}$$

$$\frac{\partial \overline{\rho} \tilde{U}_i}{\partial t} + \frac{\partial \overline{\rho} \tilde{U}_j \tilde{U}_i}{\partial x_j} = -\frac{\partial \overline{P}}{\partial x_i} - \frac{\partial \overline{\rho u_i'' u_j''}}{\partial x_j} + S_{EL}^{\tilde{U}_i} \tag{7}$$

It should be noticed that the last equation does not contain any momentum exchange terms between liquid and gaseous phases. In order to model the liquid dispersion, this set of equations is completed by the transport equation for the liquid mass fraction:

$$\frac{\partial \overline{\rho} \tilde{Y}_l}{\partial t} + \frac{\partial \overline{\rho} \tilde{U}_j \tilde{Y}_l}{\partial x_j} = -\frac{\partial \overline{\rho u_j'' y''}}{\partial x_j} + S_{EL}^{\tilde{Y}_l} \tag{8}$$

Where $S_{EL}^{\tilde{Y}_l}$ and $S_{EL}^{\tilde{U}_i}$ are the sink or source terms due to the droplet generation or absorption when the transition from Eulerian to Lagrangian formulation is activated.

In Eqs. (5) and (6), there are 2 turbulent fluxes to be closed. The turbulent stress tensor is modeled with a classical $k-\varepsilon$ model closure. Concerning the liquid turbulent diffusion flux, the gradient law approximation is applied:

$$\overline{\rho u_j'' y''} = -\overline{\rho} \frac{\nu_t}{Sc_t} \frac{\partial \tilde{Y}_l}{\partial x_j} \tag{9}$$

Liquid/gas interface density

In order to characterize the size of liquid fragments resulted from the jet atomization, the notion of liquid surface

density is introduced. This variable is defined as the quantity of liquid/gas interface per unit of volume $\overline{\Sigma}\left(m^{-1}\right)$. Using this new variable, we can obtain the Sauter Mean Diameter of droplet [Lebas R. (2005)]:

$$D_{32} = \frac{6\overline{\rho}\widetilde{Y}_l}{\rho_l \overline{\Sigma}}$$
$$n = \frac{\rho_l^2 \overline{\Sigma}^3}{36\pi \overline{\rho Y_l}^2} \qquad (10)$$

A transport equation for liquid surface density is postulated by analogy with the flame surface density.

$$\frac{\partial \overline{\rho}\widetilde{\Omega}}{\partial t} + \frac{\partial \overline{\rho}\widetilde{\Omega}\tilde{U}_j}{\partial x_j} = \frac{\partial}{\partial x_j}\left(\overline{\rho}\frac{v_t}{Sc_t}\frac{\partial \widetilde{\Omega}}{\partial x_j}\right) + S_{EL}^{\widetilde{\Omega}}$$
$$\overline{\rho}\cdot\left(\dot{\widetilde{\Omega}}_{init} + \dot{\widetilde{\Omega}}_{mean} + \dot{\widetilde{\Omega}}_{turb} + \dot{\widetilde{\Omega}}_{coll} + \dot{\widetilde{\Omega}}_{coal}\right) \qquad (11)$$

Here, Beau PA. (2005 & 2006) introduced the other notion of liquid/gas interface per unity of mass that is defined as $\widetilde{\Omega} = \overline{\Sigma}/\overline{\rho}$ (m^2/kg).

The production and destruction of liquid surface are accounted for with source terms detailed below. The first term source $\dot{\widetilde{\Omega}}_{init}$ in Eq. (8) permits to initialize the calculations since all other terms source are proportional to $\widetilde{\Omega}$:

$$\dot{\widetilde{\Omega}}_{init} = \begin{cases} 2\frac{v_t}{Sc_t}\frac{6\overline{\rho}}{\rho_l \rho_g L_t}\frac{\partial \widetilde{Y}_l}{\partial x_i}\frac{\partial \widetilde{Y}_l}{\partial x_i} if\, \widetilde{Y}_l\left(1-\widetilde{Y}_l\right) \le 0.001 \\ 2\frac{v_t}{Sc_t}\frac{\widetilde{\Omega}}{\left(1-\widetilde{Y}_l\right)\widetilde{Y}_l}\frac{\partial \widetilde{Y}_l}{\partial x_i}\frac{\partial \widetilde{Y}_l}{\partial x_i}, otherwise \end{cases} \qquad (12)$$

The second term in the right hand side stands for a general definition that was obtained by the phenomenological considerations for the spray formed of the droplets with a constant diameter. In the region closed to the injector $\widetilde{Y}_l \to 1$, the scale of the first liquid fragments is assumed to be proportional to the turbulent length scale, L_t.

The three next terms correspond to the production of liquid surface density due to the mean or turbulent stresses and due to the collisions:

$$\dot{\widetilde{\Omega}}_{mean} = \frac{\overline{\rho u_i'' u_j''}}{\overline{\rho}\tilde{k}}\frac{\partial \tilde{U}_i}{\partial x_j}\widetilde{\Omega} \qquad (13)$$

$$\dot{\widetilde{\Omega}}_{turb} = \frac{\widetilde{\Omega}}{\tau_{turb}} \quad \text{and} \quad \dot{\widetilde{\Omega}}_{coll} = \frac{\widetilde{\Omega}}{\tau_{coll}}$$

The last term in the right hand of Eq. (8) deals with destruction of surface density due to coalescence:

$$\dot{\widetilde{\Omega}}_{coal} = -\frac{1}{\tau_{coll}}\frac{\widetilde{\Omega}^2}{\widetilde{\Omega}_{crit}} \qquad (14)$$

with τ_{coll} and $\widetilde{\Omega}_{crit}$ are the characteristic time scale of collisions and the critical value of liquid/gas surface density.

I. EXPERIMENTS FOR COMPARISON

The obtained numerical results are compared with experimental data at CMT Motores Térmicos. Experimental results have been obtained from previously published data from the authors' research group R. Payri et al. (2008), and J. Gimeno (2008).

The injection velocity profile comes from measurements of mass and momentum fluxed performed in a pressurized test rig with nitrogen. The momentum flux measuring principle of this technique is explained in two references of R. Payri et al. (2005), and J. Gimeno et al. (2008), and consists of measuring the impact force of the spray in a surface with a piezo-electric sensor. As long as the whole cross-section of the spray impacts on the sensor, the measured force equals to the momentum flux at that cross section. If the measurement position is close to the nozzle exit, the time evolution of the impact force is equal to the nozzle (hole) momentum flux, $\dot{M}_o$.

II. GEOMETRY & BOUNDARY CONDITIONS

These cases have been simulated as axis-symmetric boundary-value problems. We study 2D axis-symmetric meshes (5 degree cylindrical segment along the axis). A 2D view, boundary conditions and coordinate system are shown in

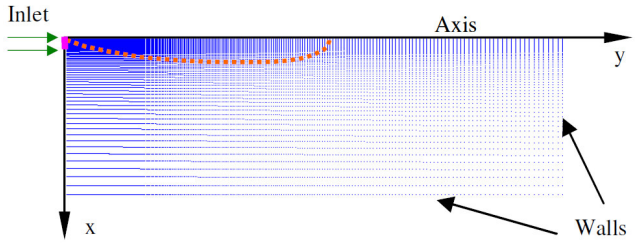

Figure 1. Boundary conditions.

Fig.1.

Within this work, we used a data as similar as CMT Diesel-type single-hole injector experiments for a diameter of 112 μm with variable velocity profile input at the injector as depicted in Fig. 2 and some key parameters in table I.

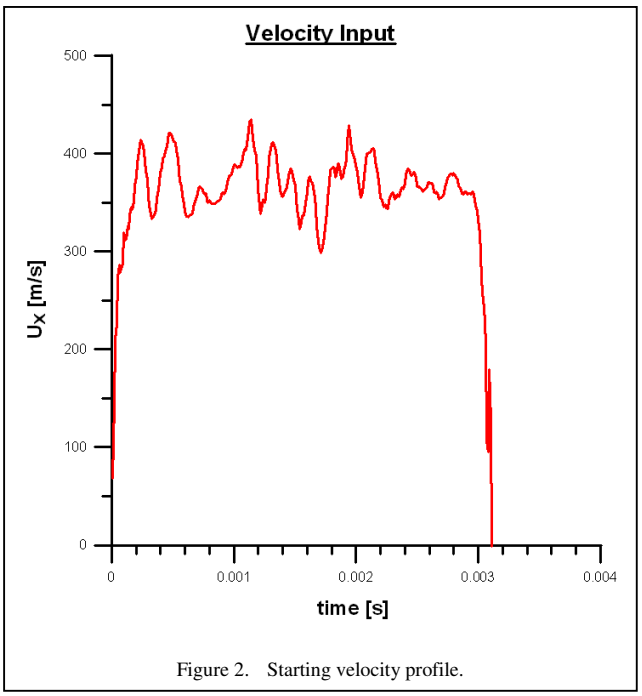

Figure 2. Starting velocity profile.

TABLE I. BASIS PARAMETERS

Ambient pressure	Injection pressure	Temperature	Fuel Density
3.53 MPa	80 MPa	307.58 K	822.10 kg/m^3

Generally, the requirement for mesh structure is especially at the nozzle where the mesh size has to be small enough to capture the spray structure and the small droplets at the injector and surroundings. Our current mesh structure is based on the following criteria:

$$\Delta x \sim 0.05 - 0.1 D_{inj} \Rightarrow \quad \Delta t \approx 10^{-8} \text{ s}$$

Hence, two different configurations with 10, and 20 cells at the nozzle are used. The computational domains with the size of 80 x 25 mm are shown in Fig. 3 according to the mesh structures in table II.

TABLE II. MESH STRUCTURES

No cells at the nozzle	No. axial cells	Axial ratio (First/Last ratio)	No. radial cells	Radial ratio (Last/First ratio)
10	**435**	72	**90**	0.006
10	218	72	45	0.006
20	250	143	50	0.003

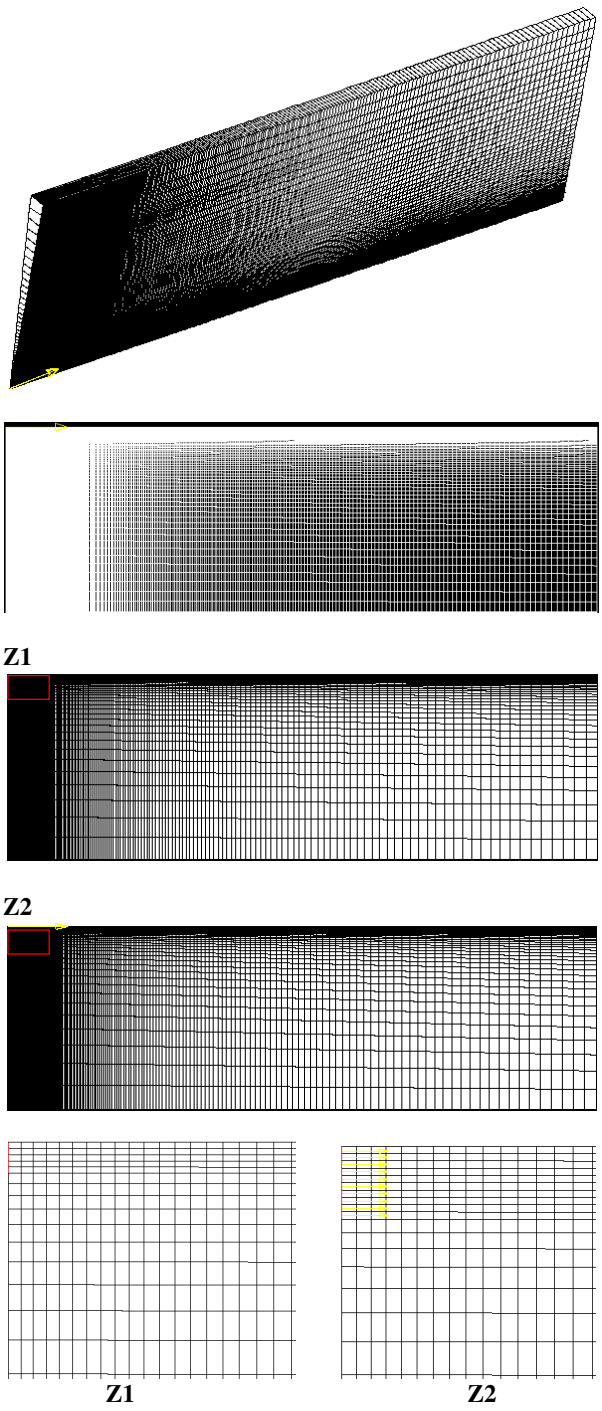

Figure 3. Geometry.

The first two graphs in Fig. 3 are for the ten cells with fine meshes in isometric and side views respectively, the third one is for ten cells with coarse mesh. The forth figure from downward position is for the case with 20 cells at the nozzle. The detailed views of two types of meshes are also showed in pairs.

We used the k-ε/High Reynolds Number turbulent model with the following constants in table 3 that are usually accepted in most of the spray calculation where C-ε1=1.44 is the standard value, and we also use the suggested value C-ε1=1.60 in order to improve predictions on round jets modeling, moreover we examine the behavior of the simulation with C-ε1=1.52. The turbulent Prandtl number has been set to 1 in order to produce similar solutions for the conservation equations of axial momentum, fuel mass and energy. We notice that the Prandtl (K.E.) in table III is another Prandtl constant which is only used for solving the k-ε equations.

TABLE III. TURBULENT PARAMETERS

	C-Mu	C-ε1	C-ε2	C-ε3	Prandtl (K.E.)	Prandtl (Eps)
Turb 1	0.09	**1.44**	1.92	1.44	1	1.219
Turb 2	0.09	**1.52**	1.92	1.44	1	1.219
Turb 3	0.09	**1.60**	1.92	1.44	1	1.219

Combining the above descriptions, we finalize six main cases in total:

TABLE IV. COMPUTATIONAL CASES

Case No.	Cells at nozzle	Turbulent constant	Vertices	Cells
Case 1	10	C = 1.60	78,916	39,150
Case 2	10	C = 1.44	19,929	9,810
Case 3		C = 1.52		
Case 4		C = 1.60		
Case 5	20	C = 1.44	25,351	12,500
Case 6		C = 1.60		

III. NUMERICAL RESULTS

Figure 4 shows the comparison of the liquid penetrations using different meshes vs. time. At first, the plot for only 20 cells at nozzle diameter with the experimental result is depicted on top. With the constant equally to 1.44, the numerical result prone to the right hand side of the experimental results meanwhile with the value of 1.60, the spray penetration tend to the other side of experimental results. This similar behavior remains for the comparison with 10 cells. For the second plot, the critical changes are observed between the three turbulent constants. In the last plot, we could see the dramatically change in the fine mesh case where the penetration curve move far way in comparison with the coarse mesh. Thus, the choice of this parameter must be considered for each numerical simulation.

As visual presentation in Fig. 5, it can be easily imagined the evolution of velocity profiles in various time steps of 0.025, 0.01, 0.5, 1, 1.5, 2 ms respectively, the structure of spray is represented for the number of cell size of 10 at the nozzle diameter and fine mesh case (case 1). It can be seen that

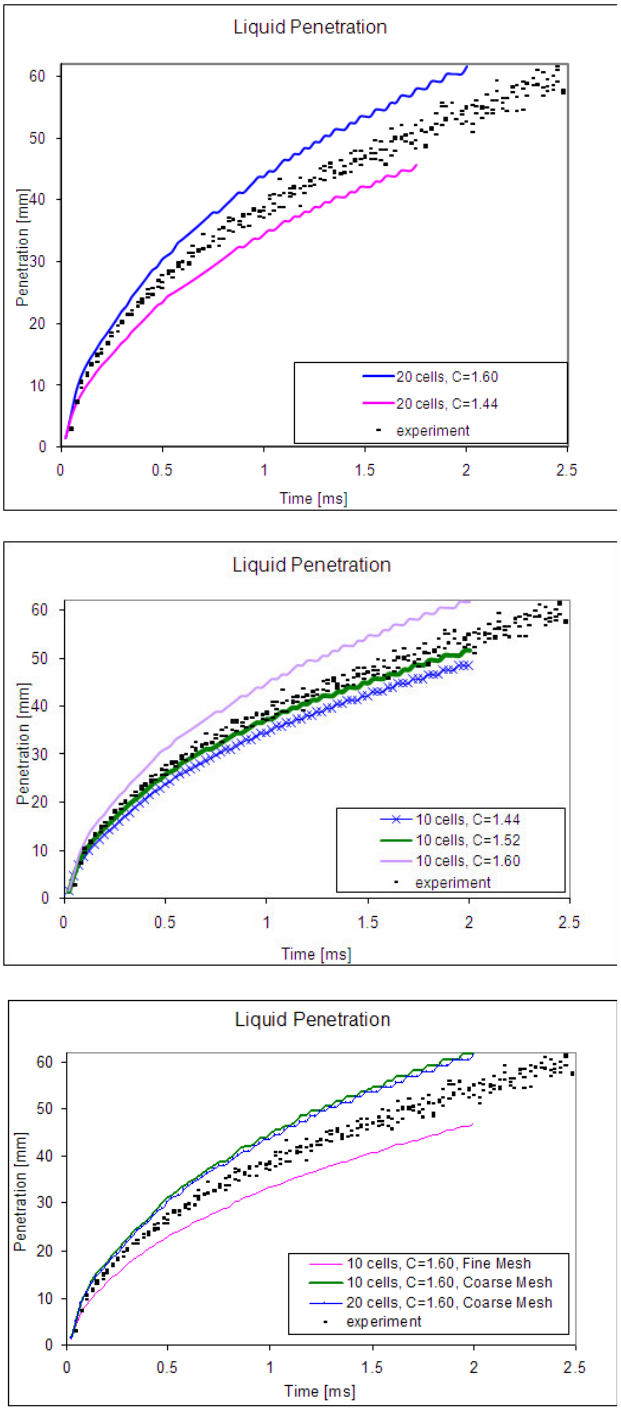

Figure 4. Liquid penetrations.

velocity magnitude is highest in the zone surrounding the nozzle and in the liquid core zone where the Eulerian approach is used and lowest in the droplet peak in the axial direction. The droplet figure describes the droplet formation is produced starting from the transition zone and continue to develop in the

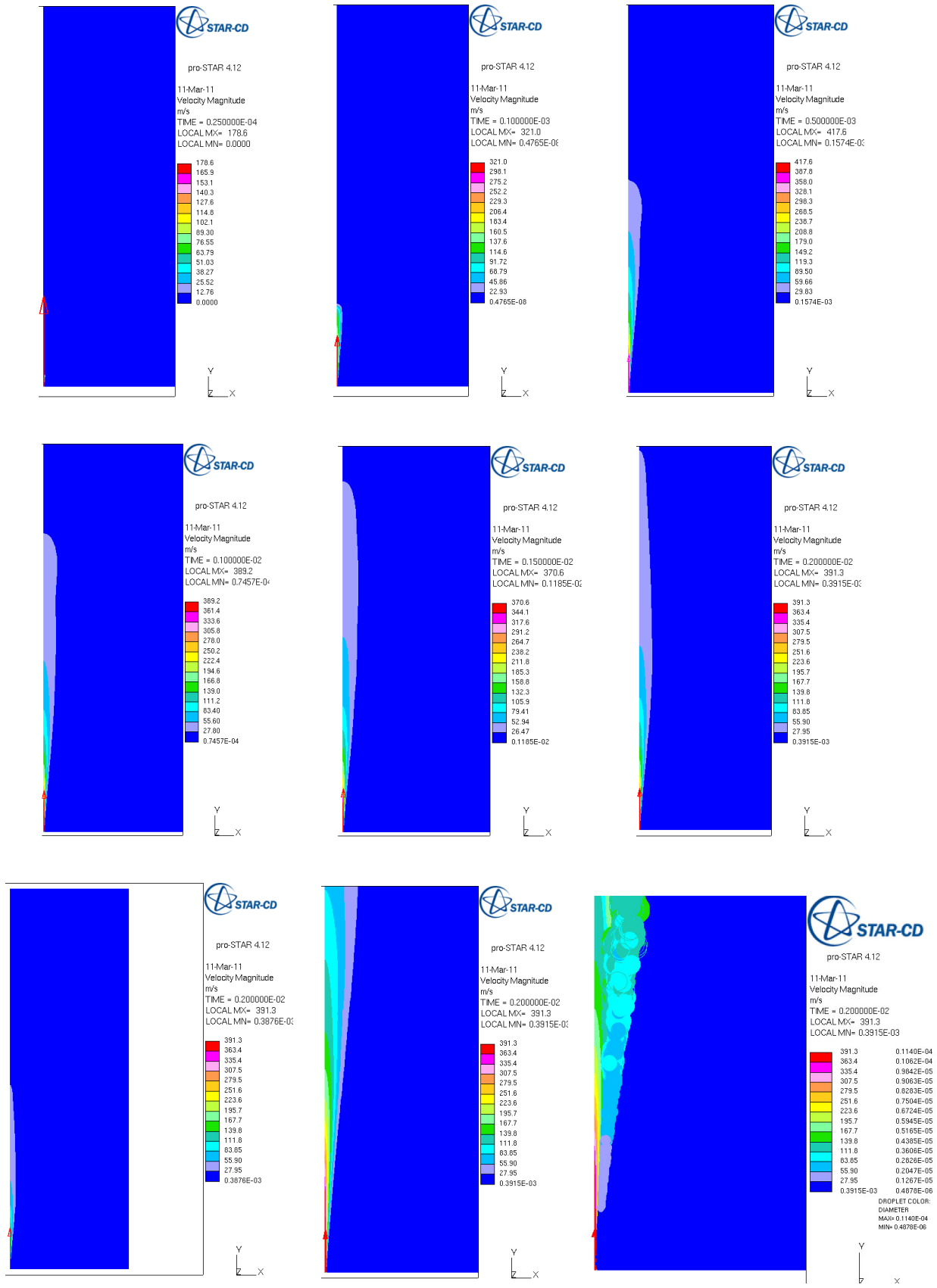

Figure 5. Spray structure and droplet formation

farther zone (Lagrangian zone) continuously. It is the combined plot where the contours profile represents for the velocity and the round circles show the droplet diameter but it shows in the same color scale. Here, droplet diameter is in mm and the velocity unit as m/s. Definitely, there is no droplet in the Eulerian mixture zone. It confirms our initial setting and formulae for ELSA model. Mean velocities and droplet velocities in different radial and axial position are shown in Fig. 5 and Fig. 6. Generally, the velocity profiles in the numerical calculation are in line with the experiments.

In Fig. 6, we plot velocity profiles in different sections with five sections at round number of distance equal to 25 30, 35, 40, and 50 mm respectively in order to compare with the available experiments from R. Payri et al. (2008). It can be seen that the velocity profiles decrease according to the penetration distance.

In Figure 7, the droplet velocity along axial direction and

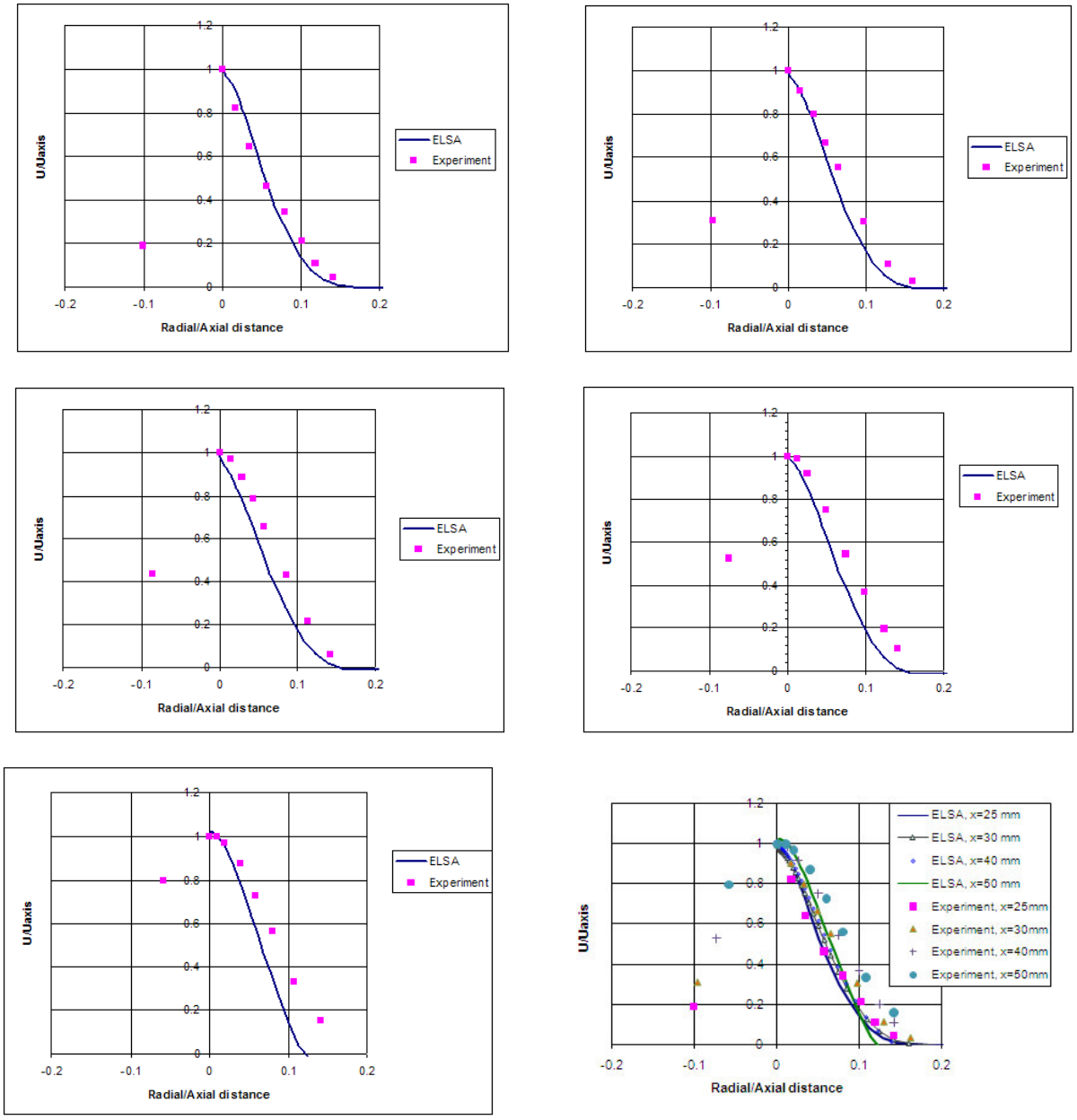

Figure 6. Velocity profiles of spray (10 cells, C-ε1=1.60).

total number of droplets are sketched. To bear in mind that we only take into account total droplets which contain within the closest cells from the axial line.

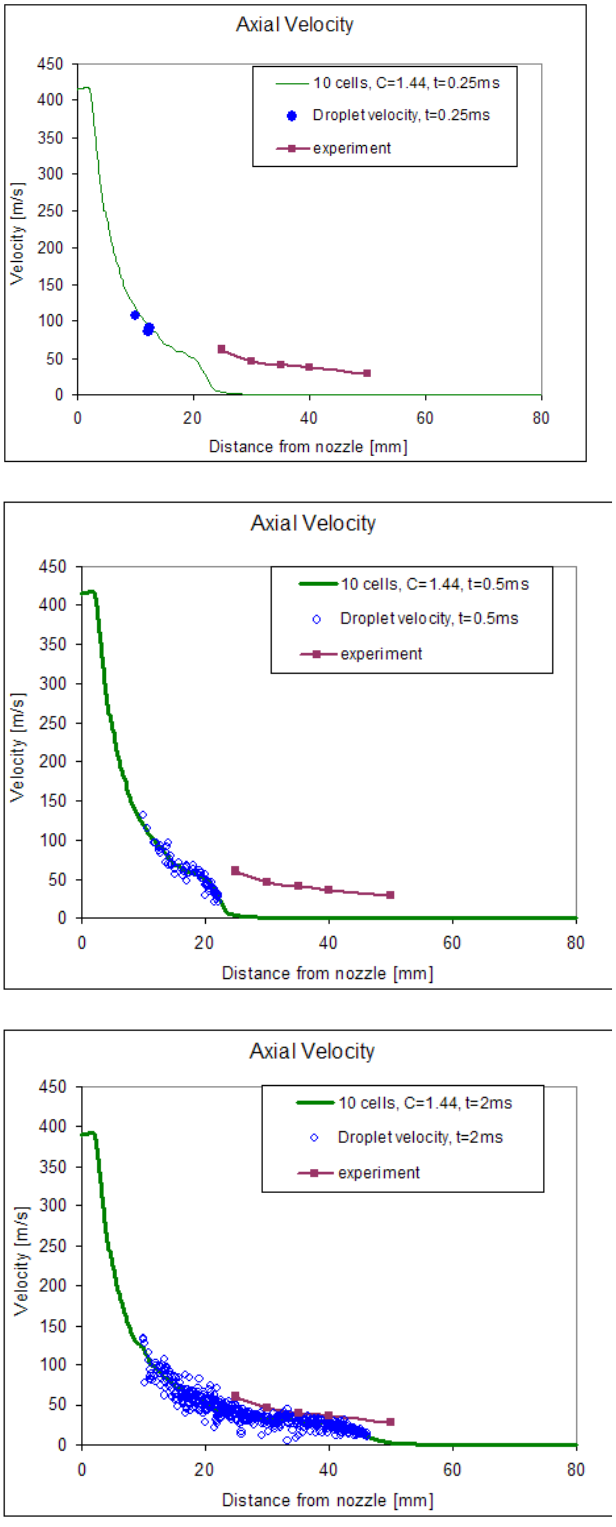

Figure 7. Droplet velocity profiles

We can see the number of droplets increase through each time steps and their velocity also change accordingly and long the mean velocity curve.

IV. CONCLUSIONS

In this report we brought out some key different amongst those computational models and typical plots for certain cases. For the rest of figures which resulted similar behavior, and don't add much value to the report aren't showed here. As stated in our target, we showed the relationships or discrepancy among key elements of penetration, velocity, turbulent parameters and different in position or number of time step and mesh effects.

In sum, mean velocity profile and droplet velocity is staying very close with the experiment index especially in the highest time step. Liquid penetration is totally depend on the mesh size, topology and of course turbulent model and parameters which we used for our simulation. Grid sensitivity is shown in our calculations, thus for 2-D RANS (Reynolds-averaged Navier–Stokes) simulations, we can use meshes as much fine as possible if time simulation and computing power allowed in order to get nearly grid independent results. We have to do more test and computations to know exactly which value should be best fit to each case.

The Diesel spray was performed with ELSA model produced a good accuracy even with the 2D axisymmetric meshes, the numerical results indicated the similar prediction in conjunction with the real experimental results conducted at CMT in 2008. Designers often focus on performance areas, thus our liquid sprays analysis and design using Computation Fluid Dynamic (CFD) simulations were performed on the Diesel spray and validated the ELSA model with the latest experimental results with almost the same configuration are very useful for them to refer to.

ACKNOWLEDGMENT

This work has been granted by Renault and VECOM (Vehicle Concept Modeling) - EU FP7 Marie Curie Initial Training Network (ITN) Grant Agreement 213543 (from October 1st, 2008 to September 30, 2012). The aim of the proposed training network is to provide dedicated research training in the emerging field of vehicle concept modeling for up-front pre-CAD functional performance engineering, bridging between industry and academia across Europe.

REFERENCES

[1] Araneo L, Soare V, Payri R, Shakal J, "Setting up a PDPA system for measurements in diesel spray", J Phys: Conf Ser 2006; 45:85-93, 2006.

[2] A. Desportes, M. Zellat, G. Desoutter, D. Abouri, Y. Liang, F. Ravet, "Validation and Application of the Eulerian-Lagrangian spray atomization (ELSA) model for the Diesel injection simulation", SAE, 2010.

[3] A. Desportes, M. Zellat, G. Desoutter, D. Abouri, Y. Liang, F. Ravet, "Application of the Eulerian-Lagrangian spray atomization (ELSA) model for the Diesel injection simulation",THIESEL 2010 conference.

[4] Beau PA, "Modelisation de l'atomisation d'un jet liquide – Application aux sprays diesel", Ph.D. Thesis, University of Rouen, 2006.

[5] Blokkeel G, Barbeau B and Borghi R, "A 3D Eulerian model to improve the primary breakup of atomizing jet", SAE Technical Paper 2003-01-0005, 2003.

[6] D. Jaime Gimeno García, "Desarrollo y aplicación de la medida del flujo de cantidad de movimiento de un chorro Diesel", PhD thesis, Universidad Politécnica de Valencia, 2008.

[7] De Lucas M., "Contribution a la modelisation de la pulverisation d'un liquide phytosanitaire en vue de reduire les pollutions", Ph.D. Thesis, University of Aix-Marseille II, 2007.

[8] G. M. Faeth, L. -P. Hsiang, P. -K. Wu, "Structure and breakup properties of sprays", International Journal of Multiphase Flow, Volume 21, Supplement 1, December 1995, Pages 99-127.

[9] Lebas R., Blokkeel, G., Beau, P.-A., Demoulin, F. –X., "Coupling Vaporization model with the Eulerian-Lagrangian Spray Atomization (ELSA) model in Diesel Engine Conditions", SAE100, 2005-01-0213, 2005.

[10] Lebas R., "Modelisation Eulerienne de l'Atomisaton haute pression – Influences sur la vaporisation et la combustion induite", Ph.D. Thesis, University of Rouen, 2007.

[11] Lefebvre, A.H., "Atomization and sprays", Taylor and Francis, 1989.

[12] Naber JD, Siebers DL, "Effects of gas density and vaporization on penetration and dispersion of Diesel sprays", SAE Technical Paper 960034, 1996.

[13] Ning W, Reitz RD, Lippert AM and Diwakar R, "Development of a nextgeneration spray and atomization model using an Eulerian-Lagrangian methodology", 17th Int. Multidimensional Engine Modeling User's Group Meeting, Detroit, MI, 2007.

[14] R. Payri, J.M. García, F.J. Salvador and J. Gimeno, "Using spray momentum flux measurements to understand the influence of Diesel nozzle geometry on spray characteristics", Fuel 84, pp. 551-561. 2005.

[15] Vallet A, Burluka AA and Borghi R., "Development of a Eulerian model for the atomization of a liquid jet", Atomization and sprays, vol. 11, pp. 619-642, 2001.

[16] R. Payri, B. Tormos, F.J. Salvador a, L. Araneo, "Spray droplet velocity characterization for convergent nozzles with three different diameters", Fuel 87, pp 3176-3182, 2008.

DEFINITIONS/ABBREVIATIONS

CAD	Computer-aided Design
CMT	CMT Motores Térmicos
CFD	Computation Fluid Dynamic
DDM	Discrete Droplet Model
ELSA	Eulerian-Lagrangian Spray Atomization
ITN	Initial Training Network
PDPA	Phase Doppler Particle Analyzer
RANS	Reynolds-averaged Navier–Stokes
SMD	Sauter Mean Diameter
VECOM	Vehicle Concept Modeling

2.2.4. Application and evaluation of the Eulerian-Lagrangian Spray Atomization (ELSA) model on CFD Diesel spray simulations. SAE Paper 2011-37-0029

SAE International

Application and Evaluation of the Eulerian-Lagrangian Spray Atomization (ELSA) Model on CFD Diesel Spray Simulations

2011-37-0029
Published
06/09/2011

Sergio Hoyas, Jose M. Pastor, Dung Khuong-Anh and Juan Manuel Mompó-Laborda
CMT, Universidad Politécnica de Valencia

Frederic Ravet
Renault

doi:10.4271/2011-37-0029

ABSTRACT

During the last fifteen years Computational Fluid Dynamics (CFD) has become one of the most important tools to both understand and improve the Diesel spray development in Internal Combustion Engine (ICE). Most of the approaches and models used pure Eulerian or Lagrangian descriptions to simulate the spray behavior. However, each one of them has both advantages and disadvantages in different regions of the spray, it can be the dense zone or the downstream dilute zone. One of the most promising techniques, which has been in development since ten years ago, is the Eulerian-Lagrangian Spray Atomization (ELSA) model. This is an integrated model for capturing the whole spray evolution, including primary break-up and secondary atomization.

In this paper, the ELSA numerical modeling of Diesel sprays implementation in Star-CD (2010) is studied, and simulated in comparison with the Diesel spray which has been experimentally studied in our institute, CMT-Motores Térmicos. Since many of the most important characteristics of the spray development, as the penetration or the axial velocity, can be captured using 2D simulations, in this preliminary validation of ELSA model only two-dimensional simulations have been performed. Moreover, the main objective of the paper is to: firstly, obtain mesh independency for further analysis and secondly, improve the classic k - ε RANS model for ELSA model. Apart from this, several characteristics of the spray as can be the droplet formation of the liquid penetration are also showed.

INTRODUCTION

Fuel injection process and subsequent fuel-air mixing formation play a major role on combustion and pollutant emissions in internal combustion engines. It is one of the most important phenomena in internal combustion engines which is still under development and with high concerns from both academic and scientific researchers, due to the complex interrelated phenomena taking place (See for instance Lefebvre, 1989 [17]). Still now, some of them, such as primary atomization or nozzle cavitation, are not fully understood.

In order to enhance Computational Fluid Dynamics (CFD) spray simulations, the ELSA model (Vallet et al., 2001 [24]) has been developed in recent years. It has been integrated very recently into the Star-CD CFD code by RSA. ELSA model is based on an Eulerian approach for the description of the dense spray region, where standard Discrete Droplet Model (DDM) method is not able to describe the flow. Within the diluted spray region, the ELSA model could switch to the traditional Lagrangian description of the liquid phase, taking advantage from well established and previously developed submodels.

The goal of the ELSA model is to realistically describe the dense zone of the spray and the spray atomization. Since the seminal work of Vallet et al. [24] it has been under development by several authors, including Blokkeel et al., 2003 [6], Beau, 2006 [5], Lebas, 2007 [15], De Lucas M., 2007 [9] or Ning W., 2007 [19]. As we have said, the ELSA model takes advantages of the Eulerian description of the

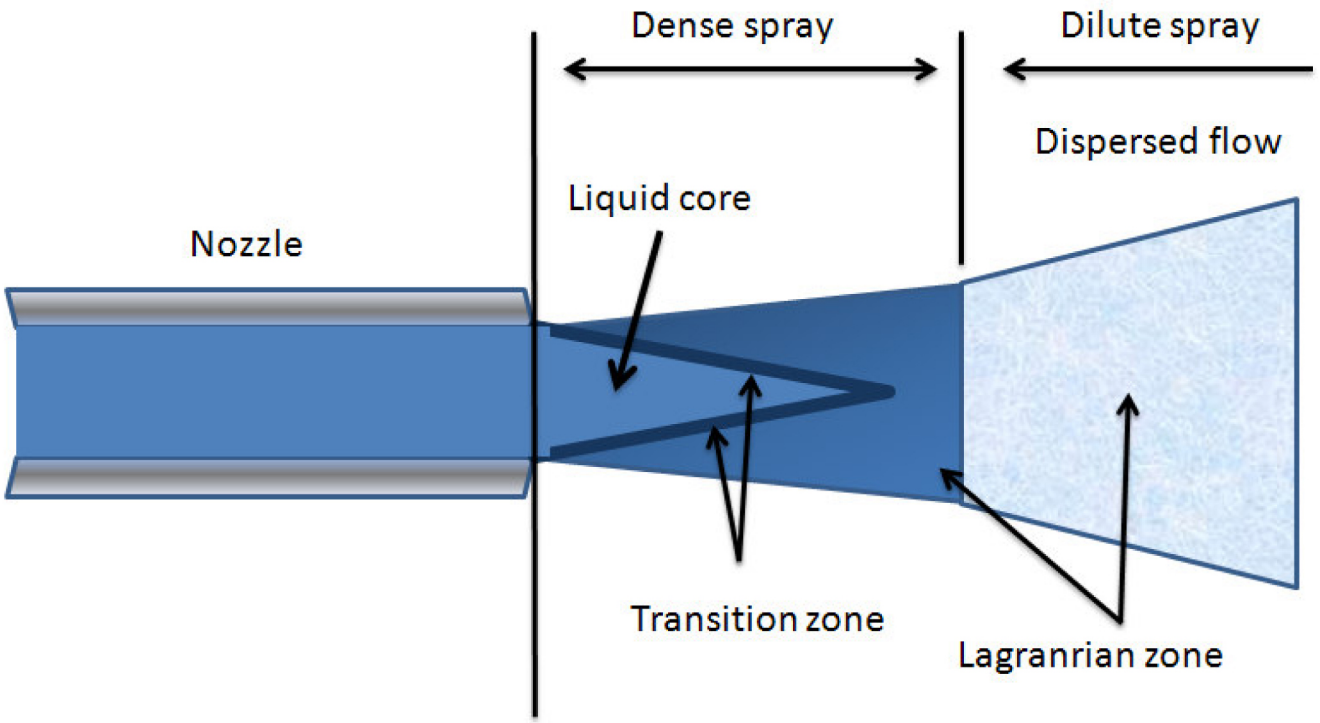

Figure 1. Illustration of the spray structure in the atomization regime (adapted from Faeth et al., 1995 [10]).

near nozzle flow where some assumptions of standard spray models based on discrete droplet method (DDM) shows strong limitations. This approach is valid only when the liquid volume fraction is small inside the computational cells and when the drops are homogeneously distributed in the computational space, neither of them is satisfied in the near field of the spray. In order to keep a low void fraction and assure numerical stability, it is necessary to use grid sizes larger than orifice diameter, which cannot adequately resolve the flow structures in this region. Additionally, it is also not required to assume any particular shape to represent drops and liquid ligaments on ELSA model, where the average area of the liquid-gas interface is introduced as a measure of the atomization extent. Moreover, the DDM method applies isolated drop based models in this region with strong interaction within the liquid phase, where its validity is hardly justified.

Basically, we have three separated zones in the ELSA model as shown in the following figure:

- **Eulerian mixture zone:** In this region (liquid core), liquid and gas phase are considered as a unique mixture flow. The classical Eulerian model is used to solve this single phase flow.
- **Transition zone:** switch from Eulerian to Lagrangian calculation.
- **Lagrangian zone:** classical Lagrangian tracking for droplets in the diluted spray zone and some regions of the Dense spray zone

The main hypothesis of ELSA, is that the flow must be a high-speed turbulent spray, where Reynolds bulk number and Weber number should be high (See Beau, 2006 [5] for a detailed study). In the case of Reynolds number, it must be at least $Re > 10^4$, (A. Doudou, 2005 [3]), whereas for Weber number, $We \sim 350$ (Lee and Reitz, 2001 [16] and Tanner, 2004 [23]). On the other hand, the main problem is that the turbulent mixing process between the liquid and surrounding gaseous phase is simulated as a single-phase turbulent fluid flow with mean properties, so it does not give a detailed information about both phases separately in the near nozzle region.

According to the previous statements, the purpose of the present study is to do a preliminary validation of the ELSA spray model implement in the Star-CD code. This work is part of a more ambitious project, with the general objective of developing and validating this spray model implementation for real-life applications on CFD engine calculations.

The structure of the paper is as follows. In the second section the model equations are written down. In the third section the geometry and the setup of the simulation are explained. Fourth section is devoted to the analysis of the results and conclusions are explained in the last section.

MODEL EQUATIONS

As we have said, the ELSA model was first described in an article of Vallet et al., 2001 [24]. Several other works as A.

Desportes et al., 2010 [2] Beau, 2006 [5], and Ning et al., 2007 [19] also discussed this set of equations, that we write down here in shake of completeness of the paper and a logical explanation of the ELSA model. These equations covered the several regions of the ELSA model, changing from one to another but, from now on and in all the regions, the subscript *l* stands for liquid and *g* stands for gas, whereas *i, j* are the direction in space. In order to facilitate the reading of the manuscript, we have added a symbol table at the end of the document.

a). Eulerian Mixture Zone

We define the mean liquid mass fraction, $\tilde{Y}_l$ as

$$\tilde{Y}_l = \frac{\overline{\rho Y_l}}{\overline{\rho}}, \tag{1}$$

where ρ is the density and Y_1 is the liquid mass fraction. Intuitively, mean density is defined as

$$\overline{\rho} = \rho_l \overline{Y_l} + \rho_g \left(1 - \overline{Y_l}\right), \tag{2}$$

which is expressed in terms of $\tilde{Y}_l$ as

$$\frac{1}{\overline{\rho}} = \frac{\tilde{Y}_l}{\rho_l} + \frac{1-\tilde{Y}_l}{\rho_g} \tag{3}$$

Favre averaged mean velocity is defined as

$$\tilde{U}_i = \tilde{Y}_l U_{l,i} + \left(1-\tilde{Y}_l\right) U_{g,i} \tag{4}$$

and mean pressure $\overline{P}$ is given by the equation of state

$$\overline{P} = \frac{\left(1-\tilde{Y}_l\right)\overline{\rho} R_g T_g}{1 - \tilde{Y}_l \cdot \overline{\rho}/\rho_l} \tag{5}$$

In this equation R_g is the gas constant and T_g is the mixture temperature.

Then, the classical transport equations are solved for these mean variables:

$$\frac{\partial \overline{\rho}}{\partial t} + \frac{\partial \overline{\rho} \tilde{U}_j}{\partial x_j} = S_{EL}^{\tilde{Y}_l} \tag{6}$$

$$\frac{\partial \overline{\rho} \tilde{U}_i}{\partial t} + \frac{\partial \overline{\rho} \tilde{U}_j \tilde{U}_i}{\partial x_j} = -\frac{\partial \overline{P}}{\partial x_i} - \frac{\partial \overline{\rho u_i'' u_j''}}{\partial x_j} \tag{7}$$

Her, $S_{EL}^{\tilde{Y}_l}$ are some source terms that are activated during the transition from Eulerian to Lagrangian when there exist droplet generation. It should be noticed that the last equation does not contain any momentum exchange terms between liquid and gaseous phases. In order to model the liquid dispersion, this set of equations is completed by the transport equation for the liquid mass fraction:

$$\frac{\partial \overline{\rho} \tilde{Y}_l}{\partial t} + \frac{\partial \overline{\rho} \tilde{U}_j \tilde{Y}_l}{\partial x_j} = -\frac{\partial \overline{\rho u_j'' y''}}{\partial x_j} \tag{8}$$

In equations (6) and (7), there are two turbulent fluxes unknown. The turbulent stress tensor is modeled with a classical k - ε model closure, which is discussed below. Concerning the liquid turbulent diffusion flux, a gradient law approximation is applied:

$$\overline{\rho u_j'' y''} = -\overline{\rho} \frac{v_t}{Sc_t} \frac{\partial \tilde{Y}_l}{\partial x_j} \tag{9}$$

In this equation v_t is the liquid viscosity and Sc_t is the turbulent Schmidt number.

b). Liquid/Gas Interface Density

In order to characterize the size of liquid fragments resulted from the jet atomization, the notion of liquid surface density is introduced. This variable is defined as the quantity of liquid/gas interface per unit of volume $\overline{\Sigma}\left(m^{-1}\right)$. Using this new variable, we can obtain the Sauter Mean Diameter of droplet, D_{32} and the drop number density (drop number per unit of volume), n (Lebas R., 2005 [14]):

$$D_{32} = \frac{6\overline{\rho}\widetilde{Y_l}}{\rho_l \overline{\Sigma}}$$

$$n = \frac{\rho_l^2 \overline{\Sigma}^3}{36\pi \overline{\rho Y_l}^2} \tag{10}$$

A transport equation for liquid surface density, $\widetilde{\Omega}$, is postulated by analogy with the flame surface density.

$$\frac{\partial \overline{\rho}\widetilde{\Omega}}{\partial t}+\frac{\partial \overline{\rho}\widetilde{\Omega}\tilde{U}_j}{\partial x_j}=\frac{\partial}{\partial x_j}\left(\overline{\rho}\frac{v_t}{Sc_t}\frac{\partial \widetilde{\Omega}}{\partial x_j}\right)+$$
$$\overline{\rho}\cdot\left(\dot{\widetilde{\Omega}}_{init}+\dot{\widetilde{\Omega}}_{mean}+\dot{\widetilde{\Omega}}_{turb}+\dot{\widetilde{\Omega}}_{coll}+\dot{\widetilde{\Omega}}_{coal}\right)+S_{EL}^{\widetilde{\Omega}} \qquad (11)$$

Where $\dot{\widetilde{\Omega}}_{init}$, $\dot{\widetilde{\Omega}}_{mean}$, $\dot{\widetilde{\Omega}}_{turb}$, $\dot{\widetilde{\Omega}}_{coll}$, and $\dot{\widetilde{\Omega}}_{coal}$, are the initial, mean, turbulence, collision and coalescence value of liquid/gas surface density respectively; $S_{EL}^{\widetilde{\Omega}}$ is the source term of the liquid/gas interface. Beau, 2006 [5] introduced other notion of liquid/gas interface per unity of mass that is defined as $\widetilde{\Omega}=\overline{\Sigma}/\overline{\rho}$ (m^2/kg).

The production and destruction of liquid surface are accounted for the five liquid/gas surface densities. The first term source $\dot{\widetilde{\Omega}}_{init}$ in Eq. (11) permits to initialize the calculations since all other terms source are proportional to $\widetilde{\Omega}$:

$$\dot{\widetilde{\Omega}}_{init}=\begin{cases}2\dfrac{v_t}{Sc_t}\dfrac{6\overline{\rho}}{\rho_l\rho_g L_t}\dfrac{\partial \widetilde{Y}_l}{\partial x_i}\dfrac{\partial \widetilde{Y}_l}{\partial x_i}, & if \quad \widetilde{Y}_l\left(1-\widetilde{Y}_l\right)\le 0.001\\ 2\dfrac{v_t}{Sc_t}\dfrac{\widetilde{\Omega}}{\left(1-\widetilde{Y}_l\right)\widetilde{Y}_l}\dfrac{\partial \widetilde{Y}_l}{\partial x_i}\dfrac{\partial \widetilde{Y}_l}{\partial x_i}, & otherwise\end{cases} \qquad (12)$$

L_t is the turbulent length scale.

Three next terms correspond to the production of liquid surface density due to the mean or turbulent stresses and due to the collisions:

$$\dot{\widetilde{\Omega}}_{mean}=\frac{\overline{\rho u_i'' u_j''}}{\overline{\rho}\tilde{k}}\frac{\partial \tilde{U}_i}{\partial x_j}\widetilde{\Omega};$$

$$\dot{\widetilde{\Omega}}_{turb}=\frac{\widetilde{\Omega}}{\tau_{turb}} \quad ; \quad \text{and}$$

$$\dot{\widetilde{\Omega}}_{coll}=\frac{\widetilde{\Omega}}{\tau_{coll}} \qquad (13)$$

τ_{turb} and τ_{coll} are the characteristic time scale of turbulence and collisions respectively and k is the turbulent kinetic energy.

The last term on the right hand side of Eq. (11) deals with destruction of surface density due to coalescence, $\dot{\widetilde{\Omega}}_{coal}$:

$$\dot{\widetilde{\Omega}}_{coal}=-\frac{1}{\tau_{coll}}\frac{\widetilde{\Omega}^2}{\widetilde{\Omega}_{crit}} \qquad (14)$$

c). Transition Zone

We rely on a critical value of the Eulerian liquid volume faction to decide whether it should turn from Eulerian to Lagrangian formulation (Beau, 2006 [5]). The Lagrangian droplets are formed where spray is assumed to be diluted enough. It follows the below equation.

$$\tilde{\Phi}_l=\widetilde{Y}_l\frac{\overline{\rho}}{\rho_l}\le\tilde{\Phi}_l^{crit} \qquad (15)$$

where $\tilde{\Phi}_l^{crit}$ is the critical value of the Eulerian liquid volume fraction.

The transitional criterion is based on the value of liquid volume fraction that is linked to the ratio of mean free path between two droplets and mean equivalent radius of the droplets in the cell. In our calculation, the transition is done when the liquid volume fraction becomes lower than 0.01 [2]. The transition zone is composed of the computational cells that form the border with the dense zone (i.e. zone where the liquid volume fraction is greater than 0.01) and only one parcel is generated per transition cell and per time step.

The velocity of the droplets is defined as

$$\overline{U}_{l,i}=\tilde{U}_i+\frac{\overline{\rho u_i'' y''}}{\overline{\rho}\tilde{Y}_l} \qquad (16)$$

The diameter of the droplet is equal to the Sauter Mean Diameter

$$D_{32}=\frac{6\widetilde{Y}_l}{\rho_l\tilde{\Omega}} \qquad (17)$$

The number of droplets per generated parcel n_{drop} is obtained from mass conservation

$$n_{drop}=\frac{\overline{\rho}\tilde{Y}_l V_{cell}}{\pi/6\,\rho_l D_{32}^3} \qquad (18)$$

where V_{cell} is the volume of one transitional cell

Table 1. Basis Parameters

Ambient pressure	Injection pressure	Ambient Temperature	Fuel Density
3.53 MPa	80 MPa	293 K	822.10 kg/m^3

MODEL VALIDATION SETUP

GEOMETRY AND BOUNDARY CONDITIONS

The geometry is to simulated an outflow of a non-cavitating single-hole injector (tapered nozzle), with an outlet diameter of 112 µm. The chamber has a size of 80×25mm. Some physical key parameters of chamber and spray are depicted in table 1.

This nozzle presents a variable velocity profile input at the nozzle exit that is showed in Figure 2. This is an average measure, not an instantaneous realization. The great irregularity showed in this picture seems to be an effect of wave reflections inside the nozzle (see R. Payri et al., 2008 [22] or J. Gimeno, 2008 [8] for more details about this issue).

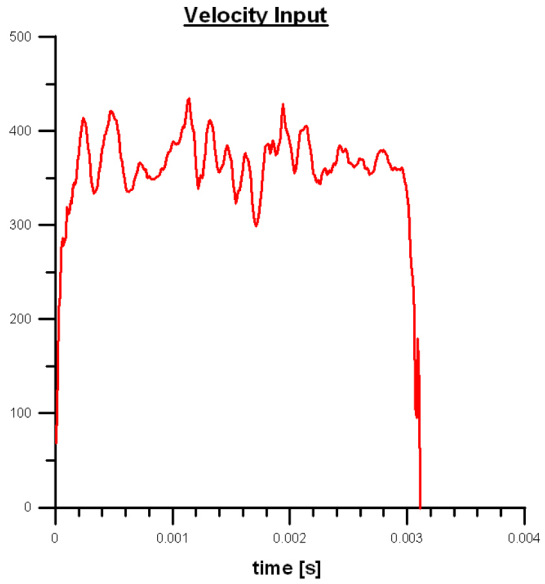

Figure 2. Velocity Profile (m/s).

In our computational cases we simulate the maximum time of 2ms, as the measurement obtained in CMT are matched well with our computational cases and velocity as explicitly shown in the later results. Moreover, the most important reason is the computational time is quite long especially once many droplets formed in ELSA modeling when time increased.

As this is axis-symmetric nozzle, a first approximation to this sort of problems is to perform 2D simulations. Of course, turbulence and engines are always 3D, but, as a first approximation to the real problem, 2D simulation can model reasonably the spray behavior. In our calculation, 2D simulations are actually a 3D simulation with only a cell in the azimuthal direction, modeling a 5° sector of the spray. This is showed in the rightmost part of Figure 4, where we also show the boundary conditions imposed on the spray and chamber. Figure 3 depicts the front view of two typical meshes.

Generally, the requirements for mesh structure are especially important at the nozzle, where the mesh size has to be small enough to capture the spray structure and droplets. The criterion used in this paper is to define the size of the first cell and then extrude the mesh, fixing the axial and radial ratio. The six cases studied in this paper are showed in table 2.

In table 3 we have the main formula based on the successive ratio used in constructing our meshes are showed. In these equations: l_1 is length of the first interval of the edge, l_n is length of the n interval of the edge, R is the interval length ratio, n is the number of intervals and L stands for the total edge length [11]. The sixth case is a little bit different. Instead of using first/last ratio of 72 on the axial direction, and the last/first ratio equal to 0.006 on the radial direction, we have taken the first segment of the mesh with $\Delta x_1 = \Delta z_1 = l_1 = 0.2R_{inj} = 0.1D_{inj} = 11.1\ (\mu m)$, and have used the same number of segments in the axial edge and radial edge, 218 and 25, respectively.

For the completeness, three different configurations with 3-, 5-, and 10-cell at the half of the nozzle are used (note that only half of the nozzle is simulated). In all of these cases we have fixed Δt in 10^{-8}, obtaining Courant numbers below 0.3. Mesh structures can be seen in Figure 3 with a zoom of the near nozzle region.

The RANS turbulent model chosen for our validation is the k - ε /High Reynolds Number, those equations are

$$\frac{\partial \tilde{k}}{\partial t}+\tilde{u}_j\frac{\partial \tilde{k}}{\partial x_j}=C_\mu\frac{\tilde{k}^2}{\tilde{\varepsilon}}\left(\frac{\partial \tilde{u}_i}{\partial x_j}+\frac{\partial \tilde{u}_j}{\partial x_i}\right)\frac{\partial \tilde{u}_i}{\partial x_j}+\frac{\partial}{\partial x_j}\left(\frac{C_\mu}{\sigma_k}\frac{\tilde{k}^2}{\tilde{\varepsilon}}\frac{\partial \tilde{k}}{\partial x_j}\right)-\tilde{\varepsilon} \quad (19)$$

and

$$\frac{\partial \tilde{\varepsilon}}{\partial t}+\tilde{u}_j\frac{\partial \tilde{\varepsilon}}{\partial x_j}=C_{\varepsilon_1}C_\mu\tilde{k}\left(\frac{\partial \tilde{u}_i}{\partial x_j}+\frac{\partial \tilde{u}_j}{\partial x_i}\right)\frac{\partial \tilde{u}_i}{\partial x_j}+\frac{\partial}{\partial x_j}\left(\frac{C_\mu}{\sigma_\varepsilon}\frac{\tilde{k}^2}{\tilde{\varepsilon}}\frac{\partial \tilde{\varepsilon}}{\partial x_j}\right)-C_{\varepsilon_2}\frac{\tilde{\varepsilon}^2}{\tilde{k}} \quad (20)$$

The constants of the model are listed in table 4. We are using the classical constants used in most of the spray calculation. However, as it is also known few decades back by Pope,

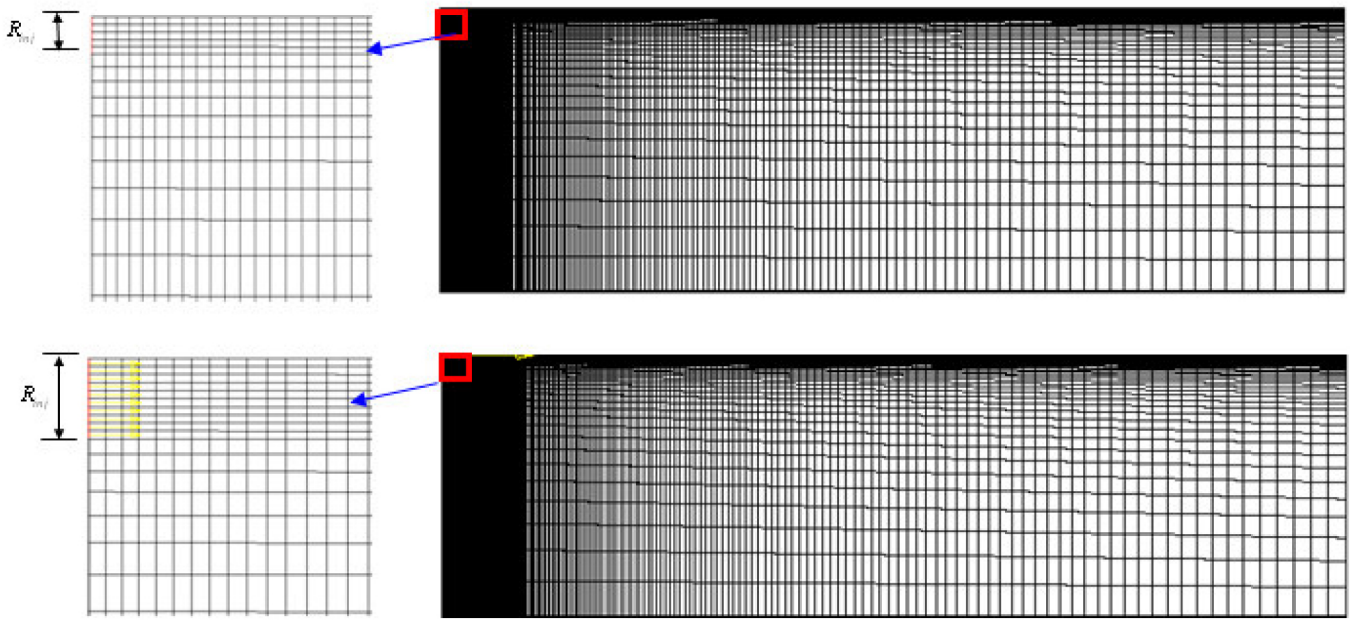

Figure 3. Computational meshes and detailed views (on the left side), for 5 cells and 10 cells at the same nozzle radius.

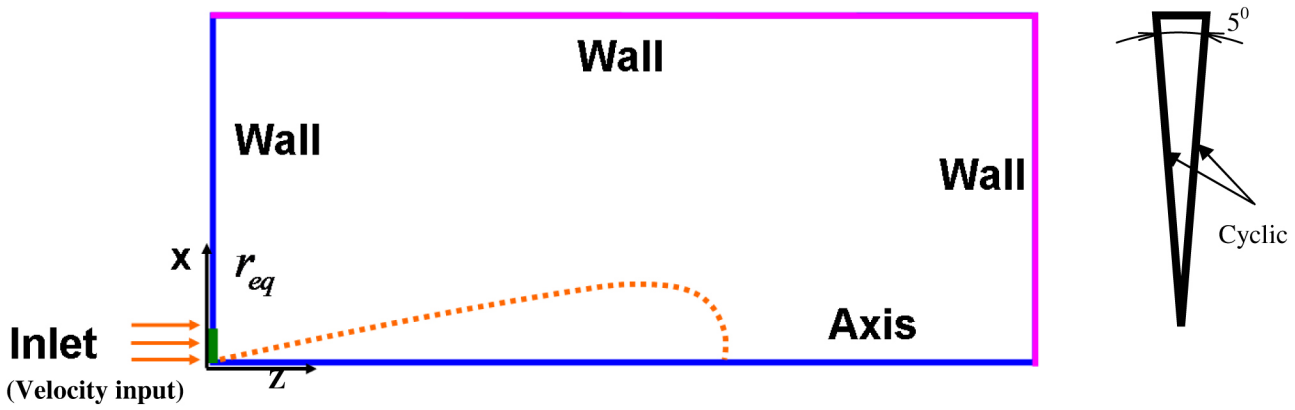

Figure 4. Geometry (front view and side view) & Boundary Condition.

1978 [20], the classical value of C_{ε_1} causes an overprediction of the spreading and decay of rate of a round jet flow.

The C_{ε_1} constant modifications are based on the suggestion of (J. Janicka et al., 1982 [13] and Dally B.B., 1998 [7]). Thus, we have used classical value $C_{\varepsilon_1}=1.44$ the suggested value $C_{\varepsilon_1}=1.60$ and an average value of 1.52 that in some cases give a better approximation. The turbulent Prandtl number has been set to 1 in order to produce similar solutions for the conservation equations of axial momentum, fuel mass and energy. Noting that the Prandtl (K.E.) in table 4 is another Prandtl constant which is only used for solving the k-ε equations which is well-known in CFD calculation and mentioned again in Diesel spray by Lebas and Blokkeel et al., 2005 [14].

Experimental Validation

The numerical results are compared with experimental data at CMT-Motores Térmicos. Experimental results have been obtained from quiescent vessel tests previously published in R. Payri et al., 2008 [22], and J. Gimeno, 2008 [8].

The injection velocity profile comes from measurements of mass and momentum fluxed performed in a pressurized test rig with nitrogen. Mass flow rate for the velocity inlet was measured by means of Bosch's method (Bosch, 1966 [4]) The momentum flux measuring principle of this technique is explained in two references of R. Payri et al., 2005 [21], and J. Gimeno, 2008 [8], and consists of measuring the impact

Table 2. Mesh parameters

Case No.	No cells at the half of nozzle	No. axial cells	Axial ratio (First/Last ratio)	No. radial cells	Radial ratio (Last/First ratio)	Total Vertices	Total Cells
1	**3**	218	72	**45**	0.006	19929	9810
2	5	218	72	**25**	0.006	11,169	5450
3	**5**	218	72	**45**	0.006	19,929	9,810
4	5	**435**	72	**90**	0.006	78,916	39,150
5	**10**	**250**	**143**	**50**	**0.003**	25,351	12,500
			First length		**First length**		
6	**5**	218	**11.1** μm	**25**	**11.1** μm	11,169	5450

Table 3. Successive Ratio of Mesh edges

Successive Ratio	Last/First ratio	First/Last ratio	First Length
Formula	$R=\left(\frac{l_n}{l_1}\right)^{1/(n-1)}$	$R=\left(\frac{l_1}{l_n}\right)^{-1/(n-1)}$	$\sum_{i=1}^{n} R^{i-1}=\frac{L}{l_1}$

Table 4. Turbulence Models

	C_μ	C_{ε_1}	C_{ε_2}	C_{ε_3}	C_{ε_4}	Prandtl (K.E.)	Prandtl (Eps)
Turb 1	0.09	**1.44**	1.92	1.44	-0.33	1	1.219
Turb 2	0.09	**1.52**	1.92	1.44	-0.33	1	1.219
Turb 2	0.09	**1.60**	1.92	1.44	-0.33	1	1.219

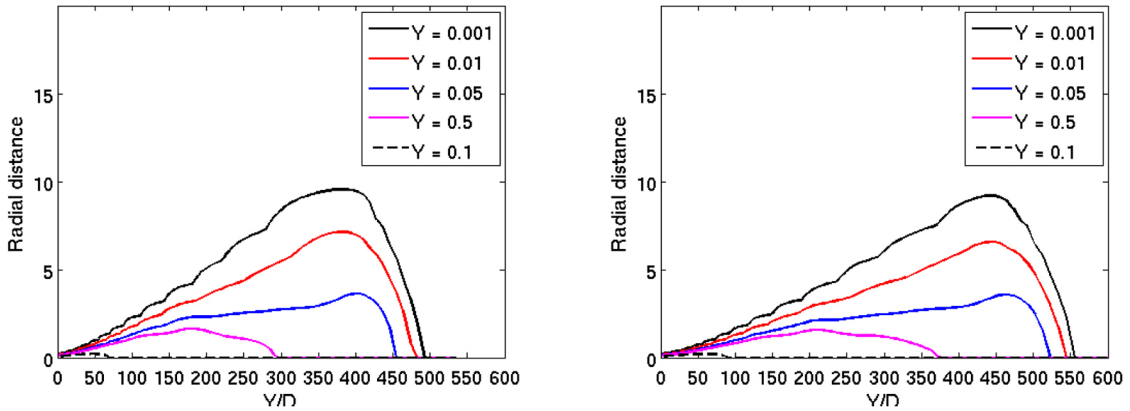

Figure 5. Comparison of iso-surfaces of 5-cell at 2ms, case 2 with C_{ε_1} =1.52 (left figure) and C_{ε_1} = 1.60 (right figure).

force of the spray in a surface with a piezo-electric sensor. As long as the whole cross-section of the spray impacts on the sensor, the measured force equals to the momentum flux at that cross section. If the measurement position is close to the nozzle exit, the time evolution of the impact force is equal to the nozzle (hole) momentum flux, Mo.

NUMERICAL RESULTS

The $C_{\varepsilon 1}$ effect of the penetration can be clearly seen in Figure 5, where several iso-surfaces of liquid mass fraction are showed. The longer axial distance of approximately 570 is obtained with C_{ε_1} =1.60, while it is only 490 with C_{ε_1} = 1.52. It is clear from the figures, the effect of C_{ε_1} reduces spray dispersion and consequently increases spray penetration.

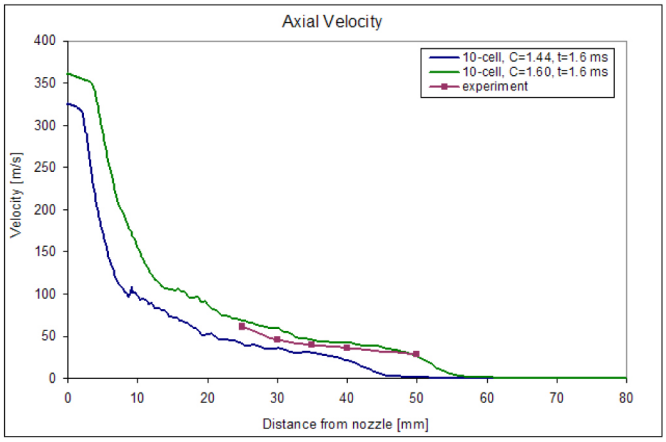

(a)

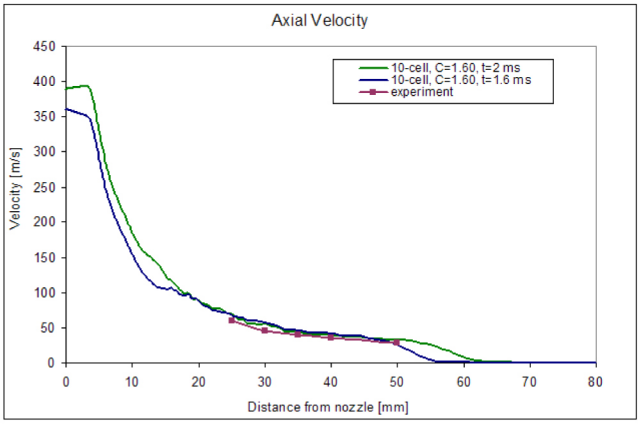

(b)

Figure 6. Axial velocity for 0.1 R_{inj} cases: (a) Changes in C_{ε_1}, (b) Changes in time.

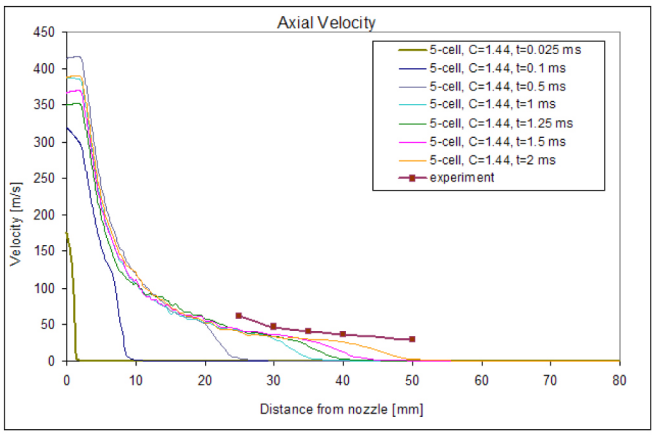

(a)

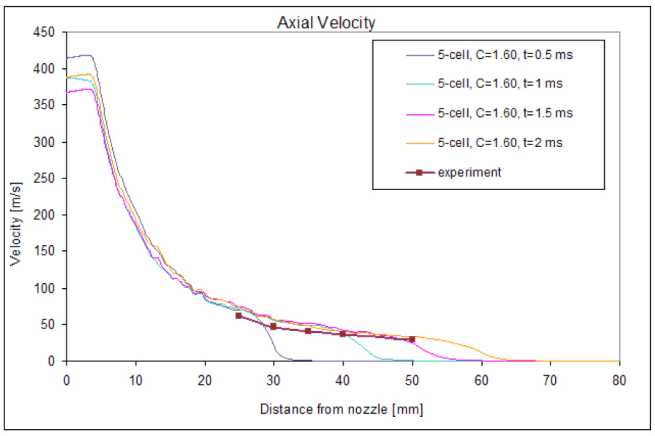

(b)

Figure 7. Comparisons of Axial velocity: (a) C_{ε_1} = 1.44; (b) C_{ε_1} = 1.60.

In the case of axial velocity, this effect is also very clear as can be seen in Figure 6, where the comparison of axial velocity for 10-cell case corresponding to two turbulent constants (1.44 and 1.60) at t=1.6 ms are illustrated. The matching of C_{ε_1} =1.60 is better than in the case of C_{ε_1} =1.44. Moreover, it seems to be clear from the figure that in the latter case, spray penetration is not enough to show an appreciable axial velocity at 50 mm from the nozzle. This result is also clear in the Figure 7, where we only have 5 cells at the nozzle. Clearly, C_{ε_1} =1.44 is underpredicting the axial velocity, whereas the 1.60 value gets more accurate results.

In Figure 8, a full view of droplet profile combined with the velocity in the same plot and a detailed view of the dense zone are depicted for 5-cell case (case no. 3), with turbulent constant equal to 1.60 at t = 2 ms. The first three figures on the left hand side are only depicted the velocity profile, and the last figure is illustrated both droplets and velocity. As it is expected, it confirms that velocity magnitude is highest in the zone next to the nozzle/inlet boundary and in the liquid core zone where the Eulerian approach is used. The farther distance from axial and radial edge, the less velocity we obtained. The last figure on the right hand side captures both velocity profile and the droplets, which are generated in regions where the velocity are approximately below 150 m/s.

The droplet formation is showed in Figure 9. According to the above description, the droplet formation starts at the transition zone and continue to develop in the farther zone (Lagrangian zone). As it was also expected, there is no droplet in the Eulerian mixture zone (regions contained the red color and its closed surroundings). These figures confirm that the initial setting and formulae for ELSA model are correctly captured in the final result. The Sauter Mean Diameters range from 8.88e- 9 µm to 4.896 µm in our computational cases, which is smaller than the smallest cell as stated in the previous part.

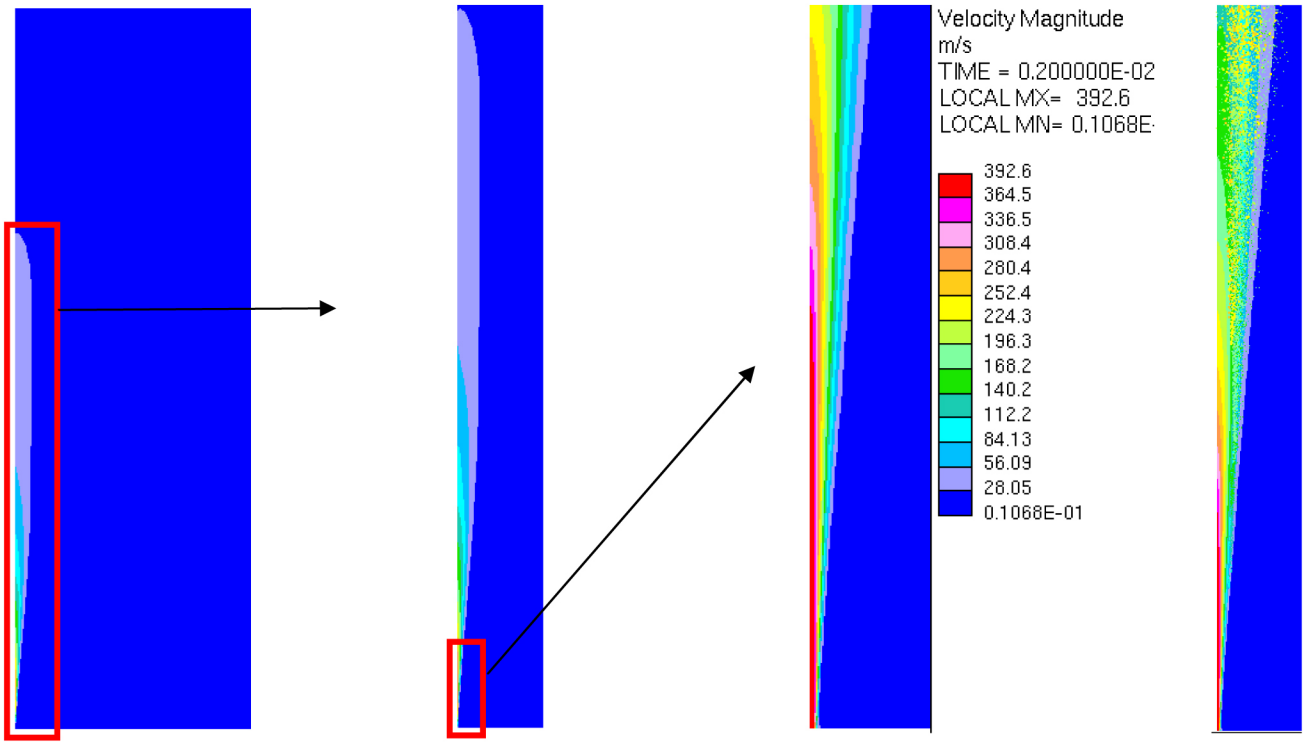

Figure 8. Velocity profile and droplet formation.

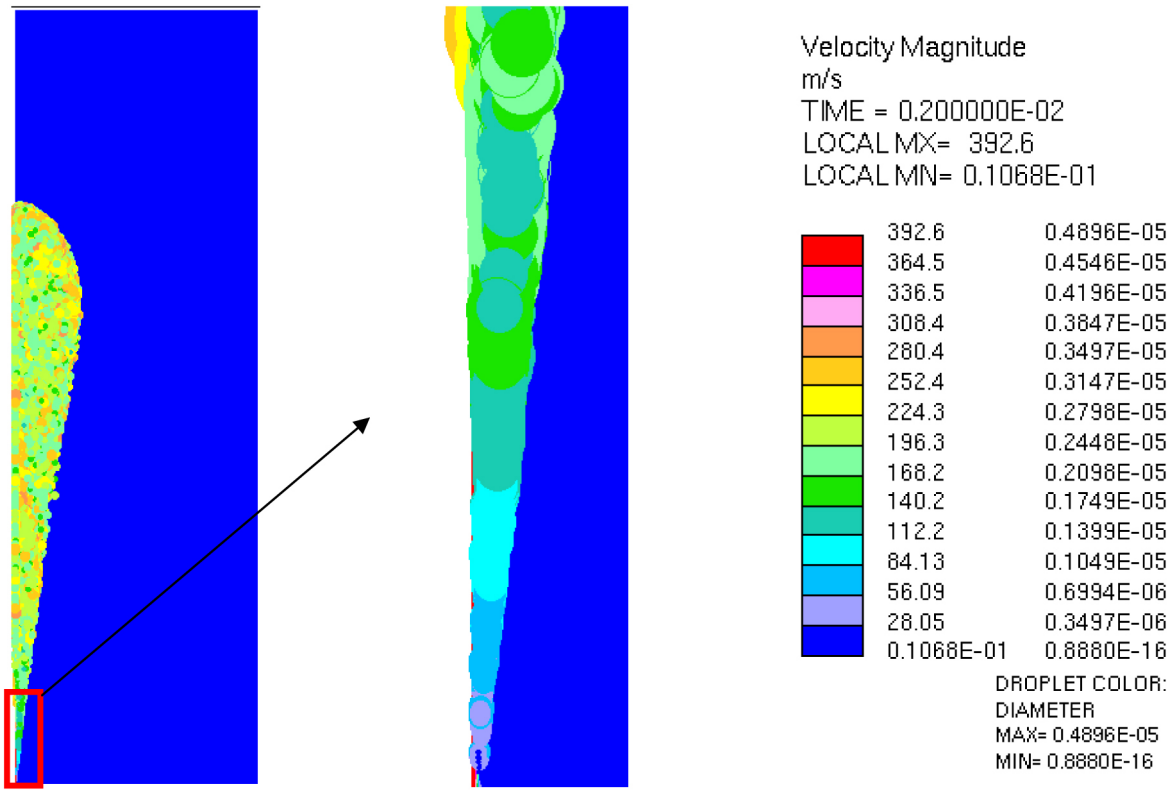

Figure 9. Droplet profile.

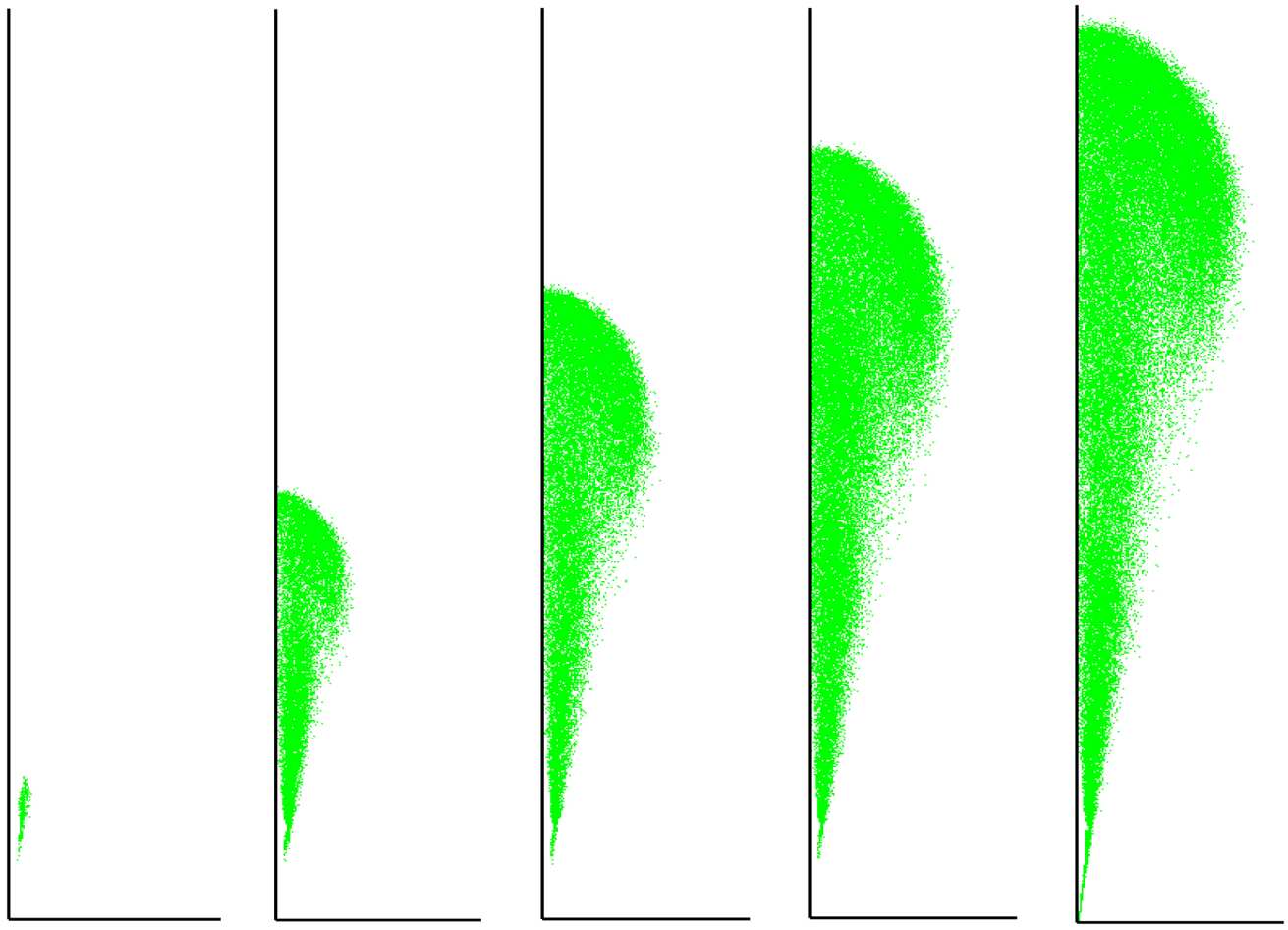

Figure 10. Droplet profiles at different time of 0.1, 0.5, 1, 1.5, and 2 ms (from left to right) for case 3, C_{ε_1} = 1.44.

Table 5. Droplet Information

	Time (ms)	Active Droplets	Evaporated / Disappeared / Absorption Droplets	Total Droplets
5-cell, C_{ε_1} **=1.44**	2	69101	422,994	492,095
5-cell, C_{ε_1} **=1.60**	2	125,739	529,320	655,059
10-cell, C_{ε_1} **=1.44**	1	706	3,734	4,440
10-cell, C_{ε_1} **=1.44**	1.5	78,894	398,061	476,955
10-cell, C_{ε_1} **=1.44**	1.75	87,969	440,249	528,218
10-cell, C_{ε_1} **=1.60**	2	107,549	630,334	737,883

Figure 10 shows the evolution of droplets in various time steps of 0.1, 0.5, 1, 1.5, 2 ms respectively for the case with 5 cells at nozzle radius. In those plots, all the droplets have the same size for the sake of visibility, independently of their actual diameter as already shown in Figure 9. A summary of the active and inactive droplets are shown in table 5. The total number of generated droplets increase rapidly after each time step for all the C_{ε_1} values. As an example, the case with 10-cell, C_{ε_1}=1.44, for t = 1, 1.5, and 1.75 in table 5 accumulated 4440, 476955, and 528218 droplets respectively. Several reasons could lead to the disappearance of droplets such as the evaporation due to the high temperature or their absoption into the Eulerian zone, where the flow is treated as a monophasic fluid.

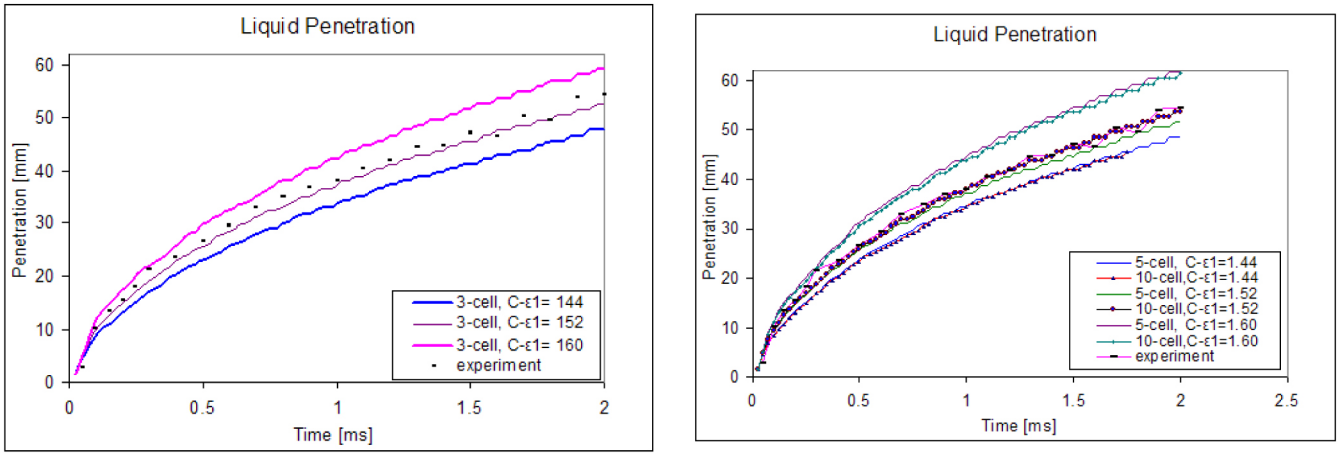

Figure 11. Spray penetration of the case with 3 cells and 5 cells.

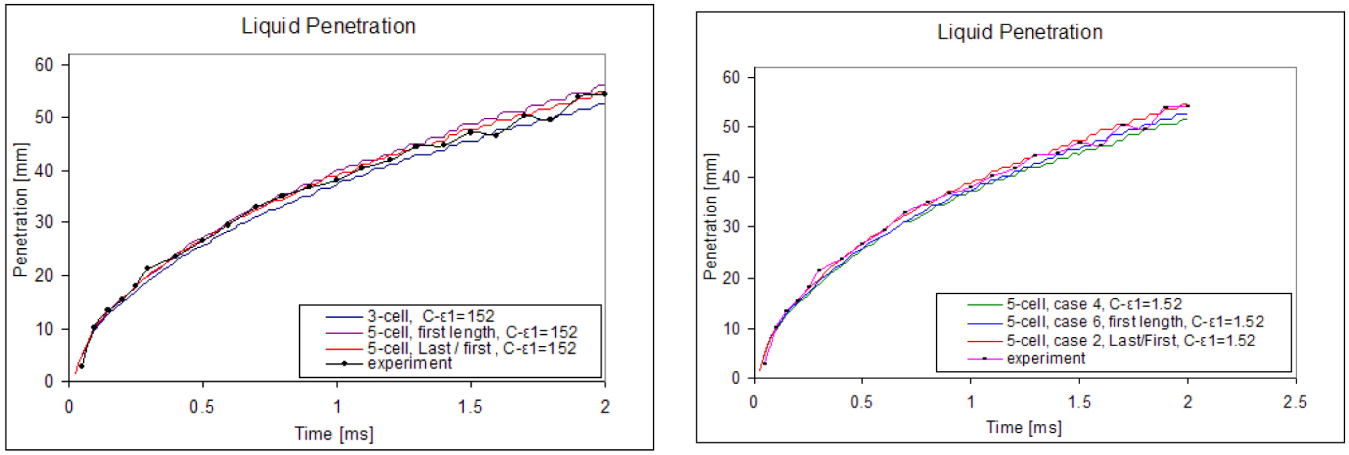

(a) (b)

Figure 12. Comparison of spray penetration.

Penetration rates also show a great dependency on the value of C_{ε_1}. Results on the penetration are showed in Figure 11 and 12. In this case, it is clear that the value of 1.60 is overprediting the penetration, while 1.44 is underpredicting in Figure 11, and for all the meshes has been tested so far. Hence, we have used a third value of 1.52 and we obtain the best fit with various meshes.

While the Figure 12 (a) illustrate the difference between 3- and 5-cell meshes, the averaged numerical errors of 3-cell case (case 1) is 0.9% whereas the 5-cell case with the first length equal to 11.1 µm (case 6) is 1%, and 5-cell case with last/first ratio (case 2) is only 0.42% as plotted in Figure 12 (b) and the detailed difference of representative errors are depicted in the Figure 13. The variance between 3-cell case and 5-cell case as in Figure 12 (a) is quite large in comparison with the discrepancy from 5-cell to 10-cell cases in Figure 11 (b). Using the same constant $C_{\varepsilon_1} = 1.52$, it only takes **138451** seconds (~39 hours) to complete one parallel calculation consisted of 6 processors for 5-cell case (case no. 3), while it must need **517741** seconds (~ 144 hours) to complete one parallel calculation consisted of 12 processors for 10-cell case (case no. 5). Hence, the 5-cell mesh with last/ first ratio consisted of 25 radial cells, and $C_{\varepsilon_1} = 1.52$ is the optimal setup, it should be enough for using the future RANS calculation of this nozzle diameter.

SUMMARY/CONCLUSIONS

In this study, several test cases are employed to have an initial validation of the ELSA model implemented in Star-CD. Mesh independency and the effect of changing C_{ε_1} constant are explored. All the simulations have been made in 2D meshes, considering axis-symmetric problems and have been validated against experimental data of a well characterized nozzle.

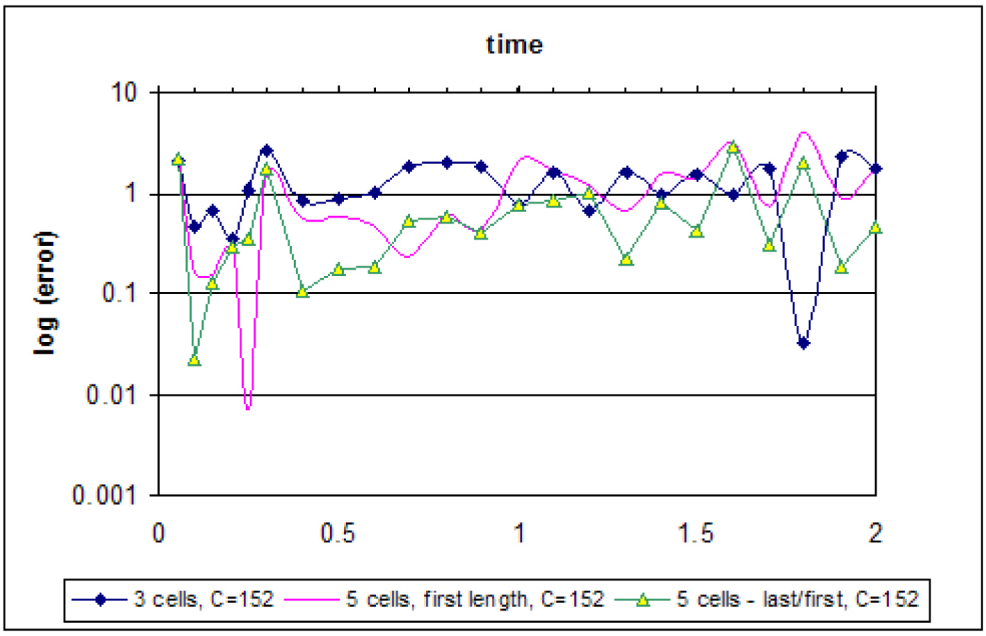

Figure 13. Numerical errors of 3-cell and 5-cell cases with turbulent constant = 1.52.

Two major conclusions are obtained from this work. Firstly, the classical value of C_{ε_1}, 1.44, leads to an overpredicting of the penetration, while the typical value used in sprays, 1.60, causes overprediticion. Secondly, mesh independency is obtained with only 5-cell at the nozzle radius, which satisfies the reasonable result, permits a considerable saving in computational time and storage space. The best fit in the penetration curve is obtained for $C_{\varepsilon_1} = 1.52$.

Obviously, a couple of 2D simulations are not a completed validation of the code. It is planned to continue with two other experimental cases analyzed in our institute, a full 3D simulation of the three nozzles, and last but not least, the effect of a cavitating nozzle.

REFERENCES

1. Araneo, L, Soare, V, Payri, R, Shakal, J (2006). Setting up a PDPA system for measurements in diesel spray. J Phys: Conf Ser 2006; 45:85-93.

2. Hoyas, S., Pastor, J., Khuong-Anh, D., Mompó-Laborda, J. et al., "Application and Evaluation of the Eulerian-Lagrangian Spray Atomization (ELSA) Model on CFD Diesel Spray Simulations," SAE Technical Paper 2011-37-0029, 2011.

3. Doudou, A., Turbulent flow study of an isothermal diesel spray injected by a common rail system, Fuel, Volume 84, Issues 2-3, January-February 2005, Pages 287-298.

4. Bosch, W., "The Fuel Rate Indicator: A New Measuring Instrument For Display of the Characteristics of Individual Injection," SAE Technical Paper 660749, 1966, doi: 10.4271/660749.

5. Beau, PA (2006). Modelisation de l'atomisation d'un jet liquide - Application aux sprays diesel. Ph.D. Thesis, University of Rouen.

6. Blokkeel, G., Barbeau, B., and Borghi, R., "A 3D Eulerian Model to Improve the Primary Breakup of Atomizing Jet," SAE Technical Paper 2003-01-0005, 2003, doi: 10.4271/2003-01-0005.

7. Dally, B.B.:'Flow and Mixing Fields of Turbulent Bluff-Body Jets and Flames, Combust.Theory Modelling, Band 2, S. 193-219 (1998).

8. García, D. Jaime Gimeno (2008). Desarrollo y aplicación de la medida del flujo de cantidad de movimiento de un chorro Diesel, PhD thesis, Universidad Politécnica de Valencia.

9. De Lucas, M (2007). Contribution a la modelisation de la pulverisation d'un liquide phytosanitaire en vue de reduire les pollutions. Ph.D. Thesis, University of Aix-Marseille II.

10. Faeth, G., Hsiang, L.-P., and Wu, P.-K. (1995). Sructure and breakup properties of sprays. Int. J. Multiphase Flow, 21:99-127.

11. Fluent, Gambit manual 13, Fluent, Inc. 05/03/00.

12. Faeth, G. M., Hsiang, L. -P., Wu, P. -K., Structure and breakup properties of sprays, International Journal of Multiphase Flow, Volume 21, Supplement 1, December 1995, Pages 99-127.

13. Janicka, J., Peters, N., Prediction of turbulent jet diffusion flame lift-off using a PDF transport equation, in: Symposium (International) on Combustion, vol. 19, 1, 1982, pp. 367-374.

14. Lebas, R., Blokkeel, G., Beau, P., and Demoulin, F., "Coupling Vaporization Model With the Eulerian-Lagrangian Spray Atomization (ELSA) Model in Diesel Engine Conditions," SAE Technical Paper 2005-01-0213, 2005, doi: 10.4271/2005-01-0213.

15. Lebas, R (2007). Modelisation Eulerienne de l'Atomisaton haute pression - Influences sur la vaporisation et la combustion induite. Ph.D. Thesis, University of Rouen.

16. Lee, S. and Reitz, R. (2001). Effect of liquid properties on the breakup mechanism of high-speed liquid drops. Atomization and Sprays, 11:1-19.

17. Lefebvre, A.H. (1989). Atomization and sprays, Taylor and Francis.

18. Naber, J. and Siebers, D., "Effects of Gas Density and Vaporization on Penetration and Dispersion of Diesel Sprays," SAE Technical Paper 960034, 1996, doi: 10.4271/960034.

19. Ning, W, Reitz, RD, Lippert, AM and Diwakar, R (2007). Development of a next generation spray and atomization model using an Eulerian-Lagrangian methodology. 17th Int. Multidimensional Engine Modeling User's Group Meeting, Detroit, MI.

20. Pope, S.: An explanation of the turbulent round-jet/plain-jet anomaly. AIAA J. 16, 279-281 (1978).

21. Payri, R., García, J.M., Salvador, F.J. and Gimeno, J. (2005). Using spray momentum flux measurements to understand the influence of Diesel nozzle geometry on spray characteristics, Fuel 84, pp. 551-561.

22. Payri, R., Tormos, B., Salvador a, F.J., Araneo, L. (2008). Spray droplet velocity characterization for convergent nozzles with three different diameters. Fuel 87, pp 3176-3182.

23. Tanner, F. (2004). Development and validation of a cascade atomization and drop breakup model for high-velocity dense sprays. Atomization and sprays, 14:20-32.

24. Vallet, A, Burluka, AA and Borghi, R (2001). Development of a Eulerian model for the atomization of a liquid jet. Atomization and sprays, vol. 11, pp. 619-642.

CONTACT INFORMATION

Sergio Hoyas, J.M. Pastor, Dung Khuong-Anh, Juan Manuel Mompó-Laborda
CMT - Motores Térmicos (Department of thermal engine)
Universidad Politécnica de Valencia.
Camino de Vera S/N, 46022
Valencia, Spain
E-mail: (serhocal, jopasen, ankh2, juamomla) @mot.upv.es

F. Ravet
Renault
1 Avenue du golf 78288
Guyancourt, France
frederic.ravet@renault.com

ACKNOWLEDGMENTS

The authors would like to thanks to the referee for his/her comments, which have greatly improved the article. This work has been granted by Renault and VECOM (Vehicle Concept Modeling) - EU FP7 Marie Curie Initial Training Network (ITN) Grant Agreement 213543 (from October 1st, 2008 to September 30, 2012). The aim of the proposed training network is to provide dedicated research training in the emerging field of vehicle concept modeling for up-front pre-CAD functional performance engineering, bridging between industry and academia across Europe. Authors also acknowledge the support of the Spanish Government in the frame of the Project "Métodos LES para la simulatión de chorros multifásicos", Ref.ENE2010-18542, the Universidad Politécnica de Valencia under the contract Reference PAID-2759 and the Generalitat Valenciana, under the contract GV/2010/039.

DEFINITIONS/ABBREVIATIONS

CAD
Computer-aided Design

CMT
CMT Motores Térmicos

CFD
Computational Fluid Dynamics

DDM
Discrete Droplet Model

ICE
Internal Combustion Engine

ELSA
Eulerian-Lagrangian Spray Atomization

ITN
Initial Training Network

PDPA
Phase Doppler Particle Analyzer

SMD
Sauter Mean Diameter

VECOM
Vehicle Concept Modeling

NOMENCLATURE

l
liquid

g
gas

i, j
direction in space

k
turbulent kinetic energy

$\overline{\Sigma}$
quantity of liquid/gas interface per unit of volume

D_{32}
Sauter Mean Diameter

n
drop number density (drop number per unit of volume)

n_{drop}
number of droplets per generated parcel

ρ
density

$\overline{\rho}$
mean density

Sc_t
turbulent Schmidt number

τ_{turb}
characteristic time scale of turbulence

τ_{coll}
characteristic time scale of collision

ν_t
liquid viscosity

$\overline{P}$
the mean pressure

L_t
turbulent length scale

R_g
the gas constant

$S_{EL}^{\tilde{Y}_l}$
source term when droplet generation during the transition from Eulerian to Lagrangian formulation

$S_{EL}^{\tilde{\Omega}}$
source term of the liquid/gas interface

T_g
the mixture temperature

$\tilde{\Phi}_l^{crit}$
critical value of the Eulerian liquid volume fraction

$\tilde{U}_i$
Favre averaged mean velocity

$\tilde{Y}_l$
mean liquid mass fraction

$\widetilde{\Omega}$
liquid/gas interface per unity of mass

$\dot{\widetilde{\Omega}}_{mean}$
mean value of liquid/gas surface density

$\dot{\widetilde{\Omega}}_{turb}$
turbulence value of liquid/gas surface density

$\dot{\widetilde{\Omega}}_{coll}$

collision value of liquid/gas surface density

$\dot{\widetilde{\Omega}}_{coal}$

coalescence value of liquid/gas surface density

$\widetilde{\Omega}_{init}$

first source term

V_{cell}

volume of one transitional cell

l_1

length of the first interval of the edge

l_n

length of the *n* interval of the edge

R

the interval length ratio

n

the number of intervals

L

the total edge length

ISSN 0148-7191

SAE Customer Service:
Tel: 877-606-7323 (inside USA and Canada)
Tel: 724-776-4970 (outside USA)
Fax: 724-776-0790
Email: CustomerService@sae.org
SAE Web Address: http://www.sae.org
Printed in USA

2.2.5. A LES approach to the simulation of Diesel-like gas jets: Boundary condition configuration. Engineering Applications of Computational Fluid Mechanics 2011

Title:

A LES approach to the simulation of Diesel-like gas jets: Boundary condition configuration

Authors:

Jose Maria Desantes, Sergio Hoyas, Antonio Gil, Juan Manuel Mompó-Laborda

Affiliation:

CMT – Motores Térmicos,

Universidad Politécnica de Valencia

Camino de Vera S/N, 46022 Valencia, Spain

E-mail: [jmdesant, serhocal, angime, juamomla]@mot.upv.es

Abstract:

Some aspects of the transient evolution of Diesel-like gas jets by means of Large-Eddy Simulation (LES) are discussed in this work. A 3D injection chamber is simulated in order to understand the relationship between the inlet boundary condition and the development of the turbulent motion of Diesel sprays. The main assumption of the set up is the turbulent gas jet theory hypothesis applied to the inlet boundary conditions. Validation of the results is presented by comparing with both experimental diesel spray measurements

and trusted Reynolds-Averaged Navier-Stokes (RANS) simulations. Results show that reasonable simulation of turbulent patterns from one diameter far away of the inlet boundary condition is achieved.

Keywords:
LES Methods; Diesel sprays; gas jets, biphasic flows

Main text

Introduction

Insight in the behaviour of an evaporating fuel spray is of great importance for engine designers. Improvements in injection system reduce emissions and increase power by a more effective combustion process. Therefore, a deep understanding of the physics of Diesel spray will provide some fundamental knowledge for the design of more efficient, less consuming and cleaner engines.

During the last years great advances on the comprehension of several physical phenomena in liquid jets and sprays have been achieved, both by means of diagnosis experimental tests and Computational Fluid Dynamics (CFD) techniques. Simulation of turbulence is still one of the most challenging

problems in physics and there is a general agreement that this simulation can be done within three levels of accuracy. The most used approaches to simulate turbulence are based on RANS. These computational methods are very useful to study the averaged flow, but they do not provide any information neither about the turbulent fluctuations nor about the processes linked with them (e.g. flow on the jet boundary). One of the key elements to model turbulent flows is the choice of a turbulent closure scheme [5]. In this sense, it is eloquent that the standard coefficients of one of most used scheme (i.e. k-ε model) need to be modified to simulate circular turbulent jets in order to achieve better agreement with the laboratory results [4].

Regarding Diesel spray injection, the most commonly used codes in the automotive industry, until very recently, are based on the RANS approach because of their reasonably accurate results and relatively lower computational cost. Moreover, coupled to probability density functions (PDF) is able to reasonably overcome combustion simulations [41].

However as the RANS approach has the highest level of modelling it can be seen as a successful interpolation between experimental data sets, and without a careful check of the results against experiments, little can be said. On the contrary, direct numerical simulation (DNS) methods solve all the significative scales of the flow, so no modelling is required and it provides the highest level of description of the flow. Since the smallest structures of the flow have to be solved, the computational cost increases as $Re^{9/4}$ and the resources required for most practical cases are above current computer hardware limitations (and will probably be in the next 20 years) [25], [23]. In this paper an implementation

of the third method is presented. LES is computationally more expensive than RANS, but modelling required by RANS is reduced, and therefore it is more accurate. Furthermore, a detailed study of the flow characteristics in zones where turbulent fluctuations are significant is allowed by means of LES, while RANS, by definition, cannot model these features [39]. For a comprehensive description of these methods, the book of Pope [40] is an excellent starting point.

As commented above, LES increases the computational cost, but this method is able to consistently simulate the complex structures related with turbulent mixing, which is decisive in the injection and combustion processes and invisible for RANS solvers [38], [37], [11]. A good knowledge of this part of the spray is crucial in order to minimize emissions in Diesel engines. Apart from the turbulence modelling, the spray behaviour itself comprises a range of complex physical and chemical processes which are difficult to incorporate in the computer models used in engine design. The nozzle internal flow greatly affects the fuel atomization characteristics and so the subsequent engine combustion and exhaust emissions [14], [34]. The transient nature of the flow is greatly affected by the needle movement which associated with cavitation has dominated recent studies as the key phenomenon connecting internal flow and spray behaviour [32], [30]. Thus simulating the transient behaviour inside the nozzle [35] and predicting the real spray characteristics is of great importance. Experimental information (refereed by Pastor [31]) shows that Diesel sprays under both non-evaporising and vaporising conditions can be properly described with a mixing-controlled approach, and thus they can be analysed in

the same way as a gas jets. However, since fuel-air mixing process is significantly influenced by fuel atomization, breakup and collision, the idea to approximate the spray evolution using gas injection cannot be completely acceptable for LES due to its degree of physical description. LES was originally developed to deal with turbulence in single phase flows. Therefore different approaches have been recently implemented in LES, in order to deal with this a priori complicated two-phase problem. The eulerian-eulerian approach (E-E) for two-phase flow has based models like the mesoscopic [19] or the VOF (volume of fluid) [7]. Regarding the lagrangian-eulerian approach (L-E), a direct use in LES can be performed by taking into account the models needed for the sub-grid two-phase interaction (viscous work, dissipation rate, turbulent viscosity, heat flux, species flux) [8]. Each of them has both advantages and disadvantages in the various regions of spray consisting of the dense zone and the downstream dilute zone. Hence, the Eulerian-Lagrangian Spray Atomization (ELSA) is an integrated model for capturing the whole spray evolution in RANS calculations [12]. Consequently, LES of atomization seems to be a necessarily step forward as depicted by Chesnel [9].

The main goal of this work is to numerically investigate the influence of the inlet boundary conditions on a LES of the flow in a Diesel fuel spray evaporation system. Therefore, in this paper we limited ourselves to the numerical simulation of Diesel-liked gas jet in a combustion chamber. By including in future works those phenomena and conditions omitted here, the effect of more complex/realistic hypothesis on the physical behavior of the spray will be noticed and its contribution on the fuel-air mixing process could be quantified.

The results are compared with the classical numerical RANS method with both eulerian-eulerian and lagrangian-eulerian approaches and are simultaneously validated with experimental data. The algorithm used in this paper has been implemented in the free all-purposes CFD code OpenFOAM.
The paper is structured as follows: after the introduction, the basis of the LES methodology and the main differences with RANS provide the needed mathematical background. In a subsequent section, the detailed description of the assumptions to set the boundary conditions together with the computational domain are presented. Finally, the numerical results with the main conclusions are exposed.

Numerical Technique

As it is said in the introduction, there are basically three types of methods to solve a CFD problem depending on the modelling and the description of turbulence: RANS, LES and DNS. DNS was the first developed method, but it is inapplicable in most practical cases. Both RANS and LES methods where developed more or less at the same time in the sixties. LES methods where first described by Smagorinsky in 1963 [44], [27] but, due to the computational resources required, it has not been wide applied in engineering until very recently [43].

Pope [40] in his book gives an excellent introduction to LES which is briefly presented in this section. There are three conceptual steps in LES. First, define a filtering operation to decompose the velocity field as:

$$u(x,t) = \overline{u}(x,t) + u'(x,t). \quad (1)$$

where the filtered component, ū, represents the motion of the large scales, once the small scale motions that occur on length scales smaller than the mesh spacing are included in the residual component u′. The motion of these sub-grid scales (SGS) can not be captured and therefore their effect on the large scales is modelled in a subsequent step.

In a second stage, the Navier-Stokes equations are spatially filtered assuming that the filtering operator is commutative with the differential operator. The filtering operation is defined as:

$$\overline{f}(x,t) = \int_{\Omega} G(x - x'; \Delta(x)) f(x',t)\, dx', \quad (2)$$

where G is the filter function and Δ is the filter width, here assigned to be the cube root of the local cell volume. As the isodense condition was set, the introduction of density filter quantities $\tilde{f} = \overline{\rho f}/\overline{\rho}$ is negligible. A deep explanation can be found in [35]. In this study the conservation equations governing the filtered velocity field ū(x',t) are obtained by applying the filtering operation to the Navier–Stokes equation, for an incompressible flow of a Newtonian fluid. Thus, the filtered continuity equation and the filtered momentum equation become:

$$\nabla \cdot \overline{u} = 0, \quad (3)$$

$$\frac{\partial \overline{u}}{\partial t} + \nabla \cdot \overline{uu} = -\frac{1}{\rho}\nabla \overline{p} + \nu \nabla^2 \overline{u} - \nabla \tau, \quad (4)$$

where ū is the filtered velocity field, t is the time, $\overline{p}$ is the filtered pressure, ρ is the fuel density, v is the uniform kinematic viscosity and τ is the stress-like tensor $(\tau = \overline{uu} - \overline{u}\,\overline{u})$. Notice that the filtered product $\overline{uu}$ differs from the product of the filtered velocities $\overline{u}\,\overline{u}$. Eqs. (3) and (4) govern the evolution of the large (energy-carrying) scales of motion and the modelled stress term is τ . Also, this sub-grid scale SGS stress tensor provides the communication between the resolved scales and the dissipation scales [35].

In the last step, closure is obtained by modelling the residual-stress tensor. The Smagorinsky [9] model is used for the sub-grid scale tensor:

$$\tau_{ij}^{d} = -2\mu_{SGS}S_{ij}, \quad (5)$$

where τ_{ij}^{d} is the deviatoric SGS stress and $\mu_{SGS} = \overline{\rho}\,(C_S\Delta^2)\left\|\widetilde{S_{ij}}\right\|$

C_S is the Smagorinsky constant, with a theoretical value in the range [0.065–0.2] and $\left\|\widetilde{S_{ij}}\right\|$ is the Frobenious norm $\left\|\widetilde{S_{ij}}\right\| = \sqrt{2\widetilde{S_{ij}}\widetilde{S_{ij}}}$ of the filtered strain tensor, $\widetilde{S_{ij}} = \frac{1}{2}\left(\frac{\partial \overline{u_i}}{\partial \overline{x_j}} + \frac{\partial \overline{u_j}}{\partial \overline{x_i}}\right)$

The Smagorinsky constant varies with both grid mesh aspect ratio as pointed out by Scotti in [42] and the mean shear ([22], [46]). Although some dynamic implementations of the Smagorinsky model allow to determine C_S as a function of time and position [20] there is little to be gained by the use of more complex SGS models in the case of high Reynolds number free flows of the type considered. As it has been already shown clearly in previous results [26] [16], the standard Smagorinsky model and even more simple models [45] give good

results for free flows. Nevertheless, LES of jets has been carried out with a dynamic model to evaluate the C_S [29]. In their work, Ma et al. had to apply some modifications to avoid the negative values and the strong variations yielded by this model.

The time derivative terms in Eqs. (3) and (4) are discretized using a first order Euler scheme. The discretization scheme for the diffusive term in Eq. (4) is a second order gaussian integration interpolated linearly by a centred scheme. The convection term in Eq. (3) and (4) is discretized implicitly using a second order Gaussian limited linear differencing scheme. Finally, The PISO [6] method is used to solve the pressure correction equation.

As mentioned above, the RANS approach has been traditionally used in order to model Diesel spray injections [36]. The RNG (Renormalization Group Theory) k-epsilon turbulence model with the default coefficients for the turbulent dissipation rate equation and turbulent viscosity is used for both Euler-Euler and Lagrangian-Euler spray calculations. Previous works [31] showed that RANS accurately predicts average velocity profiles and average spray's shape (dispersion rate, penetration), since the mean velocity profile and the spreading rate are independent of Reynolds number. Nevertheless, RANS is not valid if higher level of turbulence structure description is required during the calculations [37].

Table 1 resumes the main characteristics of RANS models compared to LES formulation. Differences are based on the statistical treatment of the turbulence (RANS) and the use of the self-similarity theory of Kolmogorov (LES). Consequently, differences can be found on the time-averaging of the Navier-

Stokes equations and the spatial filtering for the RANS and LES respectively, see Table 2.

Solutions schemes for the Eulerian-Eulerian spray simulations with the RANS formulation are exactly the same to those used and described in the previous section for the LES Eulerian-Eulerian spray calculations.

Table1 Comparison between RANS and LES

RANS	LES
Statistical phenomena	Kolmogorov theory of self similarity [a]
Time-averaged NS [b]	Spatial filtered NS
k - ε model (Jones&Launder, 1972) RNG k - ε model (Yakhot, 1992)	Smagorinsky (Smagorinsky, 1963) One Eq. model (Yoshizawa,1985)
Less computationally demanding	Predict transient flows better

[a]. Large eddies of the flow are dependent on the flow geometry, while smaller eddies are self similar and have a universal character.

[b]. NS: Navier-Stokes Equations

Table2 Time Averaging vs. Spatial Filtering.

Instantaneous = Average + Fluctuations ($u = \bar{u} + u'$)

Averaging or filtering of NS equations gives identical equations for the averaged/filtered variables plus averaged fluctuation terms.

Time Averaging	Spatial Filtering
$u_i(x) = \frac{1}{T}\int_t^{t+T} \overline{u_j}(x,s)\,ds.$	$u(x_0) = \int_\Omega u(x,t)\,G(x_0,x,\Delta)\,{}^{\llcorner 3}dx.$
$\overline{u_i'} = 0$, and $\overline{\overline{u_i}} = \overline{u_i}.$	$\overline{u_i'} \neq 0$, and $\overline{\overline{u_i}} \neq \overline{u_i}.$
Reynolds Stress Tensor	SGS[4] Stress Tensor
$\tau_{ij}^R = \overline{u_j' u_i'}$	$\tau_{ij}^S = -\left(\overline{\overline{u_i}u_j'} + \overline{u_i'\overline{u_j}} + \overline{u_i'u_j'}\right) = \overline{u_i u_j} - \overline{u_i}\,\overline{u_j}$

[3]. Spatial filter G (x_0, x, Δ) with filter size Δ

[4]. Sub-grid Scale

Boundary Conditions

In Diesel engines the fuel is injected into the cylinder by a high pressure atomizer with a nozzle hole diameter d_0 which creates the fuel spray. In terms of computational difficulty, the flow is not statistically stationary and has 3 directions of statistical inhomogeneity. Those conditions, together with the two phase appearing in the fuel at high velocity, sets the spray evolution as one of the most complicated turbulent flow to simulate [40][9]. As depicted in the introduction, besides the simplifications brought by the experimental researches, CFD still presents limitations in terms of the modelling of the atomisation process of the nearby zone which is not the goal of the present study. Consequently, the simplification of the computational domain presented by Vuorinen [25] is also assumed. In this work the inlet boundary condition is set far enough from the nozzle, avoiding the problems of the void fraction limits which grid resolution required by LES makes it more restrictive. In addition, the present work can be seen as a previous approach to the inclusion of droplets (Lagrangian term) as a source of mass and momentum. These particle-laden gas jets are considered by the authors as the logical following step as it has been widely used to analyze dilute sprays [17][18]. As it can be inferred from the description of the computational domain this is the region of the spray where the research is focused. Furthermore, by keeping the same computational

domain will provide a better application of present conclusions to future Lagrangian-Eulerian LES calculation and a more suitable framework for further comparison between them. As presented below, turbulent gas jet theory will be applied to set the fields in the inlet boundary conditions of the domain.

Studies show how under certain conditions, for any section perpendicular to the spray axis in the steady region of the gas jet or diesel spray, momentum flux is conservative, and thus equal to that existing at the nozzle exit [15][33].

Therefore, a proper implementation of the inlet boundary condition would perform the same spray development independent of where it would be placed. Hence, the inlet boundary condition must be perpendicular to the spray axis, contain the whole spray and the same momentum flux as at the nozzle exit and -in order to ensure a more realistic development of the flow- the boundary inlet has to reproduce the same profile of the fields as in a steady spray.

Since momentum flux can be obtained from experimental data, the unknown factors to set up the boundary condition can be identified by integrating momentum over the whole spray section:

$$\dot{M}_0 = \dot{M}(x) = \int_0^R 2\pi\rho(x,r)\,U(x,r)\,rU(x,r)\,dr, \tag{6}$$

where the x-coordinates coincides with the spray axis and the r is the radial coordinate, ρ is the local density in the Diesel spray and U is the axial velocity.

Writing the density at an internal point of the spray in terms of local concentration and assuming a Gaussian radial profile [10] for fuel concentration and axial velocity, Desantes et al, obtained the following expression for the spray momentum [13]:

$$\dot{M}_0 = \frac{\pi}{2\alpha} \cdot \rho_a \cdot \tan^2\left(\frac{\theta_u}{2}\right) \cdot x^2 \cdot U_{axis}^2 \cdot \sum_{i=0}^{\infty} \frac{1}{\left(1 + i\frac{S_C}{2}\right)} \cdot \left[\left(\frac{U_{axis}}{U_0}\right)\left(\frac{1+S_C}{2}\right)\left(\frac{\rho_f - \rho_a}{\rho_f}\right)\right]^i . \quad (7)$$

Here the Schmidt number (SC) represents the relative rate of momentum and mass transport and θ_u is the spray cone angle. The point of interest for the present work can be seen in Fig. 1 where the Uaxis = U0 . The spray injected under the physical conditions shown in Table 3 has been simulated [10]. In these conditions the end of the non-perturbed zone for the isodense case is located at 4.073mm, approximately $8d_{eq}$ from the nozzle exit (with $d_{eq} = d_0\sqrt{\rho_f/\rho_a}$) and the gas jet diameter is 2.07mm which is set as the inlet boundary condition diameter. The velocity and concentration reference profiles are defined as:

$$U(x,r) = U_{axis}(x) \cdot \exp\left(-\alpha\left(\frac{r}{R}\right)^2\right), \quad (8)$$

$$C(x,r) = C_{axis}(x) \cdot \exp\left(-\alpha \cdot S_C \cdot \left(\frac{r}{R}\right)^2\right), \quad (9)$$

with α (= 4.6) the shape factor of the Gaussian distribution. Since LES calculation requires perturbed inlet boundary conditions, the reference signal is randomly perturbed a 10% as a first approximation. The discussion of the convenience of this hypothesis will be overcome in the followings sections. The computational domain is a cylindrical volume (d = 40mm, L = 70mm) that represents the shape of the injection test rig chamber. The meshing methodology is fairly the same for the RANS and LES calculations, with

different grid densities depending on the turbulence formulation. Hexahedral cells have been preferred for the grid generation, since they provide better accuracy and stability than tetrahedral cells. The computational domain has been decomposed into hexahedral subparts in order to get a semi-structured topology mesh, as shown in Fig. 2(a). Cells are concentrated around the spray diameter (d = 2.07mm) to get a cell size of 57.5μm and 22.5μm for the RANS and LES meshes respectively. Downstream the nozzle the mesh is progressively adapted to the shape of the computational domain in order to obtain a homogeneous cell size at sections located downstream the inlet boundary condition, see circular sections on the right of Fig. 2. The numbers of cells are 4.05×10^5 and 4.9×10^6 for the RANS and LES formulation respectively.

Table3 Definition of experimental and gas jet CFD simulation.

	exp.[10] (M = 1.11N)	simulation
Fuel	C13 H28 (l)	fuel (N_2)
Air	N_2	N_2
P_{inj} (MPa)	73.995	-
$P_{a,\infty}$ (MPa)	3.5	3.55
$T_{f,0}$ (K)	307.58	307.58
$T_{a,\infty}$ (K)	307.58	307.58
ρ f,0 / ρ a,∞	21.26	1
U_0 (m/s)	373.27	373.27
d_{inlet} (μm)	112[a]	2070[b]
d_{eq} (μm)	516	516

[a]. Nozzle diameter

[b]. Jet diameter at the end of the non perturbed zone

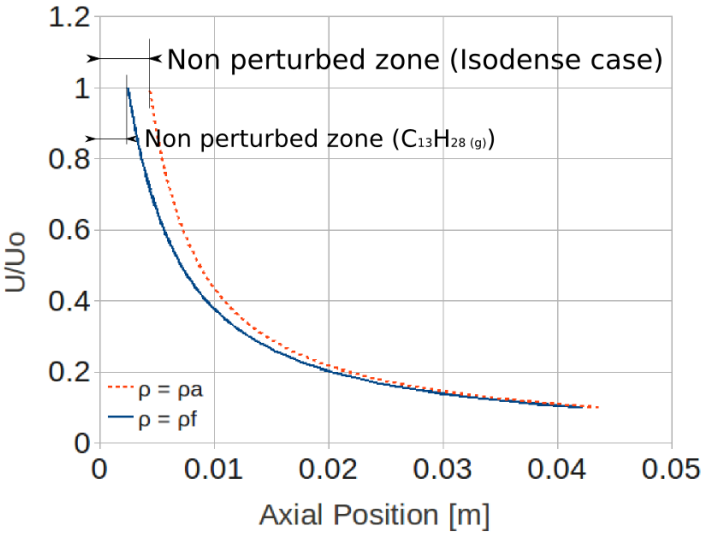

Figure1 Axis velocity. Dot line: Isodense case, Solid line: C13H28 (g) case

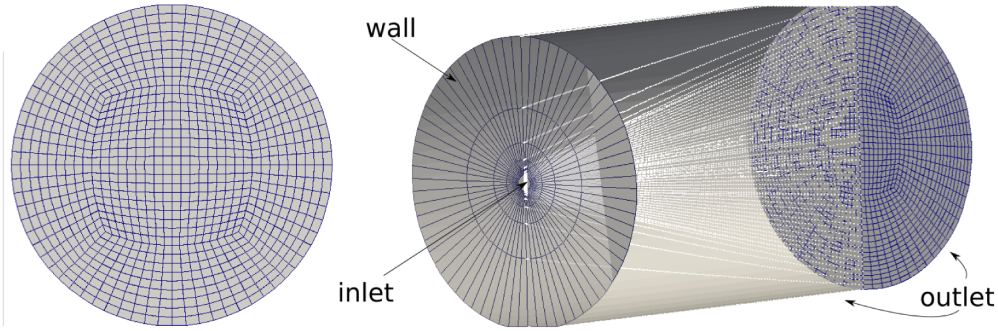

Figure2 Calculation domain and boundary conditions for the RANS case.

LES grid is a finer version of this one

In this mesh, the circular faces of the cylinder are splitted into four parts and then meshed with a non-structured hexahedral mesh using the same cell size than that described above. Previous studies performed on RANS euler-euler [1] in similar spray conditions show that the structure of the mesh and cell size are enough to get a grid independent solution. Also, the meshes used for the LES formulation have comparable and also smaller cell sizes than recent LES studies [45] for sprays characterization where the grid independence is proved.

Finally, three boundary conditions are assigned in the computational domain as depicted in Table 4.

Table4 Definition of gas jet CFD boundary conditions.

Surface	Boundary type	Defining variables
inlet	turbulent velocity inlet	U_0 (r)&C(r), T_f
wall	rigid wall, non-slip cond.	-
outlet	constant pressure, wave Transmissive	$P_{a,\infty}$ $T_{a,\infty}$

Experimental Results and Validation

Experimental data have been obtained from previously published data from the authors' research group. Mass flow rate for the velocity inlet was measured by means of Bosch's method [21]. Momentum flux data to calculate the length of the non-perturbed zone was achieved by measuring the impact force of the spray in a surface with a piezo-electric sensor [33]. The velocity of droplets is also measured under non-vaporising conditions inside a SF6 (a dense gas) atmosphere at room temperature (298K). The environmental density at low pressure (0.5MPa) was 40Kg/m3, close to the reference case [3].

A comparison with the Gaussian radial profiles is shown in Fig. 3 and Fig. 4. In both the axial velocity has been normalized with the axis velocity. In Fig. 3 the radial distance is normalized with the jet's half-width as defined by Pope [40]

where in Fig. 4 is normalized with the axial distance. A spatial average at 25mm of the nozzle of the axial velocity (t = 0.5ms) shows a good agreement with the theoretical Gaussian profile from the edge to more than the half of the jet radius (up to 30% of the axis speed) Fig. 3. Differences in simulated profiles at 20 and 25 mm in Fig. 4 can be affected by the amount of statistics for each location (around 0.05ms less data at 25mm). Experimental data is close to LES simulated profile near the edge of the spray but moves to the Gaussian one as r increases.

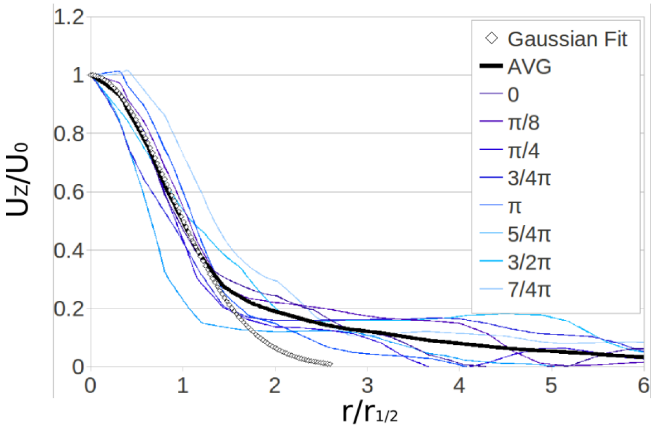

Figure3 Radial velocity profiles (t=0.5ms). Spatial average of eight different angles

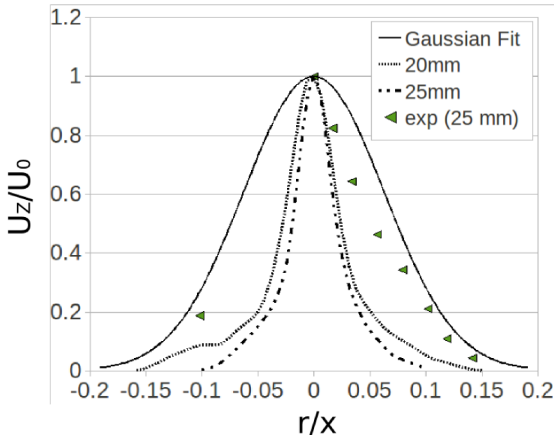

Figure4 Radial velocity profiles (t=0.5ms). Time-averaged [3].

Temporal evolution of the axial velocity at 25mm of the virtual nozzle has been used to justify the beginning for the statistical measurements. In Fig. 5 the criteria of a constant spray angle was used to set the radial position of the probes. Thus the first probe in the isodense calculation is located at the edge of the spray and the last at 4.25mm from the edge. Since no significant velocity variation is detected by the most far-off probe, its measurements do not appear. It is also shown the velocity value imposed in the center of the inlet boundary condition (4.073mm from the virtual nozzle under the isodense conditions). Differences in both the frequency content and the width of the velocity signals in the inlet boundary condition and the axis velocity at 25mm show a lack of precision of the spray fields simulated at the inlet boundary condition. Its effect in LES in terms of the classical parameters to characterize the spray is decisive as shown in Fig. 6. Therefore the improvement of the velocity field imposed at the inlet boundary condition will be a compulsory progress to work on.

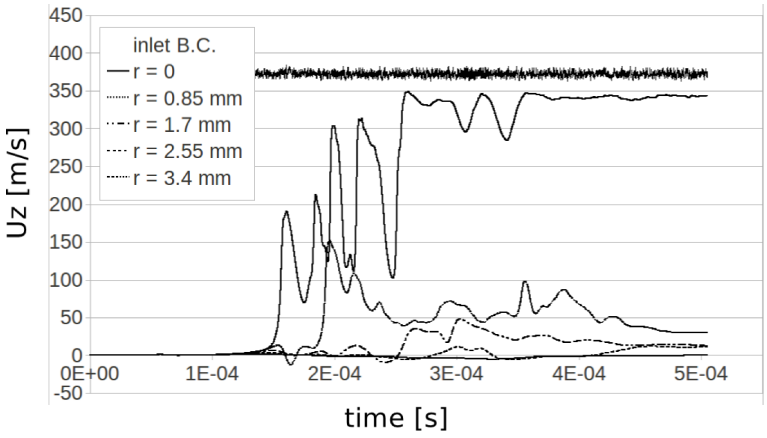

Figure5 Measurements of radial probes (x=25mm)

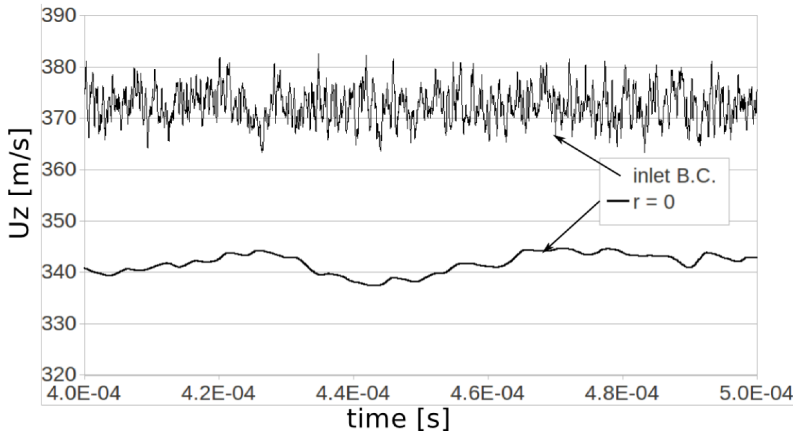

Figure6 Measurements of axys velocity

LES vs RANS

The spray penetration is defined as the maximum axial distance for the 1% fuel mass fraction iso-surface, as shown in Fig. 7. Notice that this distance is located at the edge of the spray for theoretical and RANS calculations but not necessarily for LES simulations (see Fig. 7 solid red line). The Fig. 7 shows iso-surfaces of fuel concentration for the LES simulation at 0.3ms. The red line and the green line mark the stoichiometric iso-surface for LES and RANS (E-E) simulations respectively. These areas have a relevant importance in combustion processes. The upper part of the figure plots the radial distance of these surfaces where detached surfaces far from the jet can be found.
RANS and LES (E-E) calculations correspond to isodense gas jets cases detailed in previous sections. A description of the Lagrangian-Eulerian approach will be done in future works when comparing RANS with LES Lagrangian-Eulerian calculations. This approach is outside of the scope of the present

paper and has been shown as a reference of a good experimental estimation to compare with.

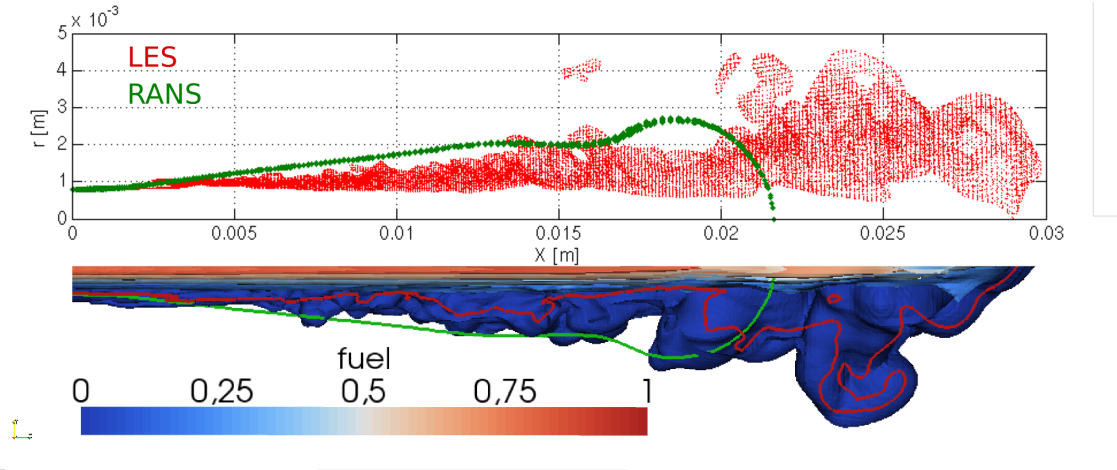

Figure7 Comparison between RANS and LES concentration iso-surfaces t=(0.3ms). Lower part: longitudinal clip of fuel concentration contours, Upper part: Radial coordinates of stoichiometric iso-surfaces

The over prediction of both the RANS and LES Eulerian-Eulerian penetration is highly affected by the different injection mass flow rate shape. The experimental injection velocity follows a progressive evolution (also shown in [21]) while the modeled injection is a constant value, simplified in this way to avoid disguising the first stages of the jet with this variable.

The over prediction of both the RANS and LES Eulerian-Eulerian penetration is also affected by the fact that spray is more effective in transferring injection momentum to the ambient than the gas jet [2] (e.g. in the L-E approach the Lagrangian term carries the 45% of the momentum at 8deq of the nozzle). Furthermore, in this initial part of the spray the local density is far from the assumption of constant density of the gas jets. Therefore the isodense hypothesis that allows comparing the gas jet with the Diesel spray is so

restrictive from the actual boundary condition placed at 8deq. The assumption is acceptable beyond the developing region (x/deq > 30) where differences in axis velocity under turbulent gas jet theory are less than 3%.

Moreover, for the LES calculation, the first 5mm can be seen as a length required developing turbulence Fig. 7. Thus, the first assumption of a 10% of velocity fluctuation at the inlet boundary condition is not a good enough turbulent initialization of the flow. Given that the inlet is placed at the end of a not well-known zone, authors think a more realistic turbulent conditions can be achieved by applying measured or more accurate calculated profiles of velocity variation [24], [28].

Conclusions

Using the OpenFOAM code, the authors have performed a completed simulation of diesel spray in LES. A comparison between the propose method and trusted (E-E) RANS sprays simulations has been performed, obtaining a very good agreement. Configuration and turbulent boundary conditions election have been justified and validated. Internal structure of the spray has been deeply studied, showing some characteristics of the spray. LES results have been also validated against experimental measurements of the velocity field. Some specific needs are presented in our paper as challenges to overcome. The results show how the hypothesis of an incompressible flow applied to obtain the governing equation imposes restrictions that distance the physical

development calculated from the real behaviour. Therefore, for future calculations under similar conditions the solver should take into account the effect of compressibility, due to closeness to sonic conditions (density-based solver).

LES modelling can become the practical tool in both industry and academic in the design process of combustion system. The future research is now focusing on identifying the important parameters that affect the model and on improving the stability and accuracy of algorithms within OpenFOAM code. By so doing, the better spray simulation will be performed and a reliable tool will be used in modelling the spray simulation in the near future.

Acknowledgment

This research has been funded by the Spanish Government in the frame of the Project “Métodos LES para la simulación de chorros multifásicos”, Ref.ENE2010-18542. The authors also acknowledge the financial support of the Universidad Politécnica de Valencia under the contract Reference PAID-2759 and the Generalitat Valenciana, under the contract GV/2010/039. We are also grateful to Dr. Franciso Javier Salvador, and Dr. José Manuel Pastor for providing experimental data and fruitful advices. In addition, we gratefully acknowledge helpful discussions with many researchers in CMT-Motóres Térmicos, specially Ms Palma González and Ms Mariany Chávez.

References

1. Abraham J (1997) What is Adequate Resolution in the Numerical Computations of Transient Jets? SAE 970051 (1997) pp. 81-95.
2. Abraham J, Magi V, Macinnes J, Bracco FV (1994) Gas versus Spray Injection: Which Mixes Faster? SAE paper 940895; (1994), pp. 163-177.
3. Araneo L, Soare V, Payri R, Shakal J (2006) Setting up PDPA system for measurement in a diesel spray, Journal of Physics, 45, (2006), pp. 85-93.
4. ASCE Task Committee on Turbulence Models in Hydraulic Computations (1988). Turbulence Modeling of Surface Water Flow and Transport. Journal of Hydraulic Engineering 114(9):970–1073.]
5. Aziz TN , Raiford JP, Khan AA (2008) NUMERICAL SIMULATION OF TURBULENT JETS. EACFM Vol. 2, No. 2, pp. 234–243
6. Barton E (1998) Comparison of simple- and piso-type algorithms for transient flows. International Journal for Numerical Methods in Fluids
7. Befrui B, Corbinelli G, Robart D, Reckers W (2008) LES simulation of the internal flow and near-field spray structure of an outward-opening gdi injector and comparison with imaging data. SAE paper 2008-01-0137; (2008), pp. 163-177.
8. Bharadwaj N, Rutland CJ (2010) A Large-Eddy Simulation study of sub-grid two-phase interaction in particle-laden flows and diesel engine sprays. Atomization and Spray (2010) 20(8), pp. 673-695.

9. Chesnel J, Réveillon J, Ménard T, Berlemont A, Demoulin FX (2010) Large Eddy Simulation of liquid atomization: From the resolved scales to subgrid spray. International Conference on Multiphase Flow (ICMF)
10. Correas D (1998) Theoretical and experimental study of isothermal Diesel free sprays (In Spanish), PhD Thesis, Universidad Politcénica de Valencia
11. De Bortoli AL (2007) SIMULATION OF A CONFINED TURBULENT NONPREMIXED PILOTED METHANE JET FLAME, EACFM Vol. 1, No.4, pp. 337–349.
12. Deportes A, Zellat M, Desoutter G, Liang Y, Ravet F (2010) Application of the Eulerian-Lagrangian Spray Atomization (ELSA) Model for the Diesel Injection Simulation. THIESEL
13. Desantes JM, Payri R, García-Oliver JM, Salvador FJ (2007) A contribution to the understanding of isothermal diesel spray dynamics, Fuel 86 (2007), pp. 1093–1101.
14. Desantes JM, Payri R, Salvador FJ, de la Morena J (2010), Influence of cavitation phenomena on primary break-up and spray behaviour at stationary conditions. Fuel 89(10), pp.3033-3041.
15. Desantes JM, Payri R, Salvador FJ, Gimeno J (2003) Measurements of spray momentum for the study of cavitation in diesel injection nozzles. SAE Paper 2003-01-0703
16. Doolan CJ (2010) LARGE EDDY SIMULATION OF THE NEAR WAKE OF A CIRCULAR CYLINDER AT SUB-CRITICAL REYNOLDS NUMBER, EACFM Vol. 4, No. 4, pp. 496–510

17. Faeth GM (1987) Mixing, transport and combustion in sprays. Prog. Energy Combust. Sci (1987), 13, pp.293-345.
18. Faeth GM (1996) Spray combustion phenomena. 26th International Symposium on Combustion (1996), pp.1596-1612.
19. Fevrier P, Simonin O, Squires KD (2005) Partitioning of particle velocities in gas-solid turbulent flows into a continuous field and a spatially uncorrelated random distribution: theoretical formalism and numerical study. J. Fluid Mech.Vol 533,(2005) pp. 1-46
20. Germano M, Piomelli U, Moin P, Cabot W (1991). A dynamic subgrid-scale eddy-viscosity model. Phys. Fluids A, 3(3):1760-65
21. Gimeno J (2008), Desarrollo y aplicación de la medida del flujo de cantidad de movimiento de un chorro diesel, PhD thesis, Universidad Politécnica de Valencia
22. Horiuti K (1993) A proper velocity scale for modelling subgrid-scale eddy viscosities in large eddy simulation, Physics of Fluids (1993), 5, 146-157.
23. Hoyas S, Jiménez J (2006) Scalling of the velocity fluctuations in turbulent channels up to Re_tau=2000. Phys. Fluids, Vol. 18 (2006), Article Number: 011702
24. Hussein HJ, Capp, George WK (1994) Velocity measurements in a high-Reynolds-number, momentum-conserving, axisymetric, turbulent jet, J Fluid Mech (1994). 258, 31-75.
25. Jiménez J (2003) Journal of Turbulence, J. turbul Vol. 4 (2003) Article Number: 022.

26. Jones WP, Lyra S, Marquis AJ (2010) Large Eddy Simulation of evaporating kerosene and acetone sprays, International Journal of Heat and Mass Transfer, Volume 53, Issues 11-12, May (2010), Pages 2491-2505.
27. Launder BE, Spalding DB (1974) The numerical computation of turbulent flows, Computer Methods in Applied Mechanics and Engineering, Volume 3, Issue 2, March 1974, Pages 269-289.
28. Levy Y, Lockwood FC (1981) Combust. Flame 40, 333
29. Ma F, Satish M, Islam MR (2007) LARGE EDDY SIMULATION OF THERMAL JETS IN CROSS FLOW, EACFM Vol. 1, No. 1, pp. 25-35
30. Margot X, Hoyas S, Fajardo P, Patouna S (2010) A moving mesh generation strategy for solving an injector internal flow problem, Mathematical and Computer Modelling (2010) 52 pp.1143-1150.
31. Pastor JV, López JJ, García JM, Pastor JM (2008) A 1Dmodel for the description of mixing-controlled inert diesel sprays. Fuel 87(08), pp.2871-2885.
32. Payri F, Margot X, Patouna S, Ravet F, Funk M (2009) A CFD Study of the Effect of the Needle Movement on the Cavitation Pattern of Diesel Injectors, Proceedings ICE2009 SAE Naples Section 2009-24-0025.
33. Payri R, García-Oliver JM, Salvador FJ, Gimeno J (2005) Using spray momentum flux measurements to understand the influence of Diesel nozzle geometry on spray characteristics, Fuel 84 (2005), pp. 551–561.

34. Payri R, Salvador FJ, Gimeno J, de la Morena J (2009) Effects of nozzle geometry on the direct injection diesel engine combustion process Appl. Therm. Eng. 29 (2009) pp.2051-2060.
35. Payri R, Tormos B, Gimeno J, Bracho G (2010) The potential of Large Eddy Simulation (LES) code for the modeling of flow in diesel injectors, Mathematical and Computer Modelling, Volume 52, Issues 7-8, (2010), Pages 1151-1160.
36. Peng-Krrholm F (2008) Numerical modelling of diesel spray injection, turbulence and combustion, Ph.D. Thesis, Chalmers Uni. of Technology
37. Pitsch H (2006) Large-Eddy Simulation of Turbulent Combustion, Annual Review of Fluid Mechanics, Vol. 38, No. 1, 2006, pp. 453-482.
38. Riley JJ (2006) Review of large-eddy simulation of non-premixed turbulent combustion, J Fluids Eng 128 (2006), pp. 209-215.
39. Roberts RA, Cui J (2010), SELECTION OF THE SIMULATION DOMAIN FOR TURBULENT FLOW AROUND AN AIRFOIL, EACFM Vol. 4, No. 3, pp. 441–449
40. S.B. Pope, Turbulent Flows, Cambridge University Press, 2000. 771 pp.
41. Safer K, Bounif A , Safer M and Gökalp I (2010) FREE TURBULENT REACTING JET SIMULATION BASED ON COMBINATION OF TRANSPORT EQUATIONS AND PDF, EACFM Vol. 4, No. 2, pp. 246–259
42. Scotti A, Meneveau C, Lilly DK (1993), Generalized Smagorinsky model for anisotropic grids. Phys. Fluids A 5, pp. 2306-2308.

43. Shalaby H, Wozniak K, Wozniak G (2008) PARTICLE-LADEN CYCLONE SEPARATOR FLOW USING LES, EACFM Vol. 2, No. 4, pp. 382–392
44. Smagorinsky JS (1963) General circulation experiments with the primitive equations. I. The basic experiment, Mon. Weather Rev. 91 (1963), pp. 99–164.
45. Vuorinen V (2010) LES of Certain Droplet Size Effects in Fuel Sprays, PhD Thesis, the Aalto University School of Science and Technology
46. Yakhot A, Orszag S, Yakhot V, Israeli M (1989) Renormalization group formulation of large-eddy simulations, J. Sci. Comput. (USA), 4, 2, pp.139-58

Figure Captions

Figure1 Axis velocity. Dot line: Isodense case, Solid line: C13H28 (g) case

Figure2 Calculation domain and boundary conditions for the RANS case.

Figure3 Radial velocity profiles (t=0.5ms). Spatial average of eight different angles

Figure4 Radial velocity profiles (t=0.5ms). Time-averaged.

Figure5 Measurements of radial probes (x=25mm)

Figure6 Measurements of axys velocity

Figure7 Comparison between RANS and LES concentration iso-surfaces

Tables

2.2.6. Large Eddy Simulation of Diesel like particle-laden flows. Mathematical Modelling in Engineering & Human Behaviour 2011

Large Eddy Simulation of Diesel like particle-laden flows

S. Hoyas, A. Gil, X. Margot, J.M. Mompó-Laborda

CMT - Motores Térmicos. Universidad Politécnica de Valencia.
Camino de Vera, s/n 46022 Valencia, Spain

E-mail addresses: serhocal@mot.upv.es, angime@mot.upv.es, xmargot@mot.upv.es
juamomla@mot.upv.es

In the automotive industry, computational fluid dynamics (CFD) tools are very useful in order to reduce experimental measurements and help understand many thermodynamic processes that take place inside internal combustion engines. These CFD codes solve the Navier-Stokes equations together with the energy equation using three different approaches to model the turbulence: Reynolds-Averaged Navier-Stokes (RANS), Large Eddy Simulation (LES), and Direct Numerical Simulation (DNS). Regarding Diesel spray injection, the most commonly used codes in the automotive industry, until very recently, are based on the RANS approach. These computational methods are very useful to study the averaged flow, but they do not provide any information neither about the turbulent fluctuations nor about the flow on the jet boundary. Nevertheless, they provide reasonably accurate results and have relatively lower computational cost.

On the contrary, direct numerical simulation (DNS) methods solve all the significative scales of the flow, and no modelling is required. Therefore, the DNS provides the highest level of description of the flow, but the computational resources required for most practical cases are above current computer hardware limitations (and will be in the next 20 years).

LES is a compromise between DNS and RANS. LES methods model only the smallest-scale fluid motions and directly represent the large-scale ones. While the use of LES increases the computational cost, LES has been a predictive tool able to consistently simulate the complex structures related with turbulent mixing, which is decisive in the injection and combustion processes and invisible for RANS solvers.

It is the aim of this paper the evaluation of numerical (LES) approach to simulate Diesel sprays by means of the open source CFD code OpenFoam. Previous works performed by these authors showed the potential of LES methodology for Diesel spray simulations, also with Euler-Euler approximations. However, since fuel-air mixing process is significantly influenced by fuel atomization, breakup and collision, the idea to approximate the spray evolution using gas injection cannot be completely valid for LES due to its degree of physical description. Therefore, Lagrangian-Eulerian particle-laden flow simulations have been carried out in order to accurately predict the mixing and entrainment processes that take place in a real Diesel spray. A parametric and sensibility study of the most significant parameters of the LES approximation has been also presented.

The modelling results are compared with the classical numerical RANS method with both Eulerian-Eulerian and Lagrangian-Eulerian approaches and are simultaneously validated with experimental data.